Mechanics and Materials Center
TEXAS A&M UNIVERSITY
College Station, Texas

EXPERIMENTAL OBSERVATIONS AND FINITE ELEMENT ANALYSIS OF THE INITIATION OF FIBER MICROBUCKLING IN NOTCHED COMPOSITE LAMINATES

An Annual Progress Report

prepared by

E. GAIL GUYNN

WALTER L. BRADLEY

NASA Research Grant NAG-1-659

December 20, 1989

Contract Monitor: Dr. Charles E. Harris

NASA Langley Research Center

Hampton, Virginia 23665

EXPERIMENTAL OBSERVATIONS AND FINITE ELEMENT ANALYSIS OF THE INITIATION OF FIBER MICROBUCKLING IN NOTCHED COMPOSITE LAMINATES

An Annual Progress Report

prepared by

E. GAIL GUYNN

WALTER L. BRADLEY

NASA Research Grant NAG-1-659

December 20, 1989

Contract Monitor: Dr. Charles E. Harris

NASA Langley Research Center

Hampton, Virginia 23665

TABLE OF CONTENTS

TABLE OF CONTENTS (Continued)

TABLE OF CONTENTS (Continued)

1.0 INTRODUCTION

The high strength-to-weight ratio of composite materials is ideally suited for aerospace applications where they are already used in commercial and military aircraft secondary structures and will soon be used for heavily loaded primary structures. One problem impeding the widespread application of composites is their inherent weakness in compressive strength when compared to the tensile properties of the same material. This result is not surprising, given that the composite's tensile and compression strength comes primarily from long narrow fibers. The effective strength of these fibers in compression is generally much lower than their strength in tension due to fiber microbuckling which leads to additional local fiber buckling and/or shear crippling, delamination, loss of structural stiffness, and macroscopic compressive failure. Nevertheless, it is desirable to develop composite systems with the smallest penalty in compressive strength possible.

Previous work[1-4] on tough matrix composite laminates containing center holes indicates that the compressive failure of these composites initiates with out-of-plane microbuckling of the 0° fibers toward an unsupported surface in 0° plies at the free surface. Compressive failure in the laminates which did not contain surface 0s initiated with in-plane fiber microbuckling into the center hole. Growth of this initial damage to a critical size at which catastrophic failure occurs required little additional load. This result suggests that the compression strength is controlled by initiation of fiber microbuckling, particularly for the PEEK system of that investigation. The in- and out-of-plane fiber microbuckling appears to preceed shear crippling damage in the systems studied in Refs. 1–4. Furthermore, the fiber microbuckling and shear crippling often lead to local delamination when the local strain necessary to accommodate the large localized interlaminar shear strains

exceeds the resin ductility. These local delaminations apparently do not propagate (to become macroscopic delaminations) until final compressive failure when large scale brooming and/or generalized delamination occurs.

The significant role of local constraints on the initiation of fiber microbuckling was also indicated in Refs. 1–4. For example, when $\pm 45°$ fibers were used as surface plies, in-plane fiber microbuckling initiated at a strain level which is much higher than the initiation strain when the $0°$ fibers were the surface plies and the microbuckling was out-of-plane. These results indicate that one reason most compression strength models overpredict the actual compression strengths observed in experiments is that they make no allowance for free surface effects, i.e. these models implicitly assume infinitely large laminates. It should be noted that the term "fiber microbuckling" used the literature and throughout this report, refers to large lateral deflections of initially wavy fibers leading to fiber breakage, rather than a bifurcation instability.

Many theories have been proposed and developed to predict the compressive strength of unidirectional composite laminates. However, few similar investigations have been conducted for multidirectional composite laminates, even though these laminates are more widely used than unidirectional laminates in composite structural components. Furthermore, an uncertainty in the modes and mechanisms of compression failures in composites remains because of the lack of a clear understanding of all possible modes of failure. In order to more accurately predict the compressive strength of composite laminates, the strain level at which fiber microbuckling initiates must be determined. Additionally, the factors that affect this strain level must be studied systematically. Accurate evaluation of this strain level is important because this process appears to control the strength of ductile composite

systems.

1.1 Objectives and Scope

The primary objectives of this research have been to develop a better understanding of the factors that determine the semi-circular edge-notched compressive strength and to identify the associated failure mode(s) of thermoplastic composite laminates with multidirectional stacking sequences.

The experimental observations[1-4] and the detailed literature review (presented in Section 2.0 of this report) suggest at least four factors that affect the determination of the strain levels at which fiber microbuckling initiates and thus, partially control the composite's compression strength. These factors are listed as follows:

1. the degree of fiber waviness,
2. the fiber/matrix interfacial bond strength,
3. the effects of the free surfaces, and
4. the nonlinear shear constitutive behavior for the composite laminate.

Two additional independent variables that are also important in the determination of the stress level at which either in- and/or out-of-plane fiber microbuckling initiates are listed below:

5. the orientation of the supporting plies adjacent to the 0° plies through the thickness of a laminate and
6. the thickness of the resin-rich region between plies.

The dependent variables studied in this research are the compressive strength of a reduced gage section compression specimen and the compression strength of a compression specimen with two semi-circular edge notches (on opposite free edges) centered along the gage section. The stress and strain at damage initiation in the

0s and the subsequent development of damage were monitored as a function of the independent variables previously described.

In this research, specimens containing two semi-circular edge notches (on opposite free edges) were loaded in compression at a relatively slow rate to provide more stable development of fiber microbuckling damage. During loading, the initiation of in- and out-of-plane fiber microbuckling was monitored prior to catastrophic failure. Several compression tests were interrupted prior to catastrophic failure to allow for more careful examination of the damage in the scanning electron microscope (SEM). To determine the extent and nature of the damage through the laminate thickness, systematic sectioning techniques (developed in Ref. 1) were used to examine damage through the thickness of selected specimens. This experimental program was used to provide a systematic understanding of the relative significance of the six variables (previously mentioned) on the initiation of fiber microbuckling, the strength limiting step of thermoplastic composites. Additionally, it provided valuable details about the fiber microbuckling process and associated damage development.

Two types of experimental information were obtained from these tests. First, the nominal strain associated with the initiation of fiber microbuckling. Second, the measured nominal strain was used in conjunctin with ABAQUS, a three-dimensional nonlinear finite element analysis, to determine the local strain at the notch for fiber microbuckling initiation.

Geometric and material nonlinear two-dimensional finite element analysis was used to show the effects of the free surfaces on the fiber microbuckling initiation strain levels for the straight fiber problem. Additionally, finite element analysis was used in preliminary studies to show the effects of initial fiber curvature on the amount of shear strain developed in the matrix for a small wavy fiber problem.

2.0 REVIEW OF LITERATURE

This section reviews the literature pertaining to the compression strength of composite materials. This review covers compression test methods, failure modes, existing failure models, and microbuckling and kinking. Additionally, the effects of each of the resin, fiber, interfacial bond, environment and initial fiber curvature on compressive strength of composite materials are reviewed. Papers encompassing the areas of delamination/inherent flaws and damage tolerance (compression after impact studies) are omitted from this review since they are not directly related to the research herein. For simplicity, the equations and figures cited in this section follow the nomenclature and units used in the corresponding reference. Additionally, the nomenclature used is explained with each reference and is not included the list of nomenclature in this report. The nomenclature list pertains only to the research herein.

2.1 Compression Test Methods

Because of the inhomogeneity of graphite/polymeric composites, the mechanical properties measured are more sensitive to testing equipment and procedures than are those properties for isotropic, homogeneous materials. A brief overview of compression test methods, fixtures, and specimens is given in Ref. 5. Leonard[5] summarized results indicating that more than one test method may be valid, depending on the type of failure being tested. Reliable compressive properties are the most difficult of all mechanical properties to acquire because of the sensitivity of compression tests to a range of factors, including test methods, quality of material, and uneven loading of specimens.[6] However, accurate prediction of the compression strength is important because this mechanical property is typically the most critical

and most susceptible to cyclic loading and environmental degradation.[6] The most common compressive test methods are reviewed within this section.

Three American Society for Testing and Materials (ASTM) approved standard test procedures for compression tests of composite materials include Test for Compressive Properties of Rigid Plastics (D695 – 85),[7] Test for Compressive Properties of Oriented Fiber Composites (D3410 – 75),[8] and Flexure Test of Flat Sandwich Constructions (C393 – 62).[9] Recently, these standard test methods have been combined into one standard, Test Method for Compressive Properties of Unidirectional or Crossply Fiber-Resin Composites (D3410 – 87).[10]

Compression test methods currently in use are generally of three types: the sandwich beam compression test method, the unsupported compression coupon test methods, and the supported compression coupon test methods. The sandwich beam compression test method was evaluated by Shuart.[11] The ASTM approved sandwich beam test method is C393 – 62.[9] The sandwich construction used in this test method is typical of many composite applications, but the beam is criticized because of its fabrication cost and the undetermined influence of the honeycomb core on the mechanical properties of the composite. Shuart's results indicate that the sandwich beam in four-point bending is a viable compression test method. However, laminate orientation, test temperature, and type of honeycomb core material were shown to affect the type of beam failure.

Many fixtures have been developed and employed to test specimens with an unsupported gage length. The standard tests are ASTM D3410-87, Procedures A and B.[10] The most widely used fixture of this type is the Illinois Institute of Technology Research Institute (IITRI) wedge-grip compression test fixture. This fixture was developed by Hofer and Rao[12] to incorporate the better features of

earlier fixtures and also eliminate many of their problems. This fixture incorporates trapezoidal wedge grips which eliminate the problems of slippage and wall friction in the Celanese test methods (ASTM D3410-87, Procedure A). The upper and lower grips are linked together with precision shafts and linear bearings to insure alignment. Additionally, the fixture is adaptable to elevated temperature tests.[13] The major disadvantage of this test fixture is that the specimen gage length (12.7 mm) is very short and the failure mechanisms are thus difficult to observe. Woolstencroft, Curtis, and Haresceugh[14] compared test techniques to evaluate the unidirectional compression strength of carbon fiber-reinforced plastic (CFRP). They compared five test techniques, all of which had an unsupported gage length. Their results indicate that the Royal Aircraft Establishment (RAE) specimen was the optimum configuration. This specimen has a tapered gage thickness with the specimen ends mounted in relatively large blocks of aluminum alloy. This specimen gives a failure level indicative of the unidirectional compressive strength (based on results from finite element analysis) and does not have an induced secondary stress state through the thickness of the gage section.

Gurdal and Starbuck[15] developed a new compression test fixture to incorporate the useful features of existing fixtures. The new fixture uses an end-loaded coupon supported by four circular support pins, rather than plates, to prevent out-of-plane displacement of the specimen. Additional benefits include a reduction of the stress concentration due to Poisson's contraction at the grips and better defined boundary conditions. A combination of experimental data and finite element analysis indicates that the fixture and test coupons are adequate for the determination of Young's moduli in the principal material directions by using specimens with 0° and 90° fiber orientations. However, the determination of Poisson's ratio requires the analysis of

the specimen to include the effects of the end constraints.

Adsit[16] evaluated four techniques, an effort undertaken by the ASTM Committee D-30 on High-Modulus Fibers and Their Composites. The test methods were the ASTM D695-85, the Celanese (D3410-75), the IITRI, and the sandwich beam. The first of these techniques introduces load into the specimen by end- loading while in the other techniques, the specimens are shear-action loaded. His results indicate that end-loading (D695-85) unidirectional specimens leads to lower compressive strengths than the other methods. This result occurs because the fibers are not exactly the same length, a consequence of machining the specimen ends. It should also be noted that the Celanese, IITRI, and sandwich beam methods all gave similar results and that the modulus of elasticity was not a function of the loading method.

The supported compression test methods include those procedures in which the coupon specimen is fully supported in the gage section to prevent Euler buckling, end brooming, and splitting during loading. Typically, the gage section for these tests is ten to twenty times the length of the unsupported gage sections. Ryder and Black[17] present a good description of these test fixtures. A more recently developed design used in the aircraft industry is the Boeing fixture.[18] In Ref. 17 the specimens were gripped on one end and pressed against a bearing plate on the other, but they can be gripped on both ends. This test procedure follows the ASTM Standard D695-85 in Ref. 7.

Compression test methods have been reviewed by many investigators (Refs. 5, 6, 11, 12, 14, 16, 19, 20). This brief review in addition to a more detailed survey of compression techniques[5,6,14,20] indicates that one specific technique is not sufficient to determine compression strength; each of the methods described have advantages

opposed by disadvantages. However, each of the three basic techniques provide consistent results for specific cases. The results presented in Refs. 6, 16, and 21 indicate the specimens should be end-loaded with some shear loading induced through the gripped specimen ends. Additionally, the specimen ends should be tabbed. Tabs help prevent longitudinal splitting and crushing of the specimen ends.[21] However, the tab surfaces must be carefully machined flat and parallel, relative to each other, to achieve the best possible specimen alignment and thus, strain uniformity across the specimen, as shown in Ref. 6.

Rehfield et al[22] developed a closed-form solution to predict the stress field at the laminate-tab interface in unidirectional composite specimens. Reasonable results (compared to finite element analysis) were presented for two end-loaded unidirectional composite material systems.

2.2 Compressive Failure Modes

The common failure modes observed in composite materials loaded in compression are reviewed in this section. These failure modes include shear and extension modes of fiber microbuckling, fiber shear, end crushing, longitudinal splitting, delamination, and Euler buckling. It should be noted that several of these failure modes may occur in the same specimen or component during compressive failure. Additionally, Ref. 23 summarizes the failure modes of the constituent materials.

2.2.1 Shear and Extension Modes of Fiber Microbuckling

Compressive strength may be controlled by fiber microbuckling, as shown in Fig. 1. Such fiber microbuckling will occur either in-phase (shear mode) or out-of-phase (extension mode). In the shear mode, the matrix material is shear deformed; in the extension mode, the matrix material between the fibers is stretched in the

direction perpendicular to the fibers. Fiber microbuckling may be assisted by fiber/matrix debonding due to transverse tensile stresses, a process that leaves the fibers with less support. Furthermore, in-plane microbuckling (contained within a given ply) may lead to delamination between plies. Generally, extension mode microbuckling is observed in composites with a lower fiber volume fraction ($< 20\%$) while shear mode microbuckling is observed in composites with a higher fiber volume fraction.[24]

Factors that may influence the initiation of fiber microbuckling are the initial fiber curvature, fiber defects, fiber misalignment, yarn twist, voids, and poor fiber/matrix adhesion. It is suspected that fiber microbuckling leads to fiber kinking followed by shear crippling of the composite.

2.2.2 Fiber Shear

A second mechanism of failure observed during compression testing is fiber shear. In this failure mode a sufficiently high compressive stress is applied to the specimen (or component), without inducing macroscopic or microscopic buckling, to induce failure in the fibers by shear deformation. This failure mechanism is usually observed in composites which have a compressive strength similar to their tensile strength. It has been suggested, as reported for example in Ref. 25, that this failure mode constitutes an upper bound in compressive strength.

2.2.3 End Crushing

This compressive failure mode is common in composite specimens, particularly unidirectional composites, that are end-loaded but have insufficient transverse support within the grips. The result is crushing damage at or near the point of end loading. These failures are a result of local stress concentrations due to end

effects and are a function of the compressive test fixture, as reported in Ref. 16. This type of failure was observed in some of the ultimate compression strength tests for multiaxial lay-ups in Ref. 1. The use of tabs[6,19] and/or greater surface support in the gripped area will help prevent this type of failure during testing.

2.2.4 Longitudinal Splitting

The difference in the Poisson's ratio between the matrix and the fibers leads to differential dilatation (being stretched beyond normal dimensions) during compressive loading. Because the matrix expands more than the fiber when loaded in compression, a tensile stress develops at the interface between the matrix and the fibers. If this stress is sufficiently large, fiber/matrix debonding occurs, leading to failure by longitudinal splitting, a so-called interaction failure. As will be presented in detail later in this review, this failure is more likely to occur in composites made with anisotropic fibers (e.g., graphite or Kevlar) rather than isotropic fibers (e.g., stainless steel or E – glass).[26] Longitudinal splitting may also result from the constraint imposed by the grips which prevents the material contained in the grips from the same Poisson expansion (due to compressive loading) as the material in the gage section. This Poisson difference results in transverse tensile stresses in the gage section, adjacent to the grips, and it leads to failure by longitudinal splitting. It is worth noting that this failure is most typically observed in unidirectional composites.

2.2.5 Delamination

Compressive loading may lead to a delamination failure mode in multiaxial lay-up composite laminates. Although the failure may initiate by either transverse tension induced longitudinal splitting or fiber microbuckling, these damage modes

can cause local delamination. If the delamination propagates to a critical size, a global failure (by buckling of the sublaminates) occurs. Furthermore, out-of-plane microbuckling causes Mode I loading between adjacent plies while in-plane microbuckling causes Mode II loading between adjacent plies. In either case, if a critical local strain level is achieved, delamination is initiated. Localized delaminations were observed in Ref. 4. If the applied compression load is sufficiently large, the delamination propagates immediately, resulting in laminate failure by buckling of the sublaminates (formed by the delaminations).

2.2.6 Euler Buckling

Euler buckling is the only mechanism of compressive failure attributed to a macroscopic, elastic instability during compression loading. This type of failure was first analyzed for isotropic materials by Leonhard Euler as a function of the material elastic properties and the specimen geometry, ignoring microstructrual details. A large thickness to length ratio in the gage section of test specimens is necessary to avoid this geometrically induced instability and thus measure the actual compressive strength of the material. Otherwise, the measured "compressive strength" is geometry dependent and not a true material property.

2.3 Compressive Failure Models

Summary papers describing the numerous compressive failure models appear to be limited. However, a few authors[23,24,26,27–30] have included detailed reviews of the existing models. Reference 29 is specifically a review of recent (1980 through August 1987) compression research on composite materials including test methods, failure theories and mechanisms, and experimental investigations. Shuart[28] includes an

historical and chronological review of proposed compression failure theories applying to the short-wavelength buckling (microbuckling) phenomenon.

In this section, mathematical theories pertaining to the failure modes described in the previous section will be thoroughly reviewed.

2.3.1 Shear and Extension Modes of Fiber Microbuckling

According to many researchers (in particular, Ref. 28), Dow and Gruntfest[31] first postulated that the compressive failure of unidirectional composites was a result of one of two phenomena: (i) high tensile stresses perpendicular to the loading direction, located at the fiber/matrix interface (so-called transverse tension failure) or (ii) buckling of the fibers within the matrix (so-called microbuckling). An equation to predict the laminate compressive strength at microbuckling was derived using Timoshenko and Gere.[32] This equation is based on a model consisting of columns supported by an elastic foundation. An empirical constant was included in this equation. Reference 31 was the first to associate fiber instability with the compressive strength of unidirectional laminates.

Rosen's classic study,[33] also referencing results from Timoshenko and Gere,[32] of the compressive failure of unidirectional composite materials focused on fiber instability in glass/epoxy laminates using a two-dimensional model. The fibers were modelled as columns supported by an elastic matrix foundation. This model assumed that the fibers were stiff relative to the matrix and that shear deformations in the fiber could be neglected relative to those in the matrix. Rosen first suggested that compressive failure of a unidirectional composite occurred when the fibers buckled in either of two possible modes, the extension mode (Fig. 1b) or the shear

mode (Fig. 1c). Using an energy formulation, Rosen obtained

$$\sigma_c = 2V_f \left[\frac{V_f E_m E_f}{3(1-V_f)}\right]^{\frac{1}{2}} \tag{1}$$

for the extension mode and

$$\sigma_c = \frac{G_m}{1-V_f} + \frac{\pi^2 V_f E_f h^2}{12\lambda^2} \tag{2}$$

for the shear mode where

σ_c = compression strength of the unidirectional composite,

V_f = fiber volume fraction,

E_m = Young's modulus of the matrix,

E_f = Young's modulus of the fiber,

G_m = shear modulus of the matrix

h = fiber diameter, and

λ = half-wavelength of the buckling mode shape.

Since the half-wavelength is much larger than the fiber diameter, i.e. $\lambda \gg h$, the magnitude of the second term in Eqn. 2 is much smaller than the magnitude of the first term. Neglecting the second term, Rosen wrote the approximate, but more familiar, relationship for the shear mode fiber microbuckling as

$$\sigma_c = \frac{G_m}{1-V_f}. \tag{3}$$

Compressive strength was predicted using the lower value from Eqns. 1 and 3. Equation 3 usually yields the more conservative compressive strength prediction for composite materials. Rosen's results for glass/epoxy showed that for low fiber volume fractions the extension mode is the lower stress, while for high volume fractions of fibers the shear mode predominates.

Rosen recognized that Eqn. 3 gave predicted strengths that were two to three times greater than the experimental strengths when the elastic shear modulus of the matrix was used. More realistic strength predictions were obtained when the matrix shear modulus was assumed to vary inelastically as a function of the applied load, from its elastic value at 1% strain to a zero value at 5% strain. It should be noted from Eqn. 3 that fiber microbuckling initiated failures are a function of the matrix shear modulus, the material property which appears to have the most significant effect on composite compressive strength.

Hayashi[34] postulated and confirmed the "shear instability mode" of compression buckling. He suggested that this type of failure occurred when the material's flexural rigidity was much larger than its shear rigidity. This concept of shear instability type failure for orthotropic materials is the same that described by Rosen[33] for composite materials. Using minimization of potential energy, Hayashi concluded that shear instability occurs for an arbitrary shear deformation when

$$\sigma_c = G \tag{4}$$

where

σ_c = compressive strength of the material and

G = shear modulus of the material.

Here, the shear modulus is a function of the applied load and usually decreases with the increase of compressive stress. According to Jones,[35] the shear modulus for a unidirectional composite material is calculated as a function of its constituent properties from

$$G_{12} = \frac{G_m}{V_f \frac{G_m}{G_f} + (1 - V_f)} \tag{5}$$

where

G_{12} = in-plane shear modulus of the unidirectional lamina, also referred to as G_{LT},

G_f = shear modulus of the fiber, and

all other variables were defined with Eqn. 2.

Since $G_m \ll G_f$ typically, the first term in the denominator may be neglected. Equation 5 is then approximated by

$$G_{12} = \frac{G_m}{1 - V_f}. \tag{6}$$

Substitution of Eqn. 6 into Eqn. 4 ($G = G_{12}$ for composite materials) yields Eqn. 3, Rosen's approximate equation for shear mode fiber microbuckling.

In a parallel study, Schuerch[36] used minimization of potential energy with assumptions similar to Rosen's[33] to also derive Eqns. 1 and 3, independent of Rosen. This analysis does assume that the shear modulus is a function of the applied strain. Schuerch showed good correlation between experiments and theory for boron/magnesium unidirectional composites. He considered these results remarkable, perhaps even fortuitous, considering the relatively crude analysis and limited experimental data.

For the extension mode of microbuckling against a plastic foundation (i.e., elastic-perfectly plastic matrix), Dow, Rosen, and Hashin[37] proposed the equation of inelastic buckling to be given by

$$\sigma_c = \left[\frac{V_f E_f \sigma_{ym}}{3(1 - V_f)}\right]^{\frac{1}{2}} \tag{7}$$

where

σ_c = compressive strength of the material,

E_f = Young's modulus of the fibers,

V_f = fiber volume fraction, and

σ_{ym} = yield stress of the matrix.

Foye[38] concluded that the instability mode of failure appeared to be the most prevalent in compression failures. Foye also proposed a macrostability model that makes no reference to the reinforcement details and, in theory, applies to all orthotropic materials. The model produced the following modified stress-strain law:

$$\tau = (G + \sigma)\gamma \tag{8}$$

where

τ = shear stress component,

σ = normal stress component,

γ = shearing strain, and

G = minimum longitudinal-transverse shear modulus.

When the direction of the tensile stress is reversed, i.e. compressive, and this stress becomes sufficiently large, the unit element would experience a complete loss of effective shear stiffness at the point where $\sigma_c = G$. Consequently, the element would be susceptible to crippling in a shearing mode as described by Eqn. 4, providing an upper bound for compression strength. Additionally, he uses the Reuss estimate or "stiffness in series" model (equivalent to Eqn. 5, Jones[35]) to show the upper bound to be the same as Eqn. 3, reported by Rosen. Foye postulated that the measured compression strengths are lower than analytical predictions due to premature failures caused by local imperfections (e.g., variations in fiber volume fraction, fiber waviness, void concentrations, and unbonded areas). Strength predictions were also modified to include void and filler contents.

Sadowski, Pu, and Hussain[39] assumed a small volume fraction of fibers so

that the mutual interference of fibers is negligible. Consequently, their model is an infinitely long single wavy fiber surrounded by an infinite matrix. The purpose of this analysis is to model the fiber instability caused by processing-induced thermal stresses. Additionally, they assumed that the fiber is subjected only to compression, but not twisting caused by the surrounding matrix. Their results predict high critical strain levels ($\approx$ 15% for $\frac{E_f}{E_m} = 5000$) and show that the same graphs are applicable for practically all values of ν, Poisson's ratio of the matrix. Additionally, the graphs indicate that including the effect of shear deformation of the fiber has a negligible effect on compressive failure strains.

Lager and June[40] used boron/epoxy (2 different matrices) to evaluate the trends of the microstability failure theory suggested in Refs. 33, 36, and 39. Their unidirectional composites were fabricated with excellent control on fiber location and volume fraction. These authors measured compression strength values approximately 63% of those predicted by Eqns. 1 and 3 using initial moduli, independent of the axial strain level. However, excellent correlations between the trends of the data and the theoretical predictions were observed. Their justification for 0.63 as an influence coefficient is that the idealized model assumes that all of the matrix material is effective in resisting buckling of the fibers. Their influence coefficient presumes the matrix material is only 63% effective.

Chung and Testa[41] applied Biot's[42] mathematical incremental deformation analysis to investigate the elastic stability of unidirectional fibers in a composite plate. Biot's analysis is modified by the following assumptions:

(i) the plate is infinitely large,

(ii) $L \gg 2h_2$,

(iii) $2h_2 \gg t$,

(iv) $\frac{E_1}{E_2} > 1$, and

(v) $\lambda \gg h_1$,

where

L = fiber length,

h_1 = fiber diameter,

$2h_2$ = fiber spacing,

t = plate thickness,

ν_2 = Poisson's ratio for the matrix,

E_1, E_2 = Young's modulus of the fiber and matrix, respectively, and

λ = fiber buckling wavelength.

The formal analysis states that the stability of an equilibrium state predicted by the equations of the classical theory of an elastic medium may be determined by considering perturbations about the equilibrium state. The equations governing the perturbations (Biot's incremental deformations) are superimposed on the initial equilibrium state (initial deformation). The solutions for sinusoidal modes of buckling is then found in the form of transcendental equations for the critical values of load and corresponding wavelengths, which can be solved numerically for fixed values of three parameters ($\frac{E_1}{E_2}$, $\frac{h_2}{h_1}$, ν_2) appearing in these equations.

Simpler expressions are obtained by introducing several approximations in the analysis. One simplification was to ignore the incremental deformation in the matrix. This formulation reduced to Rosen's[33] column on an elastic foundation analysis, Figs. 1b and 1c. Comparison of these results with the formal solution indicated that the compressive stress in the matrix has little effect on the stability of the fibers. Additionally, approximations reduced the solution to those frequently derived by energy methods (long-wavelength solution) and by considering a fiber in

an infinite medium (short-wavelength solution), e.g. Ref. 39. Experimental results for low fiber volume fraction laminates show good agreement with analytical results and show evidence of the buckling modes described in the analysis.

Guz[43] also confirmed the "shear instability mode" of failure, Eqn. 4, as the limiting value of compression. Reference 43 did not contain any experimental results or significant new ideas.

Hayashi[44] modified his previous analyses[34] for orthotropic bulk materials to unidirectional fiber-reinforced composite materials. This author proposed that failure occurs when the compressive stress in the matrix, σ_m, reaches it's shear instability limit, σ_m^*. At this point shear deformation takes place in the matrix, and the matrix loses the supporting action for the fibers. The matrix shear instability limit, rather than the fiber instability limit as described in previous analyses, is defined as

$$\sigma_m^* = G_m(\sigma_m^*) \tag{9}$$

where

σ_m^* = shear instability limit of the matrix and

$G_m(\sigma_m^*)$ = tangent shear modulus of the matrix when the stress is σ_m^*.

Using the rule of mixtures, the compressive strength of the composite is given by

$$\sigma_c = \sigma_f^* V_f + \sigma_m^*(1 - V_f) \tag{10}$$

where

σ_m^* = the stress on the matrix at which instability or yielding first occurs, Eqn. 9,

V_f = fiber volume fraction, and

σ_f^* = fiber stress corresponding to σ_m^*, the point

where matrix instability first occurs.

This analysis assumes that the strain in the fiber and the matrix are the same. The analysis is different from Schuerch[36] and Rosen,[33] Eqn. 3, by the fact that Eqn. 3 is singular for $V_f = 1$ and is different from the result in Eqn. 10. Experimental results from Lager and June[40] were compared with this analysis. Some agreement between data and analysis existed, but no explanation was suggested for irregularities between data and analysis.

Lanir and Fung[45] based their model for unidirectional composite compression strength on the assumptions that the fiber buckles inside the matrix and that both the fiber and matrix remain in the linear elastic range. These authors modelled cylindrical columns of matrix, each reinforced with a parallel, straight fiber. They consider pre-, in-situ, and postbuckling failures. In their analysis for the postbuckling range, the mode of buckling increases with increasing loads. They also concluded, that in common composites, the buckling of the fiber has no significant effect on the overall behavior of the composite in the linear elastic range. However, they predicted that fiber microbuckling significantly affects the behavior of the composite in the plastic range, particularly for high values of $\frac{E_f}{E_m}$.

Suarez, Whiteside, and Hadcock[46] appear to be the first researchers to investigate compressive failures in multidirectional laminates. They investigated the compressive strengths of multidirectional boron/epoxy laminates both theoretically and experimentally. Test specimens included coupons, honeycomb sandwich columns, and honeycomb sandwich beams. These authors modelled the composites using a beam on elastic foundation approach. They assumed that the outer ply (always 0° orientation) failed by out-of-plane fiber microbuckling, and then they treated the remainder of the laminate as an elastic foundation with both extensional and

shearing stiffness. They concluded that laminate initial waviness has a considerable effect on predicted compression strengths. Consistent assumptions of initial waviness (0.2–0.4, the ratio of waviness amplitude to lamina thickness) provided good correlation with some tests. Filament fracture and global instability were also discussed.

Hayashi and Fujikake[47] attempted to predict the ultimate compressive strength of unidirectional fiber-reinforced composites, assuming that general failure occurs by fiber buckling or fiber/matrix debonding. The critical loads were computed considering the nonlinear behavior of the matrix. The fiber microbuckling analysis presented in Ref. 47 is similar to previous analyses in that the energy method is applied. However, the analysis is unique because it is the first to consider a composite of finite size, rather than the infinite plates previously reviewed. This model is a two-dimensional, semi-infinite plate with the fiber ends simply-supported. The first fiber is considered to have a free edge, deflecting the most, and the deflections become exponentially smaller as fibers are considered from outer to inner locations. The failure strength is theoretically selected as the lower value between the fiber buckling load and the interfacial failure load. The finite size of the model leads to lower fiber buckling loads and more continuous behaviors than observed in previous analyses.

Kulkarni, Rice, and Rosen[48] investigated the compressive strength of unidirectional Kevlar 49/epoxy composites. These composites were selected because quite often their measured compressive strengths are only 20% of their tensile strengths. A unique feature that distinguishes Kevlar 49 fibers from other fibers is their anisotropy. The shear modulus is less than 2% of the axial tensile modulus of the fiber. Consequently, the fiber axial shear modulus is of the same order of

magnitude as the matrix shear modulus. Kulkarni et al,[48] using an energy approach and assuming that the buckling wavelength is much larger than the fiber diameter, derived the critical composite buckling stress for the shear mode as

$$\sigma_c = G_{12} = \frac{G_m}{1 - V_f + V_f \frac{G_m}{G_f}} \tag{11}$$

where

V_f = fiber volume fraction,

G_m = shear modulus of the matrix, and

G_f = shear modulus of the fiber.

For $\frac{G_m}{G_f} \ll 1$, Eqn. 11 reduces to Rosen's approximation in Eqn. 3. However, the expression for σ_c in Eqn. 11 is bounded for all values of V_f.

Equation 11 is identical to Eqn. 5 with $\sigma_c = G_c$, which is also the Reuss estimate of the longitudinal-transverse shear modulus, G_{LT}, of a unidirectional composite. This estimate is a "stiffness in series" model derived using rule of mixtures.

Kulkarni et al[48] modified their analysis to include the effect of an imperfect fiber/matrix bond. Equation 11 becomes

$$\sigma_c = G_m \left[\frac{1 - (1-k) V_f}{1 - \left(1 - \frac{G_m}{G_f} k\right) V_f} \right]^2 \left[1 - \left(1 - \frac{G_m}{G_f} \right) V_f \right] \tag{12}$$

where k is a bonding parameter. The bonding parameter is restricted such that

$$-\left(\frac{1 - V_f}{V_f}\right) \leq k \leq 1$$

where the limits represent no bonding and perfect bonding, respectively. Graphs presented in Ref. 48 show no quantitative conclusions but do indicate lower strengths predicted by Eqn. 12.

The most thorough investigation of the compressive strength of unidirectional composites conducted by one researcher was completed by Greszczuk in Refs. 26, 49–53. In these references, he accomplished a very systematic, but idealistic, investigation of the variables that influence the compressive strength of unidirectional composites. These studies are considered idealistic because nearly perfect model composites (straight metal rods surrounded by resin) are tested. The variables studied include specimen geometry, constituent (fiber and matrix) properties, fiber volume fraction, reinforcement shape (flat laminae or circular fibers), reinforcement size, fiber array (square, hexagonal, and arbitrary), internal imperfections (unbonded fibers, bowed fibers, misaligned fibers), and fiber end configuration.

In addition to failure by microbuckling, the following types of failure were observed: (i) compression yielding of the reinforcement, (ii) compression failure of the reinforcement (45° shear), (iii) transverse splitting of the fibers, (iv) transverse cracking of the composites, and (v) inelastic microbuckling.

An approximate micromechanics solution for interfiber stresses in unidirectional composites subjected to in-plane shear and transverse normal loadings is presented in Ref. 49. Although this investigation is not directly related to microbuckling of unidirectional composites, it does provide a foundation for other Greszczuk studies. Greszczuk's solution was shown to be sufficiently accurate for application-oriented composites (fiber volume fraction ranging between 40% and 75%). The level of accuracy is established by comparison of the results with a rigorous elasticity solution and with experimental results. The transverse and shear moduli predicted by the approximate theory also show good agreement with the values predicted by the rigorous elasticity theory.

In Ref. 26, Greszczuk compared many of the existing fiber microbuckling

analyses and showed that Rosen's[33] was the most conservative. Greszczuk's nearly perfect composite specimens were designed such that they would not fail by Euler column buckling. Greszczuk compared Rosen's shear mode microbuckling equation (Eqn. 2) with the Euler equation to derive the general relationship between σ_{Euler} and $\sigma_{microbuckling}$ as

$$\sigma_{Euler} = \left[\frac{(w/h)^2}{\frac{12G_r}{k(1-k)\pi^2 E_f}\left(\frac{L}{h}\right)^2 + 1} \right] \sigma_{microbuckling} \tag{13}$$

where

w = width of the composite specimen,

h = fiber diameter,

G_r = shear modulus of the resin,

k = fiber volume fraction,

E_f = Young's modulus of the fiber, and

L = length of the composite specimen.

Typical test-theory comparisons by Greszczuk are shown in Fig. 2. The results in Figs. 2a and 2c show that for composites reinforced with low-modulus resin, tests and theory show the same trend indicating that microbuckling is a valid failure mode. Moreover, as Young's modulus of the resin is increased significantly (from $\approx$ 2 ksi, resin A, to $\approx$ 457 ksi, resin H), the failure is independent of the length of the composite specimen and is governed by the compressive strength of the reinforcement.

Figure 2b shows very clearly that the compressive strength of the composites was found to increase with increasing resin shear modulus. Below a critical resin shear modulus, the failure was by microbuckling, and above this level, failure occurred by compression yielding of the reinforcement.

The results in Fig. 2d show that initial imperfections in the form of bowed fibers significantly reduce the microbuckling strength of composites. The author reported that other factors (misaligned fibers and unbonded fibers) were found to reduce the compressive strength of composites. For example in a composite made with a low modulus resin ($\approx$ 2.0 ksi) and aluminum rods ($k \approx 50\%$), a 5° fiber misalignment decreases the compressive microbuckling strength by 25%.

Greszczuk[50] did not observe numerous buckle waves; he stated that numerous buckle waves form in the specimen if microbuckling is in the extension mode, which requires that the reinforcement volume fraction be less than $\approx$ 5%. Additionally, Greszczuk pointed out that Rosen's[33] analysis assumes that the lamina ends are simply-supported. However, if the laminae are not simply-supported, then Eqn. 2 becomes

$$\sigma_c = \frac{G_m}{1 - V_f} + e\frac{\pi^2 E_f V_f}{12}\left(\frac{h}{\lambda}\right)^2 \tag{14}$$

where e depends on the end-fixity of the individual laminae and the variables are described with Eqn. 2. This analysis is based on Ref. 32. Consequently, when end-fixity is considered, the second term in Eqn. 14 may not be negligible, especially for nearly perfect composites. However, for graphite fibers, $\frac{h}{\lambda} \ll 1$, and the second term in Eqn. 15 will be negligible. Similar results were also presented in Refs. 52 and 53.

The authors of Refs. 30 and 54–58 also completed a very thorough investigation of the factors that affect the unidirectional compression strength and failure modes of carbon-, glass-, and Kevlar-reinforced polyester resins. The details of these results will be presented in each of the appropriate sections within this section.

Guz[59] considered a continuum and a piecewise-homogeneous medium approach to describe compressive failures in unidirectional composite materials. Both analy-

ses yielded Eqn. 4, the same result as obtained by Hayashi[34] and Guz.[43]

Gurdal and Haftka[60] recently modified Rosen's[33] beam on elastic foundation microbuckling model to include the localized shearing stresses that are either induced by the presence of a discontinuity or as a result of the externally applied loads, both for anisotropic plates with a cutout. These authors, like Rosen, also neglected the shearing deformation of the fibers and the extensional deformation of the matrix. The model is shown, for comparison, in Fig. 1d. Using an energy approach, the resulting equation for the fiber microbuckling load is

$$P_{f,c} = 2cG_m\left(1+\frac{h}{2c}\right)^2 + \frac{\pi^2}{l^2}E_f I_f \tag{15}$$

where

$P_{f,c}$ = critical fiber force,

$2c$ = matrix (foundation) width

h = fiber (beam) width

l = column length

G_m = matrix elastic shear modulus

E_f = fiber elastic Young's modulus, and

I_f = fiber first moment of inertia.

Equation 15 is similar to Rosen's (Eqn. 2); however, Rosen assumed $l \gg h$ and neglected the second term in Eqn. 2 to obtain Eqn. 3. In Ref. 60, it is assumed that $l \gg 10h$ so that the second term in Eqn. 15 significantly contributes to the critical load and may not be neglected. Additionally, this analysis allows lateral displacement of the column end, caused by the shearing stresses, prior to fiber microbuckling. While Rosen's analysis assumes the fibers are straight until the critical microbuckling load is achieved. Gurdal and Haftka assume the strength

failure criteria, rather than microbuckling instability, for the fibers of the principal load-carrying laminae. High bending stresses developed at the restrained ends (see Fig. 1d) are believed to cause the fiber breakage that leads to shear crippling. The analysis is essentially a point stress criterion, applied on a ply-by-ply basis around the cutout, that compares the resulting shear-compression coupling stresses with the fiber strength. One problem with the analysis is that the distance from the cutout or boundary to the failure point is a material constant, considered to be independent of the ply combinations and laminate stacking sequence. The fiber-kinking model predicts significant reductions in the load-carrying capacity for laminates where the 0° plies are critical. Additionally, the model predicted that rotation of the principal axis of anisotropy of the plate with respect to the loading direction caused a strength reduction under pure compression, while rotation in a direction opposite the shearing stresses (in shear compression coupling) inproved the load-carrying capacity of the plate. However, these predictions were not verified with experimental data.

Most of the fiber microbuckling models, Refs. 31–60, proposed to date are two-dimensional models in which neither initial fiber waviness, fiber/matrix debonding, nor matrix nonlinearity were considered. These idealizations have resulted in models that consistently overpredict the actual compressive strengths observed in composite materials testing. However, in Refs. 49–53, Greszczuk illustrated that these analyses were valid for ideally straight fibers with good fiber/matrix bonding. His success with the idealized composites indicates that these equations fail to predict compressive strength because they do not include the three previously mentioned.

Effects of Matrix Nonlinearity — Hayashi's and Fujikake's[47] analytical work

indicates that the compressive strength of unidirectional composite materials may be reduced as much as 50% due to the nonlinear, rather than linear, behavior of the resin.

Effects of Fiber Waviness — In earlier studies, authors[38,46] suggested that both laminate and initial fiber waviness have a considerable effect on predicted compression strengths. Hanasaki and Hasegawa[61] suggested in 1974 that the compression strength of unidirectional composites is lowered if the fibers are not straight due to their initial curvature. These authors used a moment equilibrium approach (the free body diagram contained two fibers, separated by one layer of matrix) assuming that (i) the deformation is two-dimensional, (ii) the influence of the normal strain in the matrix parallel to the fiber axis and that of Poisson's ratio may be neglected, and (iii) neither deflections nor moments exist at each end of the finite length of fibers.

From the general solution, satisfying the boundary conditions, the buckling load, and thus, compressive strength (for a straight fiber), of the composite material becomes

$$\sigma_c = \left[\frac{G_m}{(1-V)V} + \frac{\pi^2 E_f w^2}{12 l_o^2}\right]\left[V + (1-V)\frac{E_m}{E_f}\right] \tag{16}$$

where

G_m = shear modulus of the matrix,

w = width of the fibers,

W = width of the matrix,

V = $\frac{w}{W+w}$ = fiber volume fraction,

E_m, E_f = Young's modulus of the matrix and fiber, respectively, and

l_o = half-wavelength of the buckling mode.

As $\frac{l_o}{w}$ is considered to be large and $\frac{E_m}{E_f}$ small, the approximate solution obtained

is the same as that of Rosen's analysis,[33] namely Eqn. 3, for shear mode fiber microbuckling. At loads below this buckling load, assuming the initial curvature may be approximated by a sine wave, the nominal compressive stress becomes as follows:

$$\sigma' = \left[1 - \frac{a\pi}{\gamma_{max}(1-V)l + a\pi}\right]\left[\frac{G_m}{(1-V)V} + \frac{\pi^2 E_f w^2}{12l^2}\right]\left[V + (1-V)\frac{E_m}{E_f}\right] \quad (17)$$

or more simply, assuming $\frac{E_m}{E_f} \ll 1$,

$$\sigma' = \left[\frac{1}{1 + \frac{a\pi}{\gamma_{max}(1-V)l}}\right]\left[\frac{G_m}{(1-V)}\right] \quad (18)$$

where

a = amplitude of the initial curvature,

l = half-wavelength of the initial curvature, and

γ_{max}= maximum shearing strain in the matrix, and

the other variables are defined with Eqn. 16.

It should be noted that G_m is a function of γ_{max} in these equations. Additionally, when $\gamma_{max} = 0$, $\sigma' = 0$, and when γ_{max} is large, σ' (Eqn. 18) = σ_c (Eqn. 16). The compressive strength of the composite material is the maximum value of σ' at γ_{max}. At this stress level, the composite material becomes unstable elastically. Figure 3 (Ref. 61]) shows this relationship schematically. The decrease in the compressive stress at higher values of matrix shear strain is attributed to the decreasing value of G_m at higher shear strain values. Consequently, the compressive strength becomes lower than the buckling stress represented by Eqn. 16. From Eqn. 17, it may be seen that the strength depends on V, $\frac{a}{l}$, G_m, and E_m, and that the strength decrease becomes large with the increase of V and $\frac{a}{l}$.

Maewal[62] developed an analysis of the shear mode buckling as well as the initial postbuckling behavior of unidirectional composites loaded in compression.

He considered a periodically laminated medium and assumed that the constitutive equations of the two isotropic constituents are linear relationships between the Piola-Kirchoff stress of the second kind (refer to undeformed state) and the Lagrangian finite strain tensor, or equivalently, that the respective strain energy functionals are quadratic in the strain components. This theory considers only geometric nonlinearity. Maewal's analysis is different from most of the other models described in this report because it considers the instability phenomenon on the basis of continuum theory (macroscopic behavior explained disregarding molecular considerations) that includes the composite microstructure rather than a column on elastic foundation analysis. His results indicate that compressive microbuckling of the composite can occur at small strain only for those laminates where $\frac{E_f}{E_m}$ is relatively large. Additionally, his analysis of the initial postbuckling behavior suggests that the composite is not imperfection sensitive; in other words, the initial waviness of the fibers is not expected to reduce the microbuckling stress significantly. It should be noted that this result contradicts other results presented in this literature review.

Kurashige[63] also used a continuum approach, but included internal kinematical constraints of inextensibility (continuity conditions at the fiber/matrix boundary). By nature of continuum theory, a distinction between fibers and matrix does not exist. Fibers are introduced into this analysis by considering that only portions of the ends of the continuum are loaded, and thus, these portions represent the load-bearing fibers. The matrix is assumed only to transfer load to the fibers by shear at the fiber/matrix interface. Kurashige modelled the dependence of the compressive strength on fiber buckling wavelength as well as fiber volume fraction. He developed

the buckling conditions as

$$\tan\left(\frac{V_f\chi}{\zeta}\right) - \frac{(1/\chi)}{\tanh\left(\frac{1-V_f}{\zeta}\right)} = 0 \tag{19}$$

for the extension mode and

$$\tan\left(\frac{V_f\chi}{\zeta}\right) - \left(\frac{1}{\chi}\right)\tanh\left(\frac{1-V_f}{\zeta}\right) = 0 \tag{20}$$

for the shear mode where

$V_f = \frac{h}{H} =$ fiber volume fraction,

$\zeta = \frac{1}{\pi k_o}\left(\frac{l}{H}\right) =$ nondimensional buckling half-wavelength,

$\chi = \frac{k}{k_o}$,

$k = \left(\frac{p_o-\mu}{2\mu+\lambda}\right)^{\frac{1}{2}}$,

$k_o = \left(\frac{\mu}{2\mu+\lambda}\right)^{\frac{1}{2}}$,

$\mu, \lambda =$ Lamé's constants,

$h =$ fiber radius,

$H =$ matrix half-width, and

$l =$ buckling half-wavelength.

From the root of either Eqn. 19 or 20, the compressive strength, p_c is determined by

$$\frac{p_c}{\mu} = \frac{V_f}{(1+\chi^2)}. \tag{21}$$

His results are shown in Fig. 4. Additionally, Kurashige included experimental results of DeFerran and Harris[64] in Fig. 4b. The solid circles are the results for the polyester resin reinforced with hard-drawn steel wires, while the open circles for that reinforced with fully softened wires of the same steel. However, DeFerran and Harris did not include a description of the buckling wavelength in their experiment

so the theory and results cannot be compared. Figure 4a indicates that the compressive strength of unidirectional composites is an increasing function of the nondimensionalized buckling wavelength, ζ. In all cases, the shear mode appears to be more critical. However, this model predicts infinite compressive strength for the extension mode microbuckling which is not realistic. The results in Fig. 4b indicate that the compressive strength increases with increasing fiber volume fraction, but in this case, the strengths are bounded.

Kurashige[65] also analyzed the compressive strength of cross-ply composite laminates consisting of fiber-reinforced elastic layers. He assumed that the composite consisted of three types of layers: (i) axial layers that are load-bearing, incompressible, and inextensible (good approximation for $E_f \gg E_m$, (ii) cross layers that are incompressible and isotropic, and (iii) thin bonding layers made of incompressible elastic materials that connect the axial and cross layers.

Rather than using the conventional traction continuity conditions, step conditions at the layer interfaces involving singular stresses due to fiber-inextensibility were applied. The predictions indicate a sharp increase in compressive strength as the nondimensional buckling wavelength is increased from 0 to approximately 0.3, at which the compressive strength reaches a plateau. The level of this plateau was shown to decrease as the resin shear modulus decreased and/or the thickness of the resin-rich layer between the axial and cross layers increased.

Chang and Lessard[66] used energy principles to develop an analytical model to predict the fiber buckling strength of unidirectional composites. In particular, these authors wanted to understand the effect of fiber-matrix interaction due to nonuniform loading on the fiber buckling strength of these composites. The model included fiber bending energy, matrix shearing energy, and matrix extension energy

which is attributed to the interaction of the fibers and the matrix. These authors assumed that (i) the matrix does not support compressive loads, (ii) the material behaves linear elastically. Under a uniform load distribution with straight fibers, this analysis yielded Eqn. 2, Rosen's well-known buckling equation. Of particular interest, these authors considered a $[(0/90)_6]_s$ composite laminate with a center hole loaded in compression. Nonlinear finite element analysis was used to determine the normal stress distribution adjacent to the hole in the 0° plies. This analysis showed that the local stress concentration can be 1.79 times the uniaxial compressive strength before local buckling occurs. However, this analysis considers an infinite array of fibers and linear material behavior. It is possible that the local stress concentration may be considerably larger (or smaller) when the free edge effect and nonlinear material behavior are considered.

Piggott[58] developed rule of mixtures analyses to model the factors (fiber strength, matrix yield strength, degree of fiber/matrix adhesion, and degree of fiber waviness) believed to have an important influence on compression strength. Six governing equations were developed, and the actual failure stress for a given situation was determined by the failure process that operated at the lowest stress.

In Ref. 57, Martinez et al showed that the compression strength was approximately given by the expression

$$\sigma_{1cu} = \sigma_o + bR \tag{22}$$

where σ_o and b are constants and R is the minimum radius of curvature of the fibers in the region where they are kinked. These results are shown in Fig. 5.

Piggott[58] predicted the stress in a sinusoidal shaped fiber as

$$\sigma_f = \frac{2\lambda^2}{\pi^3 a}\sigma_{2m} = \frac{8R\sigma_{2m}}{\pi d} \tag{23}$$

where

d = the fiber diameter,

λ = wavelength per unit fiber length,

a = amplitude per unit fiber length,

σ_{2m} = transverse stress exerted by the fiber on the matrix,

σ_f = longitudinal stress in the fiber, and

R = minimum radius of curvature of the fiber.

Equation 23 indicates that as the composite stress is increased, σ_f will increase, and thus, σ_{2m} will increase. Unless some other failure process intervenes (e.g. fiber yielding and failure), σ_{2m} will eventually become so large that the fiber separates from the matrix on the inside of the curve, or the matrix yields, so that the fiber can push it aside. In either case, σ_f reaches some maximum value, σ_{fmax}, and the composite fails by

$$\sigma_{1cu} = \sigma_{fmax}\left(V_f + \frac{V_m E_m}{E_f}\right). \tag{24}$$

For soft matrices with perfect fiber/matrix adhesion, σ_f reaches σ_{fmax} when $\sigma_{2m} = \sigma_{my}$, the yield stress of the matrix. In this case, the compressive strength becomes

$$\sigma_{1cu} = \frac{2\lambda^2}{\pi^3 a}\left[V_f + \frac{V_m E_m}{E_f}\right]\sigma_{my}. \tag{25}$$

If $\frac{E_m}{E_f}$ is negligible, then $\sigma_{1cu} \propto \sigma_{my}$ for geometrically similar composites.

The effects of matrix nonlinearity were modelled in the analysis in Ref. 47 while the effects of fiber waviness were described in Refs. 58 and 61–66. Although including each of these effects made more realistic compression strength predictions, these analyses are still insufficient since at the limits of 0–1 for V_f they predict infinite strengths and no optimum fiber volume fraction. Consequently, both variables must be considered in one analysis.

Effects of Matrix Nonlinearity & Fiber Waviness — Davis[67] refined the previously mentioned fiber microbuckling models to include both initial fiber curvature and matrix nonlinearity. His model consisted of one fiber layer and two half-layers of matrix analyzed as a multilayered Timoshenko column in axial compression, permitting both bending and shearing deformations in each layer. He measured the initial fiber curvature in a boron/epoxy composite. The ratio of the initial amplitude of the waviness to the length of the wave, $\frac{a_o}{L}$, was measured to range from 0.001875 to 0.003750. Additionally, using compression/torsion tests, Davis observed that the apparent shear modulus $(G - \sigma)$ decreases as the axial compressive stress σ increases. However, it should be noted that no analytical effort was made to explicitly establish this relationship. Using an energy methods approach, Davis predicted interlaminar shear stresses and the onset of shear instability, which compares with Eqn. 4. These experimental and analytical results are summarized in Fig. 6. These results clearly indicate that fiber waviness causes the composite to behave like it has a reduced shear modulus. Consequently, neglecting fiber waviness effects causes much larger compressive strength predictions than observed experimentally.

From his energy analysis, Davis showed that small initial deflections, on the order of those measured experimentally, reduce the axial compressive stress at which shear instability is expected to occur from approximately 9.308 GPa to approximately 3.275 GPa. Within the region bounded by $0.001875 \leq \frac{a_o}{L} \leq 0.003750$, the maximum computed interlaminar shear stress was approximately 75,842 MPa, which is less than the interlaminar strength of the boron-epoxy composite and indicates that failure was due to shear instability and not delamination. Neglecting the initial curvature of the fibers (assuming $\frac{a_o}{L} = 0$ in Fig. 6), as assumed in Refs. 33 and 38 leads to significantly higher compression strength predictions than measured

experimentally.

It should be noted that graphite fibers have a lower modulus and are more slender than boron fibers; thus, graphite fibers have a lower stiffness. The consequence of this comparison is that graphite fibers will have larger initial fiber curvature, and thus, greater strength reductions than that measured by Davis[67] for boron.

Wang[68,69] used a moment equilibrium approach, assuming an initial fiber curvature and a nonlinear in-plane shear stress-strain relationship, to predict the compressive strength of graphite/epoxy unidirectional composites. Two additional assumptions in his analysis are quoted as follows:

(i) that an application of an incremental compressive load amplifies the deflection of the fibers which causes a rise in the in-plane shear stress; due to the nonlinear shear behavior, a rise of the shear stress decreases the shear stiffness, which in turn induces additional fiber deflection under the same compressive load; and

(ii) that compression failure of the composite occurs at the applied load which causes an unstable increase in the fiber deflection, or an excessive increase in the in-plane shear stress.

His analysis yielded

$$\tau_{LT} \approx \left[\frac{\pi G_{LT}\sigma_c}{G_{LT} - \sigma_c}\right] \frac{f_o}{l} \tag{26}$$

where

τ_{LT} = in-plane shear stress of the composite,

G_{LT} = in-plane shear modulus of the composite,

σ_c = applied uniform compressive stress,

f_o = amplitude of the initial fiber deflection (not

infinitesimal in this analysis), and

l = half-wavelength of the deflection.

The incremental increase in composite shear stress, $\Delta\tau_{LT}$, with increasing applied compressive stress, $\Delta\sigma_c$, is determined by differentiating Eqn. 26 to obtain

$$\Delta\tau_{LT} \approx \left[\frac{\pi\overline{G}_{LT}^2}{\left(\overline{G}_{LT}-\sigma_c\right)^2}\right]\frac{f_o}{l}\Delta\sigma_c \tag{27}$$

where

$\overline{G}_{LT}$= tangential shear modulus (local slope) of the composite.

Equation 27 is an approximation for the composite shear stress-strain curve using piece-wise linear segments. As shown in Fig. 7, successive increases in the composite compressive stress causes increases in the calculated shear stress. The composite shear stress-strain relationship was approximated using the method proposed by Petit,[70] utilized by Rosen,[71] and compared by Hahn.[72] In the limit, the shear stiffness of the composite approaches zero resulting in shear mode microbuckling. Figure 8 is a hypothetical graph of σ_c versus $\frac{f(\sigma_c)}{F_o}$ where $f(\sigma_c)$ is the amplitude of fiber deflection at the applied stress. Figure 8 schematically shows this increase in compressive stress (modelled by Eqn. 27) approaching an asymptotic limiting value, which is the compressive strength of the composite for failure by shear microbuckling.

In order to determine $\frac{f_o}{l}$ for the composite, the ultimate σ_c for the unidirectional composite was measured experimentally. Next, a value for $\frac{f_o}{l}$ was selected by trial-and-error such that the predicted σ_c agreed with the experimental σ_c. This value of $\frac{f_o}{l}$ then became a material property of the composite system, regardless of the test conditions. Wang determined $\frac{f_o}{l}$ to be 0.0108 for these carbon fibers. As expected, this value is larger than that for boron since the carbon fibers are

more compliant. This pseudo-empirical parameter, which should be independent of temperature, was used to predict the compressive strength over a range of temperatures. The changes in the predicted compressive strength at higher temperatures were then attributed to the shear stress-strain behavior of the composite. His analytical results were in good agreement with the experimentally measured strengths.

Shuart[28,73] investigated compressive failures in multidirectional composite laminates. In Ref. 28 Shuart studied the short-wavelength buckling of multidirectional composite laminates. In this analysis, the fibers are modelled as an infinite plate supported by matrix material which is treated as an elastic foundation. A laminate then consists of a series of plates and elastic foundations. A linear analysis is derived to determine the short-wavelength buckling response of composite laminates. This analysis was then generalized to a nonlinear analysis to include laminate short-wavelength initial imperfections. Two shearing mechanisms expected to initiate failure were analyzed. These mechanisms were interlaminar shearing caused by initial waviness of the plies (geometrically nonlinear behavior) and in-plane matrix shearing. The in-plane matrix shearing failure mode occurs in angle plies at the fiber/matrix interface and/or in the epoxy matrix between the fibers.[74] In-plane shear stresses parallel to the fiber/matrix interface cause this failure mode. These shear stresses may be a function of both fiber waviness and fiber scissoring. However, this analysis was not verified experimentally.

In Ref. 73, Shuart improved the analysis of Ref. 28 by adding the matrix compression failure mode and allowing the in-plane matrix shearing mechanism to include effects from in-plane fiber waviness and fiber scissoring. Matrix nonlinearity is introduced into the analysis in the fiber scissoring analysis. Fiber scissoring is idealized as a simply supported beam on a nonlinear foundation. Because it

possesses only shear stiffness, the foundation is modelled as a nonlinear shear spring. This stiffness is obtained from the material's shear stress-strain behavior using the method described in Ref. 71. The laminate compressive strength as a function of ply orientation is shown in Fig. 9 for $[\pm\theta]_s$-class AS4/3502 laminates. The analysis results predict that interlaminar shearing initiates laminate failure for $0° \leq \theta \leq 15°$, that in-plane matrix shearing (longitudinal splitting) initiates laminate failure for $15° \leq \theta \leq 50°$, and that matrix compression initiates laminate failure for $50° \leq \theta \leq 90°$. Experimental results are also included in Fig. 9. Comparison of the analytical and experimental results show reasonable agreement for $\theta < 45°$ and show excellent agreement for $\theta \geq 45°$.

Chang, Lessard, and Tang[75] performed an analytical and experimental investigation to study the in-plane failure of laminated multidirectional composites containing an open hole and subjected to compressive loadings. The progressive damage model consists of a stress analysis and a failure analysis. Stresses and strains in the plates were calculated by a nonlinear finite element analysis, which is based on finite deformation theory with consideration of both material and geometric (fiber waviness) nonlinearities. A plane stress condition was assumed for the analysis.

The types and size of damage were predicted by a proposed failure analysis which includes a set of proposed failure criteria and property degradation models for each mode of failure. Matrix cracking, fiber-matrix shearing, and fiber buckling (kinking) were the three basic failure modes considered in this investigation.

Basically, stresses and strains are calculated at each incremental displacement step, and these stresses are evaluated by the failure criteria to determine the occurence and mode of failure. Mechanical properties in the damaged area are reduced appropriately according to the property degradation models. Stresses and

strains are then recalculated to determine any additional damage as a result of stress redistributions at the same load. This procedure continues until no additional damage is found, and the next displacement increment is then pursued. The final collapse load is determined when the plate cannot sustain any additional load. Details of the failure analysis and experiments are given in Refs. 76 and 77, respectively.

Typical results from this analysis are shown in Fig. 10. Figure 10a shows an enhanced X-radiograph of a $[(0/90)_6]_s$ specimen before and after a test to 90% of failure. From this figure, it is clear that initial damage existed inside the specimen near the hole boundary before the test. The authors suspect this damage was an artifact of the drilling methods. The load-displacement data for two $[(0/90)_6]_s$ specimens are shown in Fig. 10b in addition to the analytical prediction. An excellent agreement was found between the calculations and the data.

Typical model predictions of damage types and sizes are presented in Fig. 10c at different load levels. The model predicted fiber/matrix shearing initiated from the hole boundary near the stress concentration, and then propagated along the loading direction (parallel to the 0° fibers). Fiber buckling (kinking) was predicted at a load of about 6000 lbs in 0° plies and grew in the direction normal to its fiber direction.

Davis and Highsmith[78,79] extended Lee[80] to incorporate material nonlinearity and compression loading. Lee[80] modelled fiber curvature with an infinite array of columns on elastic foundations under tensile loading. The analysis in Refs. 78 and 79 incorporates a closed-form solution for G_{12}, obtained from a curve fit through the shear stress-strain data.

Hahn and Williams[23] developed a nonlinear model including fiber curvature

and matrix material nonlinearity to predict the compression strength of unidirectional composites. This analysis used a free body diagram of only one fiber and assumed that the local shear stress-strain behavior was linear. In reality, this linear behavior is not expected. The compressive strength is predicted by

$$\sigma_c = V_f G_{LT} \frac{1}{1 + \frac{\pi f_o}{l \gamma_{LT}}} \tag{28}$$

where

V_f = fiber volume fraction,

γ_{LT} = composite shear strain,

G_{LT} = composite shear modulus, approximated as the secant modulus at a given γ_{LT},

f_o = amplitude of the initial fiber curvature, and

l = buckle half-wavelength.

If no initial curvature is assumed (i.e., $\frac{f_o}{l} = 0$) then

$$\sigma_c = V_f G_{LT}. \tag{29}$$

When G_{LT} is approximated by $\frac{G_m}{1-V_f}$ (Eqn. 6), Eqn. 29 is different from Eqn. 3 by the factor V_f. The difference derives from the selection of the free body. Rosen[33] used a fiber surrounded by matrix in his free body diagram. Since Eqn. 3 is known to overpredict the strength and because applying the equilibrium forces and moments to the fiber is a reasonable model, Hahn and Williams prefer Eqn. 29 over Eqn. 3.

If a bilinear shear stress-strain relation showing elastic-perfectly plastic behavior is assumed, then the compression strength becomes

$$\sigma_c^* = V_f G_{LT} \frac{1}{1 + \frac{\pi f_o}{l \gamma_y}} \tag{30}$$

where

γ_y = shear yield strain of the composite and

the other variables are defined with Eqn. 28. Equation 30 assumes that the matrix yields at γ_y and no additional shear stress may be supported. Consequently, yielding spreads over the entire length of the buckled fiber, changing the deformed configuration to the form of kinking. This change from microbuckling to kinking occurs with very little increase in the applied load.

Equation 30 indicates that the higher G_{LT} and γ_y, the stronger the composite in compression. However, a weak fiber/matrix interface will reduce γ_y, and possibly G_{LT}, and cause a reduced compressive strength.

It should be noted that this result is very similar to that obtained by Hanasaki and Hasegawa.[61] The results of Ref. 61 are given in Eqns. 16–18. To show that these results are similar, refer to Eqn. 30 and let

$$V_f = V,$$

$$\gamma_y = \gamma_{max}\,(1 - V)\,,$$

$$G_{LT} = \frac{G_m}{1 - V},$$

and

$$f_o = a.$$

Thus, the result of Hanasaki and Hasegawa (Eqn. 18), except for the V_f in the numerator of Eqn. 30 is obtained. Again, the factor of V_f appears because of the selection of the free body diagram.

The effect of fiber waviness is to give significantly larger shear stresses (and thus, shear strains) for a given axial compressive stress level. Consequently,

the composite reaches its shear instability limit at a lower applied stress level. Unfortunately, the incremental nature of the calculations used to determine this stress level does not allow the compressive strength to be expressed as a simple function of the initial fiber curvature. It is clear that the stress level at which nonlinear shear stress-strain behavior begins directly influences the compressive strength of the composite. Finally, fiber/matrix debonding causes this nonlinear behavior to initiate at an even lower applied stress level, resulting in a further reduced compressive strength.

2.3.2 Fiber Shear

Collings[81] investigated the transverse compressive behavior of unidirectional carbon/epoxy composites. In these tests, failure occurred by interlaminar shear and was limited by the strength of the fiber/matrix interfacial bond. However, when the specimen was constrained laterally (to prevent interlaminar shear), failure was by fiber shear, and the failure stresses were very close (within 8%) to longitudinal compressive strengths for the same material. Based on these results, Collings concluded that the shear strength of the fiber is much less than that of the resin and the fiber/matrix interfacial bond.

Hancox[82] suggested that since the buckling and instability models developed to date (1975) did not accurately predict the compression strength of unidirectional composites and similarities were observed between compression and tensile strengths, the compression strength of a composite must be governed by the same mechanism as the tensile strength, an inherent property of the fiber. It has been suggested in Ref. 25 that this failure mode constitutes an upper bound for compression strength.

Greszczuk[53] suggested that when a unidirectional composite specimen is loaded

to a stress level where fiber failure occurs by shear (rather than microbuckling) of the fiber, the compressive strength may be predicted by the following rule of mixtures relationship,

$$\sigma_c = F_f k + \sigma_r^* (1 - k) \tag{31}$$

where

F_f = compressive strength of the fiber,

k = fiber volume fraction, and

σ_r^* = compressive stress in the resin at failure, computed as the product of the resin modulus and the fiber failure strain, $E_m \epsilon_f$.

This type of compressive strength is only realized in practice when the composite has a relatively stiff matrix and a good interfacial bond to prevent premature failure by fiber microbuckling or longitudinal splitting.

Ewins and Ham[25] investigated the longitudinal and constrained transverse compression strengths of unidirectional graphite/epoxy composites. They proposed, based on their results, that if no other potential failure mode occurs at a lower stress, failure will occur by shear across the fibers and the matrix on a plane of near maximum shear stress. Assuming that the matrix carries only a small portion of shear load, the composite compressive strength will be limited primarily by the shear strength of the fibers. However, at approximately 100°C the failure mode changed from fiber shear to fiber microbuckling, probably due to the reduced matrix shear modulus and the change in the constitutive behavior of the resin.

2.3.3 Longitudinal Splitting

Even though the induced tensile stresses at the fiber/matrix boundary are small

compared to the applied axial compressive stresses, the transverse tensile strength is also small compared to the axial compressive strength. Thus, it is possible for the induced transverse tensile stresses to cause fiber/matrix debonding leading to longitudinal splitting (an interaction failure) and a reduction in the ultimate compression strength.

Kim[83] investigated the static strength of graphite/epoxy off-axis and angle-ply laminates under uniaxial tension and compression. Experimental data were compared with the Tsai-Wu tensor polynomial failure criterion. Both theory and experiment show greater strength in compression than in tension for these laminates. This phenomenon is explained by considering that the transverse strength in compression is four times greater than that in tension for this material system. The agreement between theory and experiment is very good except for angles smaller than $\pm 15°$. To understand this behavior, the state of stress within the angle-ply laminate was examined. When uniaxial compression is applied to the specimen, σ_1 is compressive for all angles while σ_2 changes from tension to compression at approximately 40°. Whole fiber tow breaks, sheared matrix, and cleavage indicate that all three stress components appear to play a significant role in the failure (longitudinal splitting) of these specimens.

Greszczuk[51] predicted the transverse tensile strength of glass/epoxy, graphite/epoxy, and graphite/phenolic composites using constituent properties and microstructure of the composite. The important aspect of this work is that the analysis accounts for the internal triaxial stress concentrations caused by fibers and voids individually, the interaction of stress concentrations from fibers and voids, and the volume fraction of ineffective or unbonded fibers. Good correlation between predicted and measured compressive strengths were observed.

Greszczuk[53] estimated the compressive strength of interaction failures by

$$F_{LC}^{*} \approx \frac{F_{LC} F_{Tt}}{F_{Tt} - K F_{LC}} \tag{32}$$

where

$$K \approx -\left(k - \sqrt{\frac{4k}{\pi}}\right)(\nu_f - \nu_r)\frac{E_T}{E_L} \tag{33}$$

and

ν_f, ν_r = Poisson's ratios of the fibers and matrix, respectively,

E_L, E_T = Young's moduli of the composite in the longitudinal and transverse directions,

F_{Tt} = transverse tensile strength of the composite, and

F_{LC} = longitudinal compressive strength of the composite, calculated according to the rule of mixtures, Eqn. 31.

It should be noted that a weak transverse tensile strength (e.g., a poor fiber/matrix interface) yields a compressive failure strength that is much lower than that for fiber shear controlled failure. On the other hand, a very strong transverse tensile strength causes Eqn. 32 to give a result identical to Eqn. 31 in the limit.

Broutman[24] developed an alternative expression for the compression strength of a composite that fails by longitudinal splitting. He concluded that

$$\sigma_c = \frac{(E_f V_f + E_m V_m)\left(1 - V_f^{\frac{1}{3}}\right)}{\nu_f V_f + \nu_m V_m}\epsilon_{mu} \tag{34}$$

where

E_f, E_m = Young's moduli of the fibers and the matrix, respectively,

ν_f, ν_m = Poisson's ratios of the fibers and the matrix, respectively,

V_f, V_m = fiber and matrix volume fractions, respectively, and

ϵ_{mu} = ultimate strain of the matrix, measured from a tensile test of the neat resin.

In Eqn. 34, compressive failure is assumed to occur when the transverse strain reaches the level required for failure in a transverse tensile test.

Broutman's[24] analysis implies that compression failure occurs by longitudinal splitting resulting from the Poisson's expansion in the transverse direction. However, when the specimen is rigidly supported by the grips, each end of the specimen is constrained. Consequently, the transverse tensile stresses leading to failure may be induced by constraint rather than by the Poisson's contraction difference, as assumed by Greszczuk.[53] A comparison of Broutman's predictions against Rosen's[33] predictions is shown in Fig. 11.

Piggott's[58] results showed that for stiff matrices failure occurred by splitting, rather than the controlled fiber kinking, though some kinking accompanied the splitting.[54] Even when the fibers are straight, transverse tensile stresses are present. An estimate of the stress at the fiber/matrix interface is given as

$$\sigma_r = \sigma_{1m}\left(\nu_m - \nu_f\right)\left(0.48 + 0.52V_f - 12V_f^2\right) \tag{35}$$

where ν_m and ν_f are the Poisson's ratios of the matrix and the fibers.

However, large tensile stresses can be introduced by curved fibers, and these stresses can lead to failure of the bond, especially when the fiber/matrix adhesion is poor. Piggott suggested that three distinct strengths are involved in splitting behavior, as shown in Fig. 12. In addition to the adhesive strength, σ_a, the cohesive strength of the matrix, σ_{mtu}, and the compressive strength of the matrix, σ_{mcu} (or the yield strength, σ_{my}) are involved. The ultimate compression strength for

composites made with hard matrices is given by

$$\sigma_{1cu} = \frac{8R}{\pi d}\left(V_f + \frac{V_m E_m}{E_f}\right)\sigma_{mcu} \tag{36}$$

where

R = fiber radius of curvature,

d = fiber diameter,

V_m, V_f = matrix and fiber volume fractions, respectively, and

E_m, E_f = Young's moduli of the matrix and fibers respectively.

The lines for transverse compression failure, shown in Fig. 13, were plotted using Eqn. 36.

Piggott[58] predicted that for debonding to occur, the stress must overcome the matrix cohesive strength, σ_{mtu}, in the webs of the fibers (see Fig. 12). In this case the composite strength is predicted by

$$\sigma_{1cu} = \frac{4R}{\pi d}\left\{\pi\sigma_a + \left[\left(\frac{P_f}{V_f}\right)^{\frac{1}{4}} - 2\right]\sigma_{mtu}\right\}\left\{V_f + \frac{V_m E_m}{E_f}\right\} \tag{37}$$

where P_f is the packing factor, equal to $\frac{2\pi}{\sqrt{3}}$ for hexagonal packing and π for square packing and the other variables are defined with Eqn. 36. The curves for splitting failure in Fig. 13 were plotted using Eqn. 37. Figure 13 shows the conbined effects of adhesion and fiber volume fraction. Strong nonlinear V_f effects are predicted in this plot. This figure indicates that transverse compression failure (i.e. the sideways push of the fibers will exceed σ_{mcu}) controls the strength over a range of V_f until this line intersects the appropriate adhesion line and then fiber/matrix debonding controls failure.

In summary, a weak interface, attributed to poor fiber/matrix adhesion may result in a low transverse tensile strength.[24,51,58] This strength reduction, in turn,

may give a lower compressive strength if failure is due to longitudinal splitting caused by interaction effects resulting from secondary transverse tensile stresses. A weak interface combined with secondary transverse tensile stresses may also yield a local interfacial failure which may eventually precipitate other types of failure such as fiber microbuckling or delamination.

2.3.4 Micromechanics & Damage Approaches to Compression Strength

Fried,[84] Fried and Kaminetsky,[85] and Fried[86] studied the influence of the matrix, the reinforcement, and matrix/reinforcement interface on compressive failure. Experimental results for unidirectional laminates (steel, glass, and glass roving fibers embedded in a polyester resin) led Fried to suggest the following failure sequence. The reinforcement phase in a composite material carries the compressive load until the rigid matrix phase yields; upon yielding, the matrix flows and no longer provides support for the reinforcement. Consequently, the reinforcement buckles and the composite laminate fails catastrophically. From a micromechanics (rule of mixtures) type approach, the ultimate strength of the composite was expressed as the following linear function of the matrix yield stress

$$S_{cu} = S_{ry}\left(R + G\frac{E_g}{E_r}\right) \tag{38}$$

where

S_{cu} = ultimate strength of the composite,

S_{ry} = composite stress at yield,

R = volume fraction of resin,

G = volume fraction of glass,

E_g = Young's modulus for the glass fiber, and

E_r = Young's modulus for the resin.

This model assumes that (i) the maximum stress in the matrix is its yield stress and that (ii) the strain in the matrix is the same as the strain in the reinforcement. Equation 38 was not valid for the steel reinforcement, probably due to high ductility of steel compared to glass.

Budiansky[87] completed a brief survey of the current theoretical studies in the area of micromechanics — the mechanics of very small things. Topics discussed include void collapse in metals, transformation toughening in ceramics, fiber kinking in composite materials, and thermoelastic dissipation in rocks. Of particular interest to this review is fiber kinking in composite materials, which will be discussed in the appropriate section within this section.

2.3.5 Euler Buckling

Chou and Kelly[88] used results from Timoshenko and Gere[32] with corrections for shear deformation to predict the compressive stress required to give macroscopic buckling.

The Euler buckling equation without shear deformation corrections is

$$P_e = \frac{cE_cI}{l^2} \tag{39}$$

where

P_e = critical Euler buckling load,

E_c = Young's modulus for compression,

I = moment of inertia,

l = column length, and

c = a constant determined by the end constraints of the specimen.

For the idealized end conditions,

c = 2.47 for clamped-free,

c = 9.87 for hinged-hinged, and

c = 20.2 for clamped-hinged.

In highly anisotropic materials such as unidirectional composites, the Euler buckling predictions without shear deformation corrections (Eqn. 39) overestimate the critical Euler buckling load. The additional deflections occur because of the relatively low ratio of shear to axial modulus (≈ 0.04 for composites compared to ≈ 0.31 for metals). This effect may cause another significant reduction in the Euler buckling load (typically by a factor of 4). A suitable correction factor for the low shear stiffness must be applied. The corrected critical load including shear deformation is given by

$$P_{cr} = \frac{P_e}{\left(1 + \frac{nP_e}{AG_c}\right)} \tag{40}$$

where

n = a numerical factor:

1.2 for rectangular cross-sections and

1.11 for circular cross-sections,

A = cross-sectional area,

G = composite shear modulus, and

P_e = Euler buckling load, Eqn. 39.

The critical compressive stress of the column is then given by

$$\frac{\frac{cE_c}{(l/r)^2}}{1 + \left[\frac{cnE_c}{(l/r)^2 G_c}\right]} \tag{41}$$

where

$r = \sqrt{\frac{I}{A}}$ = radius of gyration

and the other variables were defined with Eqns. 39 and 40.

Equation 41 can be simplified by considering the limiting case where

$$\frac{cnE_c}{\left(\frac{l}{r}\right)^2 G_c} \gg 1. \tag{42}$$

This condition is achieved in highly anisotropic composites where $\frac{E_c}{G_c} \gg 1$. Additionally, the condition in Eqn. 42 is obtained for relatively short specimens where $\frac{l}{r}$ is small so that the tendency for Euler buckling is also small. Under the condition of Eqn. 42,

$$\sigma_{cr} = \frac{G_c}{n}. \tag{43}$$

Equation 43, apart form the factor $\frac{1}{n}$, is the same as Eqn. 4, which assumes the composite fails in the shear instability mode.

Additionally, Chou and Kelly[88] used Eqn. 39 to determine c values of 3.34 and 16.14 for the IITRI and RAE specimens, respectively, both of which are described in the Compression Test Methods section within this section.

Wilkinson, Parry, and Wronski[89] investigated the mechanical properties of fiber-harness sateen (weft- or transverse-faced) and plain weave graphite/epoxy cloths over a range of gage lengths. Euler buckling analysis was found to be applicable for gage lengths in excess of $\approx$ 15 mm. The column was the specimen in the case of the sateen weave laminates and the longitudinal (warp) bundles in the plain weave laminates. The failure process involved bundle detachment and kinking, similar to the mechanism operating in nominally uniaxially aligned fibrous composites. Their observations indicate that the surface bundles detach and delaminate.

Lee[90] presented an equation similar to Chou and Kelly.[88] Additionally, he stresses the importance of axial alignment; misalignment introduces a bending moment causing strain divergence on either face. He reported results that an

eccentricity of 2.5% of the laminate thickness (0.095 mm for a 30-ply, 3.81 mm, laminate) reduces the apparent strength to 87% of the ultimate value.

To summarize, the strength predicted by Euler buckling corrected for shear deformation should be considered an upper limit for the compressive strength that can be experimentally measured for a given specimen of thickness, t, and column or gage length, l. In practice, one would expect to see compressive failures at lower stress levels than those predicted for Euler buckling unless specimens with long thin gage sections are used.

2.3.6 Related Studies

Whitney and Nuismer[91] developed two stress fracture criteria for tensile loaded composite laminates containing stress concentrations (circular holes and straight center cracks). These criteria[91] are based on two parameters (unnotched tensile strength, σ_o and a characteristic dimension), but do not require Linear Elastic Fracture Mechanics (LEFM). One criterion (Point Stress Criterion) assumes that failure occurs when the stress at a characteristic distance, d_o, from the discontinuity reaches the tensile strength σ_o of the unnotched material, while the other criterion (Average Stress Criterion) assumes that failure occurs when the average stress over some characteristic distance, a_o, reaches the unnotched tensile strength. These criteria were subjected to further experimental scrutiny by Nuismer and Whitney.[92] However, due to large scatter in the data, no conclusive statement concerning the accuracy of the models was presented. Although Whitney and Nuismer assumed the characteristic distances to be a material property independent of laminate geometry and stress distribution, it should be noted that these adjustable parameters have not yet been related to microstructural features and do not result from a mechanics analysis. In 1979, Nuismer[93] extended the average stress failure criterion to

compression applications for countersunk fastener holes (both loaded and unloaded), with acceptable agreement between experimental data and theoretical predictions. However, again, no conclusive statements about the accuracy of the models were made.

Reifsnider, Stinchcomb, Bakis, and Yih[94] investigated the mechanics of the damage development process of notched composite laminates. The three aspects addressed include the local mechanics associated with the damage development sequence, global changes in the stress state near the notch that relax the stress concentration, and the mechanics associated with the residual strength after damage has occurred.

Two multidirectional graphite/epoxy laminates were used to investigate the fatigue response of notched composite laminates under fully reversed ($R = -1$) cyclic loads. The earliest damage detected in the specimens was matrix cracking parallel to the fibers in the vicinity of the stress concentration. In regions with dense matrix cracks in two adjoining plies, small delaminations initiated, grew, and coalesced along the matrix cracks, particularly where two cracks of different orientation cross. These authors observed that delaminations generally initiate the earliest and propagate the fastest at interfaces nearest to the surface of the laminate, although they eventually appear in a similar fashion at all like interfaces through the laminate thickness. Additionally, they observed that laminate failure in all graphite/epoxy, low-amplitude cycled specimens was by compressive failure of the interior 0° plies after delaminations reduced the support provided by adjacent plies. Finally, they concluded that the residual compressive strength appears to be much more sensitive to damage development around a hole (or notch) than the residual tensile strength.

Renault, Valentin, Perez[95] investigated multidirectional notched graphite/epoxy laminates loaded in tension. Many of the results in this study are similar to those reported in Ref. 94. Macroscopic damage observed prior to final failure included matrix cracks parallel to the fibers and delaminations near the stress concentrator. A reduction of failure stress, described by Whitney and Nuismer[91,92] for some layups, was observed when the damage extended form the hole. A similar result was observed by Guynn[1] for compressive loading. Additionally, like Guynn[1] and Reifsnider et al,[94] these authors observed that the presence of significant damage, in the vicinity of the hole, contributed to modify the stress distributions and diminishes the stress concentrations near the hole. They propose that including these stress reductions in failure prediction models should improve the accuracy of these models.

Guz and Lapusta[96] assumed three-dimensional linearized theory for a piecewise-homogeneous medium to investigate the stability of a fiber in an elastic compressible matrix near a free cylindrical surface under small precritical deformations. The authors reference other uses of this method for similar stability problems: one fiber, two fibers, an infinite series, adouble-periodic system of fibers in an infinite matrix, a fiber near a free plane surface, and also a fiber near a free cylindrical surface under finite deformations. However these references are not readily obtainable in the United States. Their results indicate that as the fiber gets farther from the free surface the critical buckling strain approaches that for a fiber in an infinite matrix. Although the fiber in a semi-infinite matrix followed the same trend, the critical strains were as much as 20% lower than those for this cylindrical model.

Burns, Herakovich, and Williams[97] used linear three-dimensional finite element analysis and the tensor polynomial failure criterion (Tsai-Wu) to predict that failure always initiates at the $[\pm\theta]]$ interface at the hole edge for notched angle-ply laminates

loaded in compression. The angular location, around the hole edge, of initial failure was shown to be a function of θ, the fiber orientation of the lamina. The dominating stress components initiating failure are the shear stresses τ_{12} and τ_{23}.

Lee[80] used Euler-Bernoulli beam theory to develop an analysis for predicting the influence of wavy patterns in the main load-carrying layers or wrinkled fibers on the laminate behavior under tensile loading. This analysis assumed linear material behavior. The main load-carrying layers or wrinkled fibers were assumed to be corrugated beams embedded in elastic foundations of various spring constants. Young's moduli for the different laminate configurations were determined experimentally and compared to the model predictions. The model predictions were in close agreement with the present experimental results including both extensometer measurements and moiré interferometry fringe pattern analysis. Furthermore, experimental results reported by other researchers were compared with this analysis showed reasonable agreement.

2.4 Microbuckling and Kinking

Pattnaik, Koczak, and Rogers[98] studied the failure mechanisms of unidirectional metal matrix composite (MMC) cylinders loaded in compression. The normal mode of compression failure of these composites appeared to be kinking or multiple kinking, both in-plane and out-of-plane. The formation of kink bands are shown schematically in Fig. 14. Figure 14d shows the kink inclination, α, and boundary orientation, β, for both an in-plane and an out-of-plane simple kink. These authors postulate that the range of values for α and β will be a function of the post-failure deformation of the kink band, as shown in the graph in Fig. 15. Unlike graphite/epoxy composites, very few voids or delaminations were observed in

these composites because the matrix is a ductile aluminum alloy. The voids created by fiber cracking are filled by metal flow under the high compressive stresses. However, the presence of voids, fiber waviness, and possible fiber/matrix debonding yielded compressive strength values much lower than those predicted by the existing theories of compression failure.

Chaplin[99] observed and characterized the shear deformation in unidirectional glass-reinforced composites as an "elastic instability." It is therefore not determined by strength considerations, but involves shear instability in a volume of material, not failure on a plane due to a resolved stress. The author's argument is dependent on the assumption that as the shear deformation increases, the angle of the band and the length of the fibers in the band do not change. Chaplin showed that the angle $\alpha = 2\beta$ if no volume change was assumed within the kink band. Experimental results for notched compression specimens showed some difficulty was experienced in controlling the fracture to give stable damage propagation. A strong tendency existed for interlaminar shear failures to propagate from the tip of the notch. Chaplin concluded that the mechanisms of energy absorption are readily identifiable as matrix shear and interfacial failure. The difficulty lies in making allowance for load carried by the shear band after failure. Additionally, Chaplin argued that in the presence of a hydrostatic stress component, the expected effect would be an increase in compressive strength.

Parry and Wronski[100]studied the mechanisms of deformation and failure of carbon fiber-reinforced composites tested in three-point flexure. They observed a significant increase in acoustic output at the onset of nonlinear behavior on the load-deflection plot. Subsequent microscopic observations showed that the failure was initiated by fiber kinking near the compression roller. Kink growth with

decreasing load, increasing deflection, and accompanying stress resistribution led to either flexural or interlaminar failure. In the latter, the growing kink initiated interlaminar cracks in resin-rich zones. These delaminations were not confined to the neutral plane. Finally, they suggested that kink initiation, involving microbuckling of fibers and shear of the matrix, should be associated with the onset of nonlinear deformation.

Parry and Wronski[101] investigated kinking and compressive failure in unidirectional carbon fiber-reinforced composites. Based on their results, they suggested that a local surface condition initiates the first buckling and breakage of a group of fibers, which acts as the kink band. This kink band propagates by the buckling and failure of fiber groups ahead of it. Additionally, they concluded that the compressive strength properties are related to the strength, ductility, and toughness of the resin rather than its modulus.

Wronski and Parry[102] evaluated the compressive failure and kinking in unidirectional glass-reinforced composites (GRC). Because the failures were catastrophic, it was difficult to estimate the size of the microstructural unit (bundle of fibers) which initially kinked. They postulated that even for straight fibers the role of the matrix and its effect on fiber microbuckling must be considered. According to these authors, the buckling causes lateral displacement of the fiber bundles and causes pushing against the support of the matrix. If failure is initiated when the matrix support is lost locally (i.e. matrix yielding), continued loading causes localized gross deformation leading to longitudinal splitting along the bundle boundary. Based on this observation, Wronski and Parry believed that d (Eqn. 23) should be the bundle rather than fiber diameter. Additionally, they concluded that bundle buckling controlled the compressive strength of GRP unless the matrix yield strength was

very high.

In Refs. 100–102, Parry and Wronski observed that in the presence of a superposed hydrostatic pressure, the compressive strength of unidirectional composites is increased. Parry and Wronski[100] observed that the hydrostatic pressure suppressed interlaminar cracking (delaminations) in three- and four-point bending tests, but fiber kinking still preceded failure. Additionally, in Ref. 101 they again reported that in the presence of hydrostatic stress, longitudinal splitting and "shear" failures (using in-plane shear specimens) were suppressed, and the effect was to increase the compressive strength. It should be noted that all failures were associated with the propagation of kink bands. These results agree with Chaplin's[99] postulate.

Evans and Adler[103] used observations of carbon/carbon composites to identify the modes and morphology of kinking. Kinking has been attributed to three principle modes: (i) longitudinal compression, (ii) lateral compression, and (iii) lateral displacement or "shear." The kink morphologies for longitudinal compression and lateral displacement (or shear) are very similar.

A thermodynamic analysis of kinking has accounted for the observed kink morphologies in terms of the strain energy and plastic work associated with the matrix phase. Specifically, minimization of the plastic work dictates the kink inclination, α, while the minimization of the elastic strain energy determines the kink boundary orientation, β.

The mechanics of kinking were explored using a model for statistical fiber fracture and matrix stress enhancement. The appropriate fracture and deformation parameters were determined in-situ, and these parameters were used to obtain the critical kink formation stress. This expression confirmed that composites should be designed with a maximum resistance to shear kink formation by increasing the fiber

fracture strength level and enhancing the matrix yield strength.

Potter and Purslow[104,105] investigated the compressive failures of multidirectional composite laminates containing center holes. They reported that the first sign of damage (at 60%–70% of failure load, depending on lay-up) was protrusion of the discontinuous 0° plies into the hole. This damage gradually became more pronounced as the loading was increased. Additional associated and necessary damage included in-plane cracks running parallel to the 0° fibers and an area of interlaminar shear failure (localized delamination) at the ply interfaces. Further loading yielded in-plane and out-of-plane fiber microbuckling in the 0° plies. This microbuckling appeared to initiate at locations where splits or cracks, parallel to the fibers, existed in the adjacent 45° plies.

Marom, Davidovitz, Mittelman, and Roman[106] and Davidovitz, Mittelman, Roman, and Marom[107] investigated fracture mechanisms and failure modes of unidirectional Kevlar-reinforced epoxy composites, loaded in three-point bending. They reported the development of diagonal kink (shear) bands in the vicinity of the loading roller. The source of the kink bands is the compressive stress in that side of the specimen near the loading roller. The mechanism for their formation in Kevlar fibers is different than for graphite fibers. In graphite fiber composites, the kink bands consist of broken pieces of fibers, and in Kevlar fiber composites, they consist of an assembly of kink bands in the individual filaments caused by the unique compression behavior of Kevlar fibers.[54]

Rajendran, Rogers, and Koczak[108] studied the failure mode of alumina/aluminum composites under two loading conditions, an Instron testing machine (displacement-control) and dead-weight loading (load control). Both solid and hollow cylindrical specimens were tested. The typical failure mode, when tested in

displacement-control, was kink band formation. These authors proposed that local fiber buckling, initiating at a local stress concentration (e.g. inclusions,voids, and resin-rich areas), and consequent shear deformation of the matrix leads to kinking. As expected, the specimens were crushed catastrophically when loaded in load-control. The experimental compressive strength was compared with theoretical predictions, all of which overpredicted by at least a factor of 2. The largest overprediction was by a factor of 22.

Waas and Babcock[109] completed a detailed experimental investigation to understand the initiation and propagation of failure in laminates in the presence of a stress raiser. They studied damage initiation and propagation throughout the entire load history via real time holographic interferometry and photomicrography of the hole surface. Post-failure examination of the damaged specmens was accomplished using ultrasonic inspection and an optical microscope. From this study, they concluded that the damage was found to initiate by a combination of fiber microbuckling and kinking, and delamination buckling was determined to be the mechanism by which damage propagates to catastrophic failure.

It should be noted that these authors observed much more out-of-plane buckling and delamination formation than reported in in Ref. 1. However, G_{Ic} for the materials tested in Ref. 1 is much higher than that for the BP907 system in Ref. 109. This greater resistance to delamination may explain why local instability was more in-plane in Ref. 1 and more out-of-plane for Ref. 109. In the absense of delamination, in-plane fiber microbuckling requires only resin shear while out-of-plane fiber microbuckling requires out-of-plane displacement of the adjacent ply, which may be simpler or more difficult depending on the ply orientation and depth.

A very detailed study of the effects of fiber microbuckling and shear crippling on

the compressive strength of composite materials has been completed in Refs. 110–114.

Starnes and Williams[110] studied the failure characteristics of compression loaded graphite/epoxy structural components. Their results indicate that the strain concentrations near a circular hole in a graphite/epoxy laminate can cause the highly strained fibers near the hole to buckle locally. These buckled fibers can fail, and the resulting local damage propagates by a combination of shear crippling and delamination to fail the laminate. Good failure predictions were obtained when the Whitney-Nuismer[91] approach was applied to their data.

Williams[111] summarized results similar to Ref. 110. He concluded that fiber microbuckling is governed by the stiffness properties of the matrix, the fibers, and the fiber/matrix interfacial bond.

Rhodes, Mikulas, and McGowan[112] observed a sequence of failure events slightly different from that previously described in Ref. 110. To determine the sequence of failure events, these authors microscopically examined plies in several panels loaded to different percentages of the estimated failure load. The first failure was observed in panels loaded to $\approx 85\%$ of the ultimate compressive load and was an interfiber matrix failure in the 0° plies, the addition to the sequence of failure events. It is anticipated that this failure is a shear failure of the matrix due to the high stress gradient in the vicinity of the hole. Specimens loaded to a higher percentage of the predicted failure load had regions of shear crippling in the 0° plies near where the interfiber matrix failure terminated. An estimate was made of the distance from the edge of the hole to the point where the shear crippling failure was initiated. This distance was approximately equal to d_o used in the Point-Stress Failure Prediction technique for the laminates. However, no attempt was made to

accurately determine and correlate this distance with d_o.

Sohi, Hahn, and Williams[113] investigated the compressive failure mechanisms of quasi-isotropic graphite/epoxy composites, and their results are very similar to those reported in Ref. 1 from a parallel study. They concluded that these failures were triggered by the kinking of fibers in the 0° plies. The kinking was followed by delamination and subsequent sublaminate buckling. Additionally, they reported that the kinking usually initiated at the specimen free edge and quite often in the vicinity of the tab ends. They proposed that kinking initiation at the free edge may be a result of the free edge effect or less lateral support provided for the 0° plies at the edge or a combination of these two effects.

Quasi-isotropic laminates were shown to have considerably higher failure strains than the corresponding unidirectional laminates. This improvement was attributed to the better lateral support provided for the 0° plies by the adjacent off-axis plies in quasi-isotropic laminates. Additionally, they observed that the in-plane kinking in the quasi-isotropic laminate was influenced by the stiffness of the off-axis plies normal to the loading while the out-of-plane kinking was retarded by these off-axis fibers bridging over the kink band.

Hahn and Sohi[114] investigated the buckling of a fiber bundle embedded in an epoxy resin to gain insight into compressive failure mechanisms in unidirectional composites. The fibers were embedded in two different resins, one relatively compliant and one relatively stiff. In both resins, the failure mode was found to be microbuckling of the fibers for the E-glass, T300 graphite, and T700 graphite fibers; however, the high-modulus P75 fibers failed in shear without any microbuckling. Buckling induced failure was most evident for the E-glass fibers, while the kinking type of failure (fibers are broken in only 2 locations) was most common for

the T300 and T700 graphite fibers. Additionally, Hahn and Sohi observed that fiber fracture occurred immediately after fracture and that fiber/matrix debonding follows fiber buckling. Their observed failure strains and segment lengths of the bundle specimens followed the trends predicted by Lanir and Fung[45] for a single fiber embedded in an infinite matrix.

Hahn[115] improved and combined previous models describing fiber microbuckling[21] and kinking into one unified model for the compressive strength of unidirectional composites. He suggested that failure is the result of a sequential occurrence of fiber microbuckling, kinking, and fracture. Consequently, kink bands are frequently observed on failure surfaces.

When a fiber microbuckles, it pushes or pulls the neighboring fibers, and hence, a group of fibers will likely microbuckle in-phase with one another. As a result of in-phase or shear mode microbuckling, the matrix between fibers experiences shear deformation which provides resistance to further microbuckling. Eventually, with additional loading, the matrix yields, and the microbuckling changes to kinking. When the matrix cannot support any additional shear, the fibers collapse, and the composite fails, usually catastrophically.

Hahn notes that this process is very localized, and quite often, initiation occurs at a free edge where the support of neighboring fibers is reduced. Once initiated, it then propagates inward. This result is consistent with the results of Guynn and Bradley in Refs. 1, 3, and 4.

The compressive strength for fiber microbuckling predicted in Ref. 21 was given in Eqn. 30. The assumption of fiber kinking at σ_c^* leads to

$$\alpha = \frac{2\tau_y}{\sigma_f^*} \tag{44}$$

where

σ_f^* = $\frac{\sigma_c^*}{V_f}$ = fiber stress and

τ_y = shear stress level corresponding to γ_y.

Additionally, the shear strain in the kink band is given by

$$\gamma^* = \sin\alpha - (1 - \cos\alpha)\tan\beta. \tag{45}$$

It should be noted that any kink band formation caused by fiber failure rather than matrix yielding cannot be described by this analysis. He applied this analysis to data in Ref. 116 with reasonable results, although they could not be verified experimentally because of measurement difficulties. Hahn's analysis qualitatively predicts the effects of constituent phases, including interface and defects on the compressive failure of unidirectional composites.

Kulkarni et al[49] also observed kink-band formation in the longitudinal and transverse planes, inclined at 55°–60° to the horizontal axis. Lateral restraint provided by the addition of glass fibers in the 90° direction prevented the longitudinal slip plane, but involved a slip in the transverse plane.

Budianski[87] reviewed the application of kink band theories to the compression failure of composite materials. Three of the theories presented yielded $\beta = 0$ as the critical kink angle (see Fig. 14). He concluded from the results of these theories that the most important factors affecting the kink strength of composites are high stiffness in strength and shear. Furthermore, the sensitivity to fiber misalignment is large. One problem still concerning Budianski was that experimental observations by different researchers have shown that the kink angle, β, varies from $\approx 10°$ to $\approx 40°$. Budianski showed that localized deviations from the ideal fiber alignment having no particular geometrical bias induce patterns of angular misalignment due to elastic distortion that arrange themselves into inclined domains. These rotations then induce plastic kinking into similarly inclined kink bands.

Failure follows rapidly after plastic deformation begins, so that it is reasonable to identify the failure stress, σ, with the kinking failure stress, σ_s. The consequent correlations between σ_s and the kink angle, β, are

$$\tan\beta = \pm\left[\frac{1-\sigma_s/G}{E_T/G}\right]^{\frac{1}{2}} \tag{46}$$

for long wave imperfections and

$$\tan\beta = \pm\left(\sqrt{2}-1\right)\left[\frac{1-\sigma_s/G}{E_T/G}\right]^{\frac{1}{2}} \tag{47}$$

for short wave imperfections where

σ_s = stress perpendicular to the fiber direction,

G = elastic shear modulus of the composite, and

E_T = transverse modulus of the composite.

Equations 46 and 47 predict kink angles between 10° and 35° as shown in Fig. 16.

Additionally, Budianski proposed a solution for kink band width, but added that although the understanding of kink band geometry is qualitatively sound, the influence of random imperfections must also be included in the quantitative analyses.

From the literature on compression failures, it is easy to get the impression that fiber microbuckling and kinking are competing mechanisms. However, recent work has indicated that fiber microbuckling occurs first, followed by propagation of this local damage to form kinking.[1,109,115] Fiber microbuckling and the resultant kinking may form in-plane or out-of-plane. It typically initiates at free edges at the perimeter of the laminate or at an internal hole where local support to resist fiber microbuckling is reduced.

In summary, it has been shown that fiber waviness, fiber/matrix interfacial bonding, and the composite shear yield strength are all important parameters

in determining the stress level at which fiber microbuckling initiates. The shear modulus of the matrix, which esssentially controls the shear modulus of the composite, was also shown to be an important factor in the determination of the compressive strength of composite materials.

2.5 Effects of Matrix Resin Properties on Compressive Strength of Composite Materials

The shear modulus and the nonlinear constitutive behavior are both important in determining the compressive strength of a composite material when the failure mode is fiber microbuckling or macrobuckling, as indicated by Eqns. 1–18, 24–30, and 39–43. Hahn and Williams[21] illustrated the increase in compressive strength that accompanies an increase in resin modulus (see Figs. 17 and 18). Although the compressive strength in Figs. 17 and 18 is presented as a function of the resin tensile modulus, the shear modulus would show the same trend since it is proportional to the tensile modulus. In contrast, the tensile strength is relatively insensitive to the resin modulus. The consequence of the sensitivity of the compression strength to resin modulus and the insensitivity of the tensile strength to resin modulus is that the ratio of compressive strength to tensile strength increases as the resin modulus increases.

Although the unidirectional compressive strength of graphite/epoxy and metal matrix composites has been shown to correlate with the matrix modulus,[40] the results by Chang[117,118] for thermoplastic matrix composites show no such correlation. Chang states that the matrix modulus is not the key determinant for compressive strength of unidirectional carbon/thermoplastic matrix composites. He suggests that other factors such as fiber/matrix adhesion, matrix penetration, fiber alignment, and shear stability are more important.

Mabson, Wharram, Tennyson, and Hansen[119] investigated the effects of moisture content and elevated temperature on the compressive strength of graphite/epoxy composites. The sandwich beam test method yielded compressive stiffness values consistently higher than the "pure" compressive data (IITRI type fixture) for all environmental conditions studied. Elevated temperature ($\approx 100°C$) combined with high moisture content ($\approx 1.7\%$ H_2O) resulted in no significant change in compressive stiffness but a large reduction in compressive strength (21%–43%), relative to ambient condition strengths. This compressive strength reduction may be attributed to a degradation in the shear modulus of the matrix resin.

Sternstein, Yurgartis, and Srinivasan[120] studied the out-of-plane bending failure of thermoplastic matrix composites, including the effects of the graphite fibers on the ability of the matrix to deform and yield. These composites were evaluated using a four-point bending jig that allowed observation of the edge failures in the light microscope.

For these thermoplastic matrices, they observed time dependent fiber fracture which occurs in buckles or kink bands. Additionally, all failures initiated on the compression side of the bending sample. It appeared that the enhanced ductility of a thermoplastic (relative to a thermoset) composite resulted in ply buckling instability as a dominant failure mode. This result indicates that compressive properties are more critical for thermoplastic composites than thermoset composites.

Sternstein et al[120] observed large scale yielding as evidenced by shear bands and crazes or relatively large displacements of fibers only in resin-rich regions of the specimens. Observation of the delaminations indicated that matrix deformation was limited to a small interfacial region and that the crack propagated by shear (Mode II) rather than tension (Mode I).

Bishop[121] reported slightly different failure modes for carbon fiber/PEEK (APC-1) composites, compared to carbon fiber/epoxy composites. The failure mechanisms are slightly different because of the lower shear modulus, the lower compressive strength, and the greater shear strength of the carbon fiber-reinforced PEEK. Compressive failures of fibers or shear failure across the fibers is likely to occur in PEEK composites, and failure modes due to shear forces parallel to the fibers are less likely to occur.

Miyano, Kanemitsu, Kunio, and Kuhn[122] investigated the fracture strength of unidirectional CFRP for various directions and modes of loading over wide ranges of temperature and strain rates, in conjunction with similar investigations on the epoxy resin matrix. Additionally, the role of the matrix resin on these fracture strengths, based on SEM observations of the fracture surfaces, was discussed. Time and temperature dependence of tensile, compressive, and flexural strengths in the CFRP for both longitudinal and transverse directions exhibited the same viscoelastic behavior as the matrix epoxy resin. However, the longitudinal compressive and flexural fracture strengths of unidirectional CFRP was dominated by the deformation properties of the matrix, wheras the transverse tensile, transverse compressive, and flexural fracture strength of unidirectional CFRP was strongly affected by the fracture strength of the matrix.

These authors observed that for transverse tension, compression, and bending, the resin adheres to the fracture surfaces at 60°C while much less resin adhered to the fracture surfaces at 180°C. Additionally, they confirmed, using Dow's[31] equation, that the microscopic mode of failure is fiber microbuckling in both longitudinal compression and flexural in every case.

Greszczuk's[26] results presented in Figs. 2a–2c show that increasing Young's

modulus or the shear modulus of the resin significantly increases the composite strength, and if increased enough, the failure mode is then governed by the compressive strength of the reinforcement rather than microbuckling of the reinforcement.

Lee[90] conducted an experimental study of compression properties of a number of reinforced thermoplastic composites to determine the effects of these matrices on compression strength and to provide a direct comparison with carbon reinforced epoxides. His results indicate that unidirectional APC-2 gave similar compression strength to both epoxide (XA-S/Fibredux 914C and XA-S/MY750) systems tested. However, no comparison is given regarding the matrix moduli of these materials.

Hahn and Sohi[109] observed that fiber microbuckling is more uniformly distributed in a very soft resin, but quite localized in stiff resins. The results of Williams[111] indicate that a higher shear modulus resin should also increase the strain at which microbuckling initiates.

Recall that in 1963, Fried[84] proposed that in the limit the point at which the resin "yields," or flows, determines the load carrying capacity of the composite. He also hypothesized that resin physical characteristics (stiffness, shear strength, shear rigidity, and tensile strength) and content affect the stability of the reinforcement. Experimental results in a subsequent study[85] supported these initial hypotheses. In particular, the compressive strength varied directly with the resin compressive yield strength for unidirectional filament wound materials. Results from an even later study[86] showed that resin yield will be the failure mode only in laminates with low void contents and good reinforcement/matrix interfaces. Piggott and Harris[54] showed that the matrix yield stress is an important factor controlling compression properties of fiber-reinforced composites. however, beyond a certain limiting matrix yield stress, the compressive strength remains constant or declines. They postulated

that this phenomena may indicate a change from matrix control to interface control of compressive strength.

The results of many researchers (Refs. 26, 33, 54, 65, 84–86, 111, 117–122) have shown that the matrix shear modulus is the matrix property with the most significant effect on compressive strength.

The reduction in the compressive strength of a composite material that results from the nonlinear consititutive behavior in the shear stress versus shear strain relationship of the resin has been noted by many investigators (Refs. 26, 67–69, 73–79). Hahn and Williams[26] observed that although the elastic moduli of the resin varied significantly, the tangential moduli at failure were relatively consistent. This observation implies that the tangential modulus at failure, rather than the initial elastic modulus, controls the compressive failures in composite materials. Wang's[67] results support this argument. The analytical work of Hayashi and Fujikake[47] indicates that the compressive strength of unidirectional composite materials may be reduced as much as 50% due to the nonlinear behavior of the resin. Kurashige's[65] analysis predicted a decrease in the ultimate compressive strength as the resin shear modulus decreased and also as the thickness of the resin-rich layer between the axial and cross layers increased.

Shuart and Williams[74] observed in-plane shearing between the fiber and matrix (i.e., matrix shearing) as the primary compression failure mechanism for an all $\pm 45°$ laminates with a hole. However, the matrix shearing contribution to failure appeared to be reduced and delamination observation increased as the percentage of 90° plies in the laminate thickness was increased.

Sohi et al[113] investigated the effects of resin toughness and modulus on the failure modes of graphite/epoxy composites. They observed that tougher, and thus

more ductile, resins resisted delamination following fiber kinking better than the more brittle resins, even though the tougher resins allowed fiber kinking at lower strains. Regardless of the resin, failure initiation in all seven systems studied was beleived to be governed by the same mechanism, fiber kinking in the 0° plies. The mode of propagation following the initial fiber kinking changed with resin ductility. For brittle resins, delamination immediately follows fiber kinking initiation. On the other hand, tougher resins allow more stable fiber kinking and resist any delamination growth.

In summary, a high compressive strength in a composite material may only be obtained when microbuckling and macrobuckling are inhibited. Both analytical and experimental results indicate that a large shear modulus and yield strength are necessary to obtain a high compressive strength.

2.6 Effects of Fiber Properties on Compressive Strength of Composite Materials

The tensile strength of the fiber is always the limiting factor when determining the tensile strength of a composite material. However for compressive loading, the compressive strength of the fiber is significant only when fracture is initiated by fiber shear failure. In this section, the effects of the mechanical properties of the fiber, the volume fraction of the fiber, and the waviness of fiber on the compression strength of composte materials is explained.

2.6.1 Mechanical Properties of Fibers

Three investigations,[25,81,82] cited in this review, of the compressive strength of composite materials indicate fiber shear as the failure mode. However, more recent studies[1,4,68,69,115] indicate that fiber microbuckling is the limiting factor in compression strength, even when a relatively stiff epoxy matrix is used.

Van Dreumel[123] indicated that aramid fibers, compared to carbon fibers, may be very attractive, especially for compression loaded structures. He noted that the Young's modulus, E_f, for a unidirectional carbon fiber laminate is a linear function of the applied stress while it is constant for aramid fiber laminates. The data presented, considering specific stiffnesses and strengths, showed that carbon fibers are favorable for stiffness critical designs while aramid fibers are preferred for strength critical designs. However, when considering buckling behavior, structural stability is governed by stiffness. In particular, $\sqrt{E}$ is the important parameter. Although the compressive strength ratio of carbon to aramid fiber unidirectional laminates is 6, the Euler buckling strength ratio is only 1.3.

Turner and Cogswell[124] reviewed the mechanical property data base for a range of continuous fiber/PEEK composites to demonstrate the diversity of thermoplastic composite materials that may be produced. It is important to note that with most of the fibers, high efficiencies (80–90%) of fiber property utilization are observed. Experimental results indicate that the on-fiber nucleation of crystallization explains the very close physical proximity of the resin molecules to the fiber surface. Although this is a necessary condition for good adhesion, it is not a sufficient guarantee of good bonding.

Piggott and Harris[56] measured the unidirectional compression strength of hybrid composites reinforced with carbon, Kevlar, and/or glass fibers. All of the hybrid composites showed interactions, deviating from rule of mixtures behavior. The observed interactions were beneficial for the case of strength and detrimental for the case of stiffness. Microscopic examination of compression tested specimens showed highly localized transverse failure surfaces for carbon/carbon hybrids. Kevlar composites failed by a highly localized shear kinking band with no longitudinal splitting.

In carbon-glass hybrids, the kinking in the adjacent glass-rich regions appears to inhibit the progress of cracks that have initiated in the carbon.

Williams,[111] based on his results, hypothesized that the higher bending strains in a buckled fiber initiate local failure. His results showed that composites made with higher tensile strain fibers exhibited higher laminate strengths.

Hahn and Sohi[114] observed that low-modulus fibers (e.g. E-glass) are more susceptible to fiber microbuckling, while intermediate-modulus graphite fibers are more likely to fail by fiber kinking. High-modulus fibers (P75) failed by fiber shear.

DeTeresa et al[116] studied the mechanical anisotropy of an aramid polyamide fiber, Kevlar 49, in tension, compression, and torsion. Ratios of tensile-to-compressive strength, tensile-to-shear strength, and tensile-to-shear modulus of 5:1, 17:1, and 70:1, respectively, were measured for Kevlar 49. The high anisotropy of mechanical behavior for Kevlar 49 is illustrated by the measured 70:1 ratio of tensile-to-shear modulus. After compression loading, they observed lateral shifts of fiber segments, similar to slip bands in metals, called fiber kinking. No sinusoidal microbuckling instabilities were observed for these fibers. This observation implies that the microbuckling theories of unidirectional composites which satisfactorily predict the compressive strengths of composites based on isotropic glass fibers may have no bearing on the compressive strength of Kevlar composites.

The relatively low values of shear strength and modulus for Kevlar 49 may account for the relatively low in-plane shear modulus, strength, and interlaminar shear strength of Kevlar composites. For composites having a strong fiber/matrix interfacial bond, failure may occur within the Kevlar fiber, rather than in the matrix or at the interface. Therefore, any analysis of mechanical performance for Kevlar composites should consider that the fiber shear modulus and strength are in the

range of matrix shear properties.

In Refs. 126, 127, and 128, DeTeresa et al modelled highly oriented polymer fibers as a collection of chains that interact laterally. The critical stresses to buckle this fiber or collection of chains are calculated using a shear instability analysis (similar to those in Refs. 33, 34, and 36) developed to predict the compressive strengths of fiber-reinforced composites. This buckling stress is predicted to be equal to the shear modulus of the fibers, similar to Eqn. 4 for composites, and is the limiting value of fiber compressive strength. It should be noted that stresses to initiate shear instability are dominated by properties of the elastic foundation and not the column or chain geometry and properties. As with composites, the theory overestimates the fiber compressive strength, but a correlation of shear modulus with axial compressive strength exists. The authors consider it remarkable that this simple analysis, disregarding defects and inhomogeneities, predicts within an order of magnitude of the measured compressive strengths.

Based on their results, DeTeresa et al[128] suggest a possible hierarchy for compressive failure of composite materials. On a macroscopic scale, failure may occur by a golbal elastic instability first analyzed by Leonard Euler. At a smaller scale, namely the lamina, failure may occur by fiber microbuckling, modelled with an elastic instability analysis in Refs. 33, 34, and 36. Finally, the quthors have shown that the microstructure of polymer fibers undergoes an elastic instability that manifests itself as kink banding.

Hahn and Williams[23] summarized the reported compressive fiber failure modes as shear, kinking, and bending. High modulus graphite fibers fracture in shear along a maximum shear plane. These shear failures are typically observed only in a composite with a very stiff resin and minimum fiber waviness, two factors that

inhibit fiber microbuckling. When these fiber shear failures occur, the composite compressive strength is very nearly equal to its tensile strength. Fiber strength dominates compressive strength in both of these cases. In this particular case, the compressive strength is predicted using Eqn. 31, and a linear relationship between compressive strength and fiber volume fraction should be observed. Kevlar fibers, on the other hand, fail in a kink mode because of Kevlar's characteristic weak bond in the radial direction that permits individual fibers to split into fibrils. Both shear failure and fiber kinking are characteristic failure modes for fibers with well-aligned fibrillar structure. However, the low ductility for graphite fibers leads to shear fracture while the development of fibrils for Kevlar fibers results in kinking. These kinking failures are indicative of a low compressive strength fiber and thus, a low compressive strength composite. Brittle fibers with amorphous structure (e.g., glass) usually fail in bending, starting from the tension side. Medium to high-strength fibers also fail in bending. Bending failures occur after fiber microbuckling in which case the fiber strength does not play an important factor in determining the compressive strength.

It has been established from this review that fiber tensile modulus is not a particularly significant variable in the determination of the compressive strength of composite laminates. The fiber tensile modulus appears explicitly in Eqns. 1, 2, 7, 13–17, 24, and 25, which give the compressive strength for fiber microbuckling failures. The fiber shear modulus is explicit in Eqns. 5, 11, and 12 which also predict the compressive strength for fiber microbuckling failures. However, the contribution of the fiber modulus to the calculated compressive strength in each case is small, unless the fiber shear modulus is the same order of magnitude as the matrix shear modulus and/or the microbuckling wavelength is less than or equal to ten times the

fiber diameter.

Indirectly, the fiber modulus may be more important in the determination of the composite's compressive strength if it reduces the fiber waviness, which would increase the compressive strength (see Eqns. 16–30). However, fiber waviness ultimately depends on fiber stiffness which is more sensitive to fiber diameter than fiber modulus.

2.6.2 Fiber Volume Fraction

All of the models for compressive strength described previously in this review indicate that the fiber volume fraction, V_f, is an important variable in determining compression strength. When V_f does not appear explicitly in the equations, it is present implicitly through the composite shear modulus G_{12}, as shown in Eqn. 5. The monotonic increase in compressive strength with increasing fiber volume fraction has been observed by a number of investigators (see Refs. 47, 51, 54, 55, 23, 63, 81, 84, 85, and 88).

The results from Hayashi and Fujikake,[47] showing the variation in compression strength as a function of fiber volume fraction, are given in Fig. 19. The results shown in Figs. 19a and 19c indicate that an optimum fiber volume fraction ($\approx$ 50%–60%) yields a maximum compressive strength for polyester composites. The results in Ref. 47 suggest that the fiber distribution is also important. A heterogeneous fiber distribution facilitates interfacial failures at a lower average fiber volume fraction than a homogeneous distribution. The fiber volume fraction results shown in Fig. 19 are more continuous than those presented by Rosen.[33]

Piggott and Harris[54] tested unidirectional Kevlar-, carbon-, and glass-reinforced composites. The results indicate that both strength and modulus are a linear function of volume fractions for moderate volume fractions, $\leq$30% and $\leq$45%,

respectively. It is interesting to note that beyond these fiber volume fractions, both the strength and modulus appear to decrease and that deviations from the rule of mixtures type behavior increase. At 30% fiber volume fraction, the Kevlar fiber composites behaved as though their compression modulus and strength were significantly smaller than their tensile values, while carbon fiber composites were only slightly more compliant and weaker in compression than tension.

Piggott and Wilde[55] concluded that the compressive strength of fibers play a very important role in the compressive strength of steel-reinforced composites when failure occurs at strains that are less than the matrix yield strain. They observed a linear relationship, sufficiently predicted using rule of mixtures (Eqn. 31), for the variation of the composite compressive strength as a function of fiber volume fraction.

Martinez et al[57] also showed that both the composite compressive strength and modulus are very linear functions of fiber volume fraction, as shown in Fig. 20, up to a limiting V_f. The limiting fiber volume fractions for strength and modulus are $\approx$ 40% and $\approx$ 50%, respectively. Beyond these limiting values of V_f, both the strength and modulus decrease. They attributed these maximums in compressive strength at intermediate V_f values to interfacial bond failures (see Eqns. 32–34). This result also suggests (like Ref. 47) that fiber distribution is important. A heterogeneous fiber distribution would facilitate interfacial failures at lower V_f values than a homogeneous fiber distribution.

Kurashige[63] predicted increasing compressive strength with increasing fiber volume fraction (see Fig. 4).

Hancox[82] observed a very linear increase in unidirectional compression strength as the fiber volume fraction of the carbon/epoxy composites was increased, as shown

in Fig. 21. The results shown in Fig. 21 would be predicted by Eqn. 31 for a fiber shear failure mode, which was the fracture mode described by Hancox.

Fried[84] concluded that the effectiveness of the reinforcement is influenced by the nature and physical characteristics of the basic material (compressive modulus and strength, shear characteristics, and degree of ductility or brittleness) and by geometric factors (straightness, distribution uniformity, and cross-sectional shape). A later study[85] showed that the compressive strength was maximized when the fiber volume fraction was optimized.

Chou and Kelly[88] found that compressive strength increased with increasing fiber volume fraction in a manner consistent with Eqn. 41 for fiber microbuckling as shown in Fig. 22. The solid lines (IITRI) and broken lines (RAE) are the predictions for the upper and lower limits of the slenderness ratio. Greszczuk[53] observed a similar trend, shown in Fig. 23. In both cases, the trend in the experimental data was well described by Eqn. 41, although the absolute values of the experimentally determined strengths were lower than the predictions. The theoretical values probably overpredict because Eqn. 41 neglects the effects of initial fiber waviness and resin nonlinearity at the higher stress levels.

Lager and June[40] varied the fiber volume fraction from 0.05 through 0.46 for boron/epoxy laminates. They observed excellent correlation between the trends of the data and the theoretical predictions from Eqns. 1 and 3. However, measured compressive strengths were 63% of those predicted. As postulated by Rosen,[33] the shear mode failure dominated the higher fiber volume fraction composites.

2.6.3 Fiber Waviness

Models that attempt to describe the effect of fiber waviness on compression strength have been reviewed in two sections of this section (see Eqns. 16–30, and

Refs. 26, 57, 61–66], 67–80.

Woven fabrics are attractive materials for load-bearing structural applications for many reasons. Two-dimensional woven fabrics provide more balanced (compared to unidirectional tape) in-plane material properties, provide excellent impact resistance because of the 2-D reinforcement, handle easily, and have relatively low fabrication costs.[129] Fabrics may be made using many types of weaves.[130] Each 2-D weave consists of two sets of yarns. By definition, warp corresponds to the length direction of the fabric, and fill or weft corresponds to the width direction of the fabric.

Yau and Chou[129] evaluated the open hole strength of carbon/PEEK and carbon/epoxy composites with drilled and molded holes. Molded holes were formed in the prepreg layer-by-layer, prior to curing. These holes were made by allowing the woven fiber bundles to wrap around a steel pin. Different hole diameters were formed by using different diameter steel pins. The authors attribute the strengthening mechanisms in the molded holes to an increase in local fiber volume fraction and the maintaining of fiber continuity. The molding process forces the fibers to have a higher local in-plane fiber waviness. However, this curvature is convex away from the free surface, which should inhibit local in-plane fiber microbuckling into the hole. Their results indicate that the molded hole, compared to the drilled hole, greatly increased (up to 47%) the open hole tensile and compression strengths of woven fabric composites (epoxy and PEEK). Considering the normalized strength ($\sigma_{notch}/\sigma_{unnotched}$), PEEK composites exhibited higher tensile and compressive strengths than epoxy composites.

Schapery[131] attributed a 10% increase in the tensile secant modulus for AS4/3502 composites to the straightening of initially wavy fibers.

Greszczuk's[26] results, presented in Fig. 21d showed that bowed fibers significantly reduce the compressive strength of composites.

Martinez et al[57] used a fixture to deliberately kink fibers (induce fiber waviness) during the processing of the composite. This kinking process increased the fiber curvature, and they expressed the waviness using the radius of curvature. Smaller radii of curvature corresponded to larger amplitude waviness. These results are shown in Fig. 5 and indicate that fiber waviness significantly reduces the compressive strength.

Maewal,[62] contrary to other investigators, suggested that the initial fiber waviness of the fibers should not reduce the fiber microbuckling stress significantly.

Kurashige[63] predicted that increasing fiber waviness caused a reduction in compressive strength (see Fig. 4). However, his strength results were not bounded for the extension mode of fiber microbuckling.

Kurashige[65] predicted a sharp increase in compressive strength as the nondimensional buckling wavelength was increased from 0 to approximately 0.3, at which point the compression strength reaches a plateau.

Davis[67] observed primarily in-plane fiber waviness for boron/epoxy composites. The ratio of the initial amplitude of the waviness to the length, $\frac{a_o}{L}$, was measured to range from 0.001875 to 0.003750. His calculations indicate that this magnitude of fiber waviness caused the compressive strength to be reduced by 65% from the ideal strength expected for a composite with perfectly straight fibers.

Wang[67,69] back calculated, using an iterative technique, $\frac{a_o}{L}$ to be 0.0108 for AS1/3501-6 graphite/epoxy composites. As expected, this value is larger than that for the boron[67] fibers since the carbon fibers are more slender and more compliant. Wang's observed compressive strength (1.2 GPa) is less than 20% of the G_{12} value

(7.1 GPa)[125], indicating the significant degradation in compression strength that results from fiber waviness.

It is generally noted that composites made with thermoplastic matrices have a compressive strength that is a smaller fraction of their tensile strengths than composites made with thermoset matrices. This difference is generally attributed to a weaker fiber/matrix interfacial bond in thermoplastic composites. However, it is quite possible that another contributing factor is the greater tendency for fiber waviness in thermoplastic composite materials. These composites are more susceptible, compared to thermosets, to fiber waviness because they are processed at higher temperatures, pressures, and viscosity levels, and consequently, they have higher residual thermal stresses. The results reviewed in this section and compared with the models clearly indicate that fiber waviness leads to premature fiber microbuckling due to larger matrix shear stresses at a given applied compresive stress.

2.7 Effects of Interfacial Bonding on Compressive Strength of Composite Materials

The characteristics between the fiber and the matrix control the properties of the final composite. Thus, the effects of the interfacial bond on compression strength is important and is reviewed in this section.

Landro and Pegoraro[132] accurately evaluated the shear strength at the fiber/matrix interface for two materials, polyethersulphone (PES) and polyetherimide (ULTEM), using a statistical method based on the measurement of the mean critical fiber length. Post-mortem SEM examination showed bare fibers, indicating that the chemical bond between the fiber and matrix was weaker than the matrix strength. However, the experimental data showed that the limiting interfacial

shear strength was approximately equal to the matrix shear yield stress. They attributed this interfacial strength to the differential thermal shrinkage of the fiber and matrix which gives rise, at the interface, to a pressure that increases the Van der Waal's forces. Additionally, they concluded that this shrinkage phenomena was most important because of the high transition temperatures (softening) of the thermoplastics investigated.

Lanir and Fung[45] showed that the prebuckling separation of the fiber and the matrix, debonding, decreases the buckling load and may affect the postbuckling behavior of the fiber.

The interfacial failure analysis by Hayashi and Fujikake[47] assumed that the composite fails when the maximum tensile stress at the fiber/matrix interface ($\hat{rr}_{cr}$) reaches the interfacial bonding strength. Figure 19c is a comparison of experimental data with the fiber buckling and interfacial bonding failure theories developed in Ref. 47. These authors have indicated that the flattening of the compressive stress versus fiber volume fraction curve (see Fig. 19c) is a result of poor interfacial bonding.

Additionally, Hayashi and Fujikake[47] and Greszczuk[51] have indicated that both fiber arrangement and fiber volume fraction are important in the determination of compression strength. Different arrangements result in different nearest neighbor distances between fibers which influences the magnitude of the interfacial stresses. Consequently, fiber arrangement is more critical in composites containing relatively weak fiber/matrix interfaces. This result also suggests that a homogeneous fiber arrangement, which maximizes the distance between fibers (for a given fiber volume fraction), will make composites less susceptible to longitudinal splitting.

Kulkarni et al[48] developed a fiber microbuckling model that included the effect

of an imperfect fiber/matrix interfacial bond (Eqns. 11–12). The results of this analysis are shown in Fig. 25. Although no quantitative conclusions are made, it is clear that the significance of the interfacial strength increases with increasing fiber volume fraction. For the case of poor adhesion, increasing the fiber volume fraction is actually detrimental to the composite compressive strength.

Greszczuk[51] predicted the transverse tensile strength of glass/epoxy, graphite/epoxy, and graphite/phenolic composites using constituent properties and microstructure of the composite (Eqns. 32 and 33). This analysis indicates that a reduction in the transverse tensile strength (e.g., a poor fiber/matrix interfacial bond) causes a reduction in the compressive strength.

In Greszczuk's[53] nearly perfect composites, he observed fan-shaped internal helical cracks initiating at the fiber/matrix interface. The failure appeared to initiate at the fiber/matrix interface, to propagate along the interface, and then terminate in a helical crack. These experimental observations led to an additional study on the effect of the fiber/matrix interface on compressive strength. As a first approximation, Greszczuk assumed that the shear modulus of a composite with unbonded fibers was equal to the shear modulus of a solid containing cylindrical voids in the amount equal to the amount of unbonded fibers. Experimental data did not correlate well with this analysis. The test/theory ratio of strengths ranged from $\approx$ 0.84–0.92.

Greszczuk's explanation for the mechanism that causes fiber/matrix debonding is as follows. Because of the differences in Poisson's ratios between the fibers and the matrix, transverse stresses are induced when a composite is subjected to compressive loading in the fiber direction. Even though the induced tensile stresses at the fiber/matrix boundary are small compared to the applied axial compressive

stresses, so is the transverse tensile strength compared to the axial compressive strength. Thus, it is possible for the induced transverse tensile stresses to cause fiber/matrix debonding leading to longitudinal splitting (an interaction failure) and a reduction in the ultimate compression strength.

Martinez et al[57] varied the interfacial bond strength of unidirectional glass-polyester composites by using different fiber surface treatments. These results are shown in Figs. 5 and 24. The results in Fig. 5 show that poor fiber/matrix adhesion has a detrimental effect on the compressive strength of composites. Figure 24 shows the compressive strength as a function of fiber volume fraction for composites with good and poor fiber/matrix adhesion. Again, a significant reduction in compression strength is observed for composites with poor fiber/matrix interfaces. These trends are similar to those reported by Hayashi and Fujikake.[47]

Hancox[82] also observed a flattening of the compressive stress versus fiber volume fraction curve (see Fig. 21) for composites made with non-surface treated fibers. He reported that the fracture mode for these specimens was usually massive delamination. Poor interfacial bonding, associated with non-surface treated fibers, probably caused the flattening of the data in Fig. 21 which is very similar to that reported by Hayashi and Fujikake[47] (shown in Fig. 19c). He concluded that poor adhesion between the fibers and the matrix produces composites weaker in compression than those produced with strong fiber/matrix interfaces.

Fried[86] studied filament wound $[0/90]_s$ laminates. In this study, he observed that orthogonal materials fail in shear and compression by debonding at the reinforcement/matrix interface. Experimental results showed that the laminate compressive strength was inversely proportional to the void content.

The trends presented in this section indicate that poor interfacial bonding may

degrade the compressive strength in two ways. First, it allows failure to occur by longitudinal splitting due to differential Poisson's contraction between the fiber and the matrix.[24,51,53] Poor interfacial bonding may lead to a reduction in the transverse tensile strength[53,132] or the matrix ultimate strain[24] which results in a reduction in the compressive strength, as calculated in Eqns. 32–34. Second, it can effectively reduce the composite shear modulus, G_{12}, and allow fiber microbuckling at a lower compressive stress level, as indicated in Eqns. 4, 5, and 11 (Refs. 24, 51, 68, 69).

2.8 Environmental Effects on Compressive Strength of Composite Materials

It has been reported that elevated temperature causes a reduction in compression strength of composites by degrading the shear modulus of the resin[119] and the fiber/matrix interfacial bond.[122] Thus, a brief survey of the literature, describing the effects of temperature on the compressive strength of composite materials follows.

Ewins and Potter[133] illustrated the effects of temperature and humidity (see Fig. 26) on the unidirectional compressive strength of carbon fiber-reinforced plastics (CFRP). They postulated that if the fiber shear failure mode remains dominant, the compressive strength will decrease only slightly with increased temperature, probably due to a decrease in the matrix contribution to strength. However, as temperature increases, the matrix shear modulus and fiber/matrix interfacial bond strength decrease, and at some critical temperature the failure mode changes to one governed primarily by fiber instability (see Fig. 26a.).

The absorption of moisture causes matrix plasticization, a reduction in the matrix modulus, and a reduction in the fiber/matrix interfacial bond strength. Again, following a failure mode change to one of fiber instability, further moisture

absorption and a corresponding reduction in shear modulus are likely to result in a rapid reduction in compression strength. The hypothetical combined effect of temperature and moisture absorption is illustrated in Fig. 26b.

Malik, Palazotto, and Whitney[134] investigated graphite/PEEK (APC-1) quasi-isotropic composites at 21°C, 121°C, and 149°C in tension and compression. These authors reported a rapid reduction in moduli at the glass transition temperature (135°C) of this material and reduced fiber/matrix adhesion at the higher temperatures.

Ramey, Palazotto, and Whitney[135] continued the test program of Ref. 134 to compare the notched strength (tension and compression) of quasi-isotropic graphite/PEEK (APC-2) and graphite/epoxy composites at 21°C, 121°C, 135°C, and 149°C. This discussion is limited to the results for APC-2 composites. The results indicate that APC-2 composites are less resistant to compression loading than tensile loading over the entire range of temperatures. For a given hole diameter, both the tension and compression strengths are reduced as the temperature is increased. However, the tension strength does not illustrate a strength reduction until very near the glass transition temperature, T_g, and this strength reduction is smaller than that for the compression strength. For the graphite/epoxy laminates, the notched tensile strength increases with temperature. This result is attributed to a reduction in the local stress concentrations at the notch, caused by the higher temperatures, that allow the laminate to become tougher than at room temperature where the matrix is brittle.

The compression specimens tested at room temperature broke into two pieces at failure, while those tested at the higher temperatures remained in one solid piece. This failure pattern supports the idea that the room temperature matrix

supports the fiber more efficiently than the elevated temperature matrix. The room temperature system stores more energy and thus, releases more energy at failure, large enough to cause catastrophic failure of the specimen.

Post-mortem examination of the failure mechanisms indicates that fibers in the 0° surface ply have failed in-plane into the notch and also out-of-plane of the laminate, an intra-laminar failure. Matrix deformation between the 0° crippled fibers and the adjacent 90° ply was attributed to inter-laminar stresses.

Observation shows that the matrix fails in at least a partially cohesive mechanism. Although the fiber/matrix adhesion is reduced at elevated temperatures, the matrix failure was more ductile and also more cohesive than adhesive. Examination of the matrix deformation at the previously mentioned 0/90 interface indicates that at elevated temperatures, the matrix flows, providing less fiber support and less load transfer as it becomes more fluid. The consequent inter-lamina strength reduction and reduced fiber support are believed to account for the compression strength reduction for APC-2 composites at elevated temperatures.

Kar, Herfert, and Kessler[136] investigated AS1/3501-6 multidirectional composites and also found a breakdown of the fiber/matrix bond, leading to reduced compressive strengths, under conditions of elevated temperature and high humidity.

Ewins and Ham[25] reported a change in the failure mode from fiber shear to fiber microbuckling at approximately 100°C. They attributed this mode change to a reduced matrix shear modulus and an altered matrix constitutive behavior, thus providing less support for the fibers.

Potter and Purslow[104,105] observed a reduction in fiber/matrix interfacial bond strength due to hot-wet conditions. In the room temperature-dry specimens, failure occurred within the matrix while in the hot-wet specimens, failure occurred at the

fiber/matrix interface. They concluded that hot-wet conditions cause a massive loss of interlaminar shear and axial compressive strengths because of the reduced bond strength and modulus.

In conclusion, the results presented in Refs. 25, D-5.1], 105, and 133–136 indicate that environmental conditions (elevated temperatures and moisture content) cause a reduction in compressive strength of composite materials. This strength reduction has been attributed to degradation of the fiber/matrix interfacial bond[122] and a reduction in the matrix moduli.[119]

3.0 EXPERIMENTAL PROCEDURES

3.1 Materials

The material selected for this investigation is APC-2, an Aromatic Polymer Composite manufactured by Fiberite Corporation — An ICI (Imperial Chemical Industries) Company.[137–142] APC-2 is an advanced structural composite composed of continuous carbon fibers and "Victrex" PEEK (Polyetheretherketone) semi-crystalline thermoplastic matrix. Compared with other types of thermoplastic resins, PEEK has a potentially higher service temperature, $\approx$ 121°C) and is unaffected by solvents.

The glass transition temperature, T_g, for PEEK is 143°C, and the melting temperature, T_m, is 335°C. A compatible high strain carbon fiber (AS4) has been chosen for this composite system. The carbon fibers are well dispersed and thoroughly wetted in the PEEK matrix to give a fiber content of 61% by volume and 68% by weight. APC-2 is recognized for its specially developed interface science to provide effective stress transfer between the fibers and the matrix, and thus, the full properties of the carbon fiber are realized. This thermoplastic system was selected for this investigation because the compression strength of thermoplastics in general is a primary concern for industry applications. Typically, thermoplastics have compression strength values approximately 50% less than the observed tensile strength, compared to 75–80% for graphite/epoxy systems.

Literature regarding the mechanical property data base for the thermoplastic composites, in particular APC-2, includes mechanical property characterization (Refs. 117, 118, 123, 137, 138, 139), the effects of processing variables on mechanical properties,[117,137,140,141] the effects of fiber characteristics on mechanical

properties,[123] and the effects of matrix properties on mechanical properties.[117,118] The effects of the crystallinity on the mechanical properties is described in Ref. 140. The morphology of the PEEK resin is described in Refs. 137 and 142. These references provide a data base for material property comparison with the results of this report research.

In order to evaluate the factors that affect the compressive failure strength, the laminate stacking sequence has been varied systematically. A relatively simple baseline stacking sequence, $[(\pm 45/0_2)_3/ \pm 45/0]_s$, has been selected. Systematic variations of this stacking sequence allow for a detailed study of the effects of supporting fiber orientation, fiber waviness, interfacial bond strength, and resin-rich regions between plies. For consistency, these variations are made through the laminate thickness. Experimental results[143] indicate that the strength of symmetric composite laminates containing identical ply orientations can be strongly dependent on the detailed stacking sequence. Consequently, the Pipes and Pagano analysis[143] was used to verify that the interlaminar peel stresses for each stacking sequence were a reasonable.

The complete test matrix, including all variables (supporting fiber orientation, fiber waviness, interfacial bond strength, and resin-rich regions) is shown in Table I. The following discussion summarizes the laminates to be tested to determine the effects of each of the previously mentioned independent variables on fiber microbuckling initiation.

Table II details the laminates used to study the effects of the local constraint (supporting fiber orientation) on fiber microbuckling initiation. Five stacking sequences of APC-2 will be used to vary the support to the 0° fibers. The ±45° plies in the baseline stacking sequence were replaced with either ±15°, ±75° plies, or 90_2°

plies. Additionally, the 45s and 0s are interchanged in one laminate to determine the effect of surface 0s on compression strength.

Table III lists the 3 laminates used to determine the effects of fiber waviness on fiber microbuckling initiation. Note that the baseline lay-up has been altered slightly for this study. The APC-2 baseline lay-up has become $[\pm 45/0/90]_{3s}$ so that the theoretically straight 0/90 tape plies in this stacking sequence may be replaced with Quadrax $\langle 0/90 \rangle$ interlaced plies, where $\langle\ \rangle$ designates one interlaced ply. Quadrax Unidirectional Interlaced Tapes[144] are formed by interlacing ribbons or strips of APC-2 prepreg. Ribbons may vary from 3.175 mm to 12.7 mm in width. The Quadrax process is different from traditional weaving in that the fibers are impregnated first and then interlaced rather than weaving the fiber tows and then impregnating the resin. Consequently, the process is only applicable for thermoplastic composites. Two degrees of waviness and thus, interlacing, have been selected: (1) plain weave, 1-harness Quadrax and (2) 8-harness Quadrax.

The interfacial bond strength is varied by using two different materials, both with the baseline stacking sequence (Table IV). One panel is made with APC-2 which has a strong interfacial bond, and the other panel is made with non-surface treated AS4 fibers (provided by Hercules, Inc.) in PEEK matrix. Experience and previous work at ICI indicates this combination will provide a very poor fiber/matrix interface.

The effect of the resin-rich regions (Table V) is evaluated by adding a PEEK resin film at each 45/0 interface through the thickness of the baseline stacking sequence. In the stacking sequences, the addition of the resin film is denoted by "f." Two differeng thicknesses, 0.025 mm (f) and 0.075 mm (f_3), of resin film were added to the laminates.

C-2

3.2 Methods

3.2.1 Compression Specimen Geometry

The compression specimen is 2.54 cm wide by 10.16 cm long with a semi-circular notch (3.175 mm diameter) at each free edge, centered along the gage section. The gage length for this specimen in is 2.54 cm. Preliminary experimental results, detailed in Ref. 145, indicate that reducing the gage length from 5.08 cm (used in Refs. 1–4) to 2.54 cm does not introduce significant end effects but does minimize specimen bending and the incidence of Euler buckling. It should be noted that for the end-loading type test methods, the effects on the stress field in the test section are less pronounced than stress concentrations that are a consequence of the shear loading mechanism inherent in the IITRI fixture. These specimens were strain-gaged front and back (at the specimen's center) with longitudinal strain gages to monitor any specimen bending and to provide accurate measurement of the fiber microbuckling initiation strains. For the room temperature tests, 21°C, the strain gages were bonded to the specimens using M-Bond 200 adhesive and catalyst, and for the high temperatures tests, 77°C, M-Bond 600 adhesive was used. Both adhesives and the catalyst were manufactured by Micromeasurements Group, Inc.

3.2.2 Compression Test Methods

Although many compression test methods for composite materials are summarized in Section 2.0 of this report, the author suspects that a large percentage of these methods inhibit the natural failure mode for a laminate by supporting the specimen's test section in a manner that suppresses or prevents short-wavelength buckling.

Compression tests were conducted in a specially designed ultra high axial

alignment Material Test System (MTS) machine in the Materials and Structures Laboratory of Texas A&M University. The specimens were loaded in compression to microbuckling initiation and/or failure in the servo-controlled hydraulic test stand at three relatively slow rates in displacement control to provide more stable growth of the damage zone. The fiber microbuckling process occurring in the radius of the semi-circular edge notches was monitored using a Wild M8 Zoom Stereomicroscope equipped with a video system for real-time recording or a 35 mm camera to obtain intermittent photographs. This testing system is shown in Fig. 27. Tests were interrupted at the first indication of fiber microbuckling and subsequently observed in the SEM.

The specially designed MTS (previously described) contains a collet-type grip arrangement. The collet inserts which grip the specimen are machined for an ideal specimen thickness, e.g. 5.334 ± 0.025 mm. However, due to the nonuniform thickness of laminated composite panels, most specimens in past compression tests (Refs. 1–4, 145) were shimmed symmetrically with precision brass shims to properly fit into the MTS grips.

To further improve the alignment and gripping support provided during the compression tests, a fixture has been designed to allow resin shims to be cast symmetrically onto the specimen ends. The Shim Casting Fixture, including appropriate component labels, is shown in Fig. 28. The composite specimen (A) is centered in Teflon (annealed prior to machining) molds (B) using two Mitutoyo micrometer heads (C) with nonrotating spindels. Set screws (D) hold the micrometer heads in the fixture. Each Teflon mold contains a 3.175 mm diameter resin injection port (E). Steel end caps (F) are pulled tight against the specimen ends using a set screw and dovetail arrangement (G) to prevent the resin from

covering the already machined specimen ends and to prevent leakage. After the specimen is properly centered in the fixture, resin is injected into the bottom mold until the mold is completely filled. To prevent leakage, a 3.175 mm diameter Teflon rod is inserted into the injection port. After the resin is cured, the fixture is turned upside down and resin shims are cast, by the same method, onto the other end of the specimen. Consequently, the thickness of the specimen plus the cast shims is within the thickness tolerances required by the collet inserts, and the shims are uniformly bonded to the specimen ends. The specimen design reduced the global bending significantly.

The epoxy used as shim material consists of an all-purpose resin, D.E.R. 31[146], and a curing agent or hardener, D.E.H. 24[146], supplied by The Dow Chemical Company[147], Freeport, Texas. The epoxy was mixed using the recommended ratio of 13 parts by weight (8.22 cc) of hardener per 100 parts by weight (50 cc) of resin. The cure schedule for the epoxy was one hour at 100°C.

Some preliminary high temperature tests were conducted at 77°C to provide variation in the constitutive behavior of the PEEK matrix, and thus, additional variation in the support provided to the 0° fibers.

To provide easier observation and access to the specimen, a forced-air heat gun (also used in Ref. 135) with a controller, rather than an environmental chamber, was used to heat the specimen gage section. In addition to easier access, the heat gun heats the specimen to the test temperature much quicker (10 min. compared to 1 hr) than the traditional environmental chamber which also must heat the massive MTS grips. The high temperature test set-up is shown in Fig. 29. These tests will also be conducted in displacement control at the same three rates previously mentioned. It should be noted that General Dynamics in Fort Worth, Texas used

the forced-air heat gun because it more realistically, compared to an environmental chamber, simulates the heat spikes typically experienced by aircrafts.

Two types of experimental information were obtained from these notched compression tests. First, the nominal strain associated with the initiation of fiber microbuckling was measured. It should be noted that this value is the strain at which either in- or out-of-plane fiber microbuckling is sufficiently general to be observed with the stereomicroscope. This strain level has been defined as fiber microbuckling initiation, ϵ_I. Second, the measured nominal strain was used in conjunction with two-dimensional finite element analysis to determine the local strain at the notch during fiber microbuckling initiation.

3.2.3 X-radiography

Dye-penetrant enhanced X-radiography was the nondestructive technique used to monitor matrix cracking. To act as an enhancing agent, a zinc iodide solution is applied to the surface damage to infiltrate to the connected interior damage. The zinc iodide solution consists of 60 grams of zinc iodide, 10 ml of water, 10 ml of isopropyl alcohol, and 10 ml of Kodak "Photo-Flo 600" to act as a wetting agent.

3.2.4 Scanning Electron Microscopy

Most nonconductive specimens examined in the scanning electron microscope (SEM) need to be coated with a thin film of conducting material. This coating is necessary to eliminate or reduce the electric charge which builds up rapidly in a nonconducting specimen when scanned by a beam of high-energy electrons. Because of the high conductivity of the carbon fibers and low conductivity of the resin and plastic cold-mount, charging was anticipated as a problem for the uncoated specimen. Therefore, each specimen surface for SEM examination was

sputter-coated with a thin film of gold palladium approximately 100$\mathring{A}$ thick, and then it was examined in a JEOL JSM T330A. Delamination fracture surfaces and unpolished shear crippling zones were examined at a relatively long working distance (48 mm) to provide a greater depth of field, and thus, facilitate the observation of the topography of the fracture surfaces. Polished specimen surfaces, specimen cross-sections, and sectioning surfaces were examined at a shorter working distance (10 mm) to increase the resolution and contrast highlights of the damage. Additionally, a low accelerating voltage of 5 kV was used to further increase the contrast of the specimen surfaces.

3.2.5 Sectioning Studies

Guynn[1] developed techniques for sectioning, polishing, and observing (in the SEM) damage caused by compressive loading of the previously described specimens. This methodology is used to accumulate a more detailed understanding of the effects of the six independent variables in this investigation on the micromechanisms of compressive failure. The Struers Precision Saw usa utilized for the major sectioning cuts while the thinner cuts and final polishing (preparation for microscopy) was accomplished using a microprocessor controlled grinding and polishing machine also manufactured by Struers (Abramin Automated Polishing Unit).

3.2.6 Material Property Characterization

Material Data — The mechanical properties for the constituent materials, PEEK matrix and AS4 fibers, are given in Table VI. The fiber diameter is 7μm. Additionally, the lamina material properties are summarized in Table VI. Table VII summarizes the two coefficients of thermal expansion, α_1 and α_2, valid for two different temperature ranges. The laminate engineering constants, E_x, E_y, G_{xy},

and ν_{xy} for each stacking sequence were computed using a basic laminate theory program, and these constants are summarized in Table VIII.

Determination of Lamina Constitutive Behavior — The constitutive behavior for shear loading was determined from tensile and compressive tests of a $[\pm 45]_{ns}$ laminate where n is 2 for tension and n is 8 for compression tests, listed in Table IX. These tests were conducted at the same temperatures (21°C, 77°C, and 132°C) as the notched compression tests. The elevated temperature tests give a considerable change in the shear stress "yield strength."

The specimens for the tensile tests were 2.54 cm wide by 22.9 cm long with two 2.81 cm long glass/epoxy tabs bonded to each end of the coupon.[148] The specimens for the compression tests were prepared in a manner similar to the notched compression specimens except without the edge notches. High-strain (5%) longitudinal-transverse strain gages were bonded onto both types of specimens using M-Bond AE-15, a high strain (15%) adhesive manufactured by Micromeasurements Group, Inc. The tests were conducted in displacement control at a rate of 1 mm/min.

Two specimens, one compression-loaded and one tension-loaded, were monitored for matrix cracking with nondestructive examination, namely dye-penetrant enhanced X-radiography. Each of these tests was paused at every one percent increment of longitudinal strain. The dye-penetrant was applied, allowed to soak, and then the X-ray was taken.

The nonlinear shear stress-strain relationship for these laminates was calculated using the method described by Refs. 70–72, 149. From the remotely applied axial stress, σ_x, the longitudinal strain, E_x, and the transverse strain, E_y, the in-plane shear stress, τ_{12}, and the in-plane shear strain, γ_{12}, in each lamina are computed

by the following equations:

$$\tau_{12} = \frac{\sigma_x}{2} \tag{48}$$

and

$$\gamma_{12} = \epsilon_x - \epsilon_y = |\epsilon_x| + |\epsilon_y| \tag{49}$$

so that the in-plane shear modulus of a lamina, G_{12}, is computed by

$$G_{12} = \frac{\tau_{12}}{\gamma_{12}} = \frac{\sigma_x}{2(\epsilon_x - \epsilon_y)} \tag{50}$$

from the linear portion of the shear stress-strain data. Using Eqns. 48 and 49, the nonlinear shear stress-strain behavior of the lamina was determined.

Measurement of Initial Fiber Curvature — A technique to measure either in- and/or out-of-plane fiber waviness is presently being developed by Dr. Alton Highsmith at Texas A&M University. This technique employs a Hewlett Packard plotter, a personal computer, and a cross-haired eyepiece or stylus that replaces the plotter pen. Points are digitized along a fiber to track the waviness. This technique will be used to compare the degree of fiber waviness of the laminates listed in Table III.

Determination of Fiber/Matrix Interfacial Bond Strength — Techniques to measure the fiber/matrix bond strength are summarized in Ref. 150. The fiber/matrix interfacial bond strength will be determined in a semi-quantitative way using the Interfacial Testing System[151–153] developed at Dow Chemical in Freeport, Texas. This test is very similar to the "microdebonding test" developed by Mandell et al.[154] In this test, the load is applied to one fiber end within a laminate

cross-section until local fiber/matrix debonding occurs. This test will be applied to specimens from each of the two panels in Table IV. Additionally, the interfacial bond strengths may be compared qualitatively with results from the Mode I fracture toughness tests.

Delamination Fracture Toughness — The delamination fracture toughness, or the resistance to fracture in the presence of a crack, is normally expressed in terms of the critical energy release rate, G_c. G_c for Mode I loading (G_{Ic}) will be determined using three double cantilever beam (DCB) specimens from each of the two unidirectional laminates listed in Table IV. One of these laminates will be made of APC-2 (good fiber/matrix bond). The other laminate will consist of non-surface treated AS4 fibers (provided by Hercules, Inc.) in PEEK resin, a combination known to produce a poor fiber/matrix interfacial bond. These tests will provide a comparison of G_{Ic} between the APC-2 composite with a strong interfacial bond and an otherwise identical system with a poor interfacial bond. G_{Ic} will be computed using the area method as described by Whitney et al[155] and/or Keary et al.[156] The area method allows nonlinear elastic behavior with inelasticity limited to a small volume of material surrounding the crack tip. This method has been selected in anticipating that the APC-2 behavior will be nonlinear elastic. The DCB specimens will be 2.54 cm wide, 25.4 cm long, containing a Kapton insert at the midplane of one end of the specimen to provide a starter crack. The insert will be 2.54 cm square and approximately 0.025 mm thick. Additionally, it should be noted that each laminate in Table I (except $[\pm 45]_{ns}$) contains a Kapton insert in one corner of the laminate. Consequently, if significant discrepancies are evident in the experimental results, up to three fracture toughness tests may be conducted on each of these multidirectional laminates in the proposed test matrix.

FINITE ELEMENT ANALYSIS

Geometric and material nonlinear two-dimensional finite element analysis (implementing ABAQUS) is being used to investigate the free surface effects in the straight fiber problem and the initial fiber curvature effects on the shear strain developed in the matrix.

4.1 Theory

4.1.1 The Straight Fiber Problem

The buckling analysis of perfectly straight fibers embedded in matrix (bifurcation instability[157,158]) is the classical Euler column analysis which has the form of the generalized eigenvalue problem

$$[A]\{v\} = \lambda[B]\{v\} \tag{51}$$

where $[A]$ and $[B]$ are symmetric matrices, λ is a scalar, and $\{v\}$ is a vector. When λ_i and v_i satisfy Eqn. 51, they are called an eigenvalue and eigenvector, respectively. The main objective of an eigenvalue formulation and solution in instability analysis is to predict whether small disturbances, imposed on the equilibrium configuration, increase substantially. The load or strain level at which this situation occurs corresponds to the critical load or strain of the system.

In a stability problem, a load may be reached where deflections increase more rapidly than predicted by linear solution. It is even possible to reach a state where the load carrying capacity decreases with increasing deformation. Consequently, for accurate determination of the displacements, geometric nonlinearity (finite

rotations) must be considered. The Lagrangian nonlinear strain-displacement relations (displacements are referred to original configuration) are of the form

$$\epsilon_x = \frac{\partial u}{\partial x} + \frac{1}{2}\left[\left(\frac{\partial u}{\partial x}\right)^2 + \left(\frac{\partial v}{\partial x}\right)^2\right]$$

$$\epsilon_y = \frac{\partial v}{\partial y} + \frac{1}{2}\left[\left(\frac{\partial u}{\partial y}\right)^2 + \left(\frac{\partial v}{\partial y}\right)^2\right] \tag{52}$$

$$\epsilon_{xy} = \frac{\partial u}{\partial y} + \frac{\partial v}{\partial x} + \frac{\partial u}{\partial x \partial y} + \frac{\partial v}{\partial x \partial y}$$

The generalized eigenproblem to be solved for the classical Euler problem described is of the form

$$([K_o] + \lambda[K_g])\{u\} = 0 \tag{53}$$

where $[K_o]$ represents the usual, small displacements or linear stiffness matrix, $[K_g]$ is the initial stress matrix or geometric matrix, and $\{u\}$ is the displacement vector. The initial stress matrix represents the change in stiffness going from the initial state to the applied load state and is proportional to the change in load. In the solution of this problem, λ denotes the increase factor on applied strains necessary to achieve instability.

4.1.2 The Wavy Fiber Problem

Once the fibers are no longer considered perfectly straight, as typically observed in composites, the problem to be solved is not the classical Euler problem. Recall that the term "fiber microbuckling" refers to large lateral deflections of initially wavy fibers leading to fiber breakage, rather than a bifurcation instability.

Compared to bifurcation instability, fiber microbuckling is a gradual process. In the wavy fiber case, instability is defined as the point at which additional applied displacement no longer gives an increase in the load carried by the column. Although geometric nonlinearity (Eqn. 52) is still considered, the problem solution is an incremental plastic stress-strain analysis.

4.2 Models

Two-dimensional finite element analysis was used to model fiber microbuckling in two different configurations: 1) straight fibers surrounded by matrix and 2) wavy fibers surrounded by matrix. The straight fiber problem was modelled for two reasons. First, the straight fiber problem illustrates the ideal situation for composites, and second, this model was used to show the effects of the free surface on fiber microbuckling initiation. The effects of initial fiber curvature and matrix nonlinearity on the amount of shear strain developed in the matrix are demonstrated for a preliminary wavy fiber model.

Three types of configurations were modelled for the straight fiber problem. For these models, symmetry was utilized, so that only one-half of the column length was modelled. The three configurations were the infinite plate, the semi-infinite plate, and the finite plate consisting of ten fibers and matrix. The geometries for these three models are shown in Fig. 30. It should be noted that these descriptive names are meant to imply that the model is sufficiently wide so that the interior fibers are not near a free surface; the names do not imply that the model is infinitely wide. The infinite plate (Fig. 30a) consisted of ten fibers (cross-hatch regions) separated by matrix (white regions) with support provided on each side by an equivalent homogeneous orthotropic material (dotted regions). The equivalent

regions replace the heterogeneous unidirectional lamina and effectively represent a set of smeared elastic properties. Note that since these equivalent properties are from a unidirectional lamina, they include the initial fiber curvature. The purpose of these regions is to simulate the stiffness of adjacent material in the lamina. Each of these regions are the same width as the ten fibers and matrix. A half-matrix layer exists between the outer fibers and the equivalent regions. The semi-infinite plate (Fig. 30b) was similar to the infinite plate, but contained only one equivalent region. Consequently, a fiber and a half-matrix were located at a free surface. Finally, the ten fiber model (Fig. 30c) consisted of ten fibers separated by matrix with half-matrix layers at both outer surfaces. In this case, two free surfaces exist.

To show the initial fiber curvature effects on the shear strain developed in the matrix, a preliminary model with one fiber with half-matrix on either side was modelled, as shown in Fig. 31. In progress work includes adding multipoint constraints to the preliminary model previously described to make it an infinitely wide model. This model will be used to show the fiber curvature effects on the shear strain developed in the matrix in an infinitely wide model, as an upper bound. Other models include two fibers and matrix with two homogeneous equivalent regions on each side, similar to the infinitely wide straight fiber problem. This model will be used to show the curvature effects on models of finite width. Additionally, the meshes in these models are being refined to verify convergence. Four different values of initial fiber waviness are being modelled. The initial fiber curvature is expressed as the ratio of the amplitude to the length, $\frac{a_o}{L}$, of the wave. A sine wave is used to approximate the fiber curvature.

In these models (both straight and wavy fiber), the fiber volume fraction, V_f, is 60% and the diameter of the fiber modelled, d_f, is 7.6 μm. The width of the

modelled matrix regions are equal and were determined to be 5.1 μm, based on d_f and V_f. The length of the fiber, L, was selected based on measurements from SEM micrographs. The ratio $\frac{L}{d_f}$ was measured ,from the micrographs (e.g., Fig. 37), to be 87. All of the geometries are modelled with one end of the column fixed and nodal displacements applied at the symmetry line of the column.

4.3 Implementation

The finite element analysis was accomplished using ABAQUS Version 4.7-25 (1987), developed by Hibbitt, Karlsson & Sorenson. PATRAN, Release 2.3A-1, developed by PDA Engineering, was used for mesh generation and post-processing. Data were translated between ABAQUS and PATRAN using PATABA: The PAT/ABAQUS Application Interface, Release 3.0A, ABAPAT: The ABAQUS/PAT Application Interface, Release 3.0A, both developed by PDA Engineering, and a translator, written by the author, to prepare the stress-strain data from the elements in the model for x–y plotting.

The matrix, fibers, and homogeneous regions were modelled using ABAQUS S8R5 elements. These elements are doubly curved shells with eight nodes and reduced integration, primarily used for thin shell applications. The elements allow five degrees of freedom (three displacements and two in-surface rotations) per node at all nodes except those with specified boundary conditions. At nodes where the boundary conditions are specified, these elements allow six degrees of freedom per node.

4.3.1 ABAQUS Procedures

ABAQUS contains a capability for estimating elastic buckling by eigenvalue extraction. This estimation is typically useful for "stiff" structures, where the pre-

buckling response is almost linear. The buckling load estimate is obtained as a multiplier of the applied loads. The nontrivial solutions to Eqn. 53 provide the estimated buckling strain as $\frac{\lambda_i q}{L}$ (q is the magnitude of the applied nodal displacements), while the corresponding eigenvector $\{u_i\}_i$ gives the associated buckling mode. ABAQUS only provides an eigensolution for symmetric systems, which means $[K_o]$ and $[K_g]$ must be symmetric, implying that the system has real, positive eigenvalues only. ABAQUS implements the subspace iteration method, using the Householder and Quarter-Rotation algorithm for the reduced eigenproblem.

4.3.2 Constituent Properties

The equivalent stress-strain behavior of the resin was derived from the lamina τ_{12}–γ_{12} data. For the analysis it was assumed that the resin is isotropic, homogeneous, and has constitutive behavior which can be expressed in the form of the Ramberg-Osgood equation. Additionally, it was assumed that $G_f \gg G_m$ ($\frac{G_m}{G_f} = 0.046$), and thus, the shear is primarily transferred by the resin. Using these assumptions, $\tau_{12} = \tau_{12f} = \tau_{12m}$ and $\gamma_{12m} = \frac{\gamma_{12}}{V_m}$. The subscripts f and m correspond to the fiber and matrix, respectively. Once the shear constitutive behavior of the resin was derived, the equivalent stress-strain ($\overline{\sigma}$–$\overline{\epsilon}$) behavior of the resin was computed using

$$\overline{\sigma} = \left[\frac{1}{2}\left[(\sigma_x - \sigma_y)^2 + (\sigma_y - \sigma_z)^2 + (\sigma_z - \sigma_x)^2\right] + 3\left[\tau_{xy}^2 + \tau_{yz}^2 + \tau_{zx}^2\right]\right]^{\frac{1}{2}} \qquad (54)$$

and, for proportional loading (the components of applied stress remain in constant ratio to one another throughout the straining process) only,

$$\overline{\epsilon} = \left[\frac{2}{9}\left[(\epsilon_x - \epsilon_y)^2 + (\epsilon_y - \epsilon_z)^2 + (\epsilon_z - \epsilon_x)^2\right] + \frac{1}{3}\left[\gamma_{xy}^2 + \gamma_{yz}^2 + \gamma_{zx}^2\right]\right]^{\frac{1}{2}}. \qquad (55)$$

Proportional loading may be assumed because this data is derived from a tensile test. For the stress state in the $[\pm 45]_{ns}$ specimens, the equivalent stress-strain behavior was reduced to

$$\overline{\sigma} = \sqrt{3}\tau_{xy} \tag{56}$$

and

$$\overline{\epsilon} = \frac{1}{\sqrt{3}}\gamma_{xy}. \tag{57}$$

The nonlinear constitutive behavior of the resin was fit using the Ramberg-Osgood stress-strain relation

$$\overline{\epsilon} = \frac{\overline{\sigma}}{E} + \frac{\alpha\overline{\sigma}}{E}\left[\frac{|\overline{\sigma}|}{\sigma_o}\right]^{n-1} \tag{58}$$

where α is the yield offset, σ_o is the yield stress, E is the Young's modulus, and n is the hardening exponent for the plastic term. Assuming $\alpha = 1$ and E as given in Table 1, the values determined for n and σ_o for the best fit through the data are given in Table XI. It should be noted that all computations were completed in U.S. units, and the constants were then converted to S.I. units.

For the straight fiber problem, the fibers were assumed to be transversely isotropic, having the properties of the AS4 fiber given in Table VI. However, for the wavy fiber problem, the fiber was assumed to have the isotropic behavior shown in Table VI. Two types of isotropic fiber properties were assumed for this analysis. In one case (Type *a*), E_{11} and ν_{12} are fixed ($E_{22} = E_{11}$) to the actual values and G_{12} necessary for isotropy is computed. In the other case (Type *b*), G_{12} and ν_{12} are fixed to the actual values and E_{11} necessary for isotropy is computed ($E_{22} = E_{11}$).

However, in shear instability models (Refs. 33, 34, 36, 126–128), the researchers have shown that the resistance to failure is controlled by the shear properties of the foundation and the column. Addtionally, the results of Hayashi[34] and Kulkarni et al[48], analyses that neglect $\frac{G_m}{G_f}$, indicate that as G_f is increased, the compressive strength of the composite is increased. Consequently, the Type *b* properties are used for the wavy fiber models. For these fibers, $\frac{G_m}{G_f} = 0.046$.

The unidirectional lamina properties for APC-2 were given in Table 1. These properties were used for the equivalent homogeneous properties in the infinite and semi-infinite models. The equivalent regions were assumed to be linear elastic and in a state of plane stress, consistent with laminate theory.

5.0 EXPERIMENTAL RESULTS AND DISCUSSION

5.1 Lamina Constitutive Behavior

The shear stress-strain curves obtained from both tension and compression testing (see Table IX) for the APC-2 laminae, derived from Eqns. 48 and 49, are shown in Fig. 32. Radiographs, shown in Figs. 33 and 34, indicate that matrix cracking has initiated in the tension-loaded specimens (Fig. 33) by the 2% axial strain level while the radiograph of the compression specimen (Fig. 34) shows no signs of damage at axial strain levels up to 9.7%. The flatter curve in Fig. 32, obtained from tension testing, is attributed to matrix cracking in the laminate. Consequently, compression testing of $[\pm 45]_{8s}$ specimens was selected for determination of the lamina constitutive behavior. Lamina shear constitutive behaviors obtained from compressive loading, derived using Eqns. 48 and 49, for 21°C and 77°C tests are shown in Fig. 35. The derived resin shear constitutive behaviors for 21°C and 77°C are shown in Fig. 36. Additionally, an assumed theoretically linear behavior has been added to the figure. From this data the elastic shear modulus of the resin, G_m, was measured to be 2.0 GPa, significantly higher than given in Table VI.[137] The higher PEEK shear modulus is attributed to the fiber contribution and the fiber/matrix interaction. These curves indicate a significant reduction in the shear stress "yield strength" of the resin for the 77°C data. It is anticipated that this reduction decreases the amount of support for the fibers and reduces the strain level at which fiber microbuckling initiates.

5.2 Effects of Supporting Ply Orientation

The test matrix used to illustrate the effects of supporting ply orientation on

the initiation of fiber microbuckling in 0° plies was given in Table II. Data showing these effects are presented in this section.

Figure 37 shows a surface view of in-plane and out-of-plane fiber microbuckling of a $[(0_2/\pm 45)_3/0/\pm 45]_s$ laminate tested at 21°C. Figures 37a and 37b show the in-plane fiber microbuckling into the semi-circular notch and also fiber buckling out-of-plane toward the free surface. Higher magnifications of typical fiber damage, both shear and tensile/bending-type fiber breaks, are shown in Figs. 37c and 37d. Figure 37a was one of the micrographs used to measure the column length modelled in the finite element analysis.

Figure 38 is a bar chart showing the average remote axial strain for fiber microbuckling initiation, ϵ_I, for two lay-ups, one with ± 45 plies as surface plies and one with 0_2 plies as surface plies. In-plane fiber microbuckling initiated in specimens with ± 45 plies as surface plies at strain levels of $\approx 7042\ \mu\epsilon$. On the other hand, out-of-plane fiber microbuckling toward the free surface initiated in the specimens with 0_2 plies as surface plies at strain levels of $\approx 4580\ \mu\epsilon$. These strain levels indicate a 35% reduction in the remote initiation strain level for specimens with out-of-plane fiber microbuckling, compared to initiation by in-plane fiber microbuckling. This 35% reduction emphasizes the importance of including the effect of the free surface in fiber microbuckling models for accurate predictions. Similar reductions were reported in Ref. 96.

The effects of supporting ply orientation on in-plane fiber microbuckling are shown in Fig. 39. This bar chart shows the average remote axial strain level for in-plane fiber microbuckling initiation in specimens with ± 15, ± 45, ± 75, and 90_2 plies as surface plies. The data indicates the ± 75 plies provide the most resistance to fiber microbuckling while the ± 15 plies provide the least resistance. However, this

result did not seem intuitive to the authors. Consequently, the SCFs were computed using the two-dimensional finite element analysis of an orthotropic plate with two semi-circular edge notches. Additionally, fringe plots of the stress distributions (not included) were examined to verify that the strain gages were in remote locations, with respect to the notches, on the specimens. The SCFs are listed in Table XII for these laminates, and the local fiber microbuckling initiation strain levels are shown as a function of the supporting ply orientation in the bar chart in Fig. 40. The trend in Fig. 40 also indicates that an optimum angle ($\approx 75°$) of supporting ply orientation exists, maximizing the resistance to in-plane fiber microbuckling, a direct consequence of the local constraint. More indirectly, the various supporting ply orientations cause different residual stresses in the laminate, and thus, a different initial stress state that may influence the fiber microbuckling process and initiation levels.

Observation of the local strain values in Fig. 40 poses another question; namely, what about fiber failure? Tensile failure strains for AS4 fibers are reported to be 1.45%.[159] However, DeTeresa[160] has observed fiber shear failure strains of $\approx 3.6\%$ for a single AS4 fiber embedded in matrix and loaded in compression. To investigate this phenomenon, one of the notches of a baseline specimen was observed in the SEM, prior to testing. Then, the specimen was loaded to a local strain level of $\approx 1.7\%$ at the notch and unloaded. Observation of the specimen under an optical microscope indicated that the discontinuous 0° plies have protruded into the notch, similar to the result in Refs. 104 and 105. Subsequent SEM examination of the same notch showed failure by fiber shear and microbuckling. Micrographs showing the multiple fiber failures are shown in Fig. 41. Figure 41a shows an overview of the fiber damage in one of the group of 0s closer to the specimen free surface.

Figure 41b is a higher magnification (from a) of multiple failures by fiber shear. Figure 41c shows the fiber damage in the center group of 0s; these plies had the highest apparent density of fiber breaks. Figure 41d is an excellent example of a fiber shear failure. One possible explanation for fiber shear failures is as follows. Assume that each of the fibers in a ply have different initial in-plane curvatures. Consequently, the straighter fibers support a higher local stress than those with the larger initial curvatures. These straighter fibers then reach the stress level necessary to cause fiber shear, prior to ply microbuckling and catastrophic damage development. These micrographs indicate that failure by fiber shear may precede failure by fiber microbuckling in these thermoplastic laminates, although failure by fiber microbuckling still appears to be the strength limiting stage of compression strength of composites.

5.3 Effects of Resin-Rich Regions Between Plies

The test matrix for the effects of resin-rich regions between plies was summarized in Table V. The room temperature data illustrating these effects are shown in the bar chart in Fig. 42. In-plane fiber microbuckling initiated at strain levels of $\approx$ 7042 $\mu\epsilon$ for the baseline lay-up, $\approx$ 6580 $\mu\epsilon$ for the laminate with one layer of neat resin at the 0/45 interfaces, and $\approx$ 5475 $\mu\epsilon$ for the laminate with three layers of neat resin at the 0/45 interfaces. Compared to the baseline lay-up, the introduction of one layer of neat resin at the 0/45 interfaces through the laminate thickness causes a 7% reduction in the strain level for in-plane fiber microbuckling initiation. Coincidently, the addition of three layers of neat resin at 0/45 interfaces through the laminate thickness causes a 22% reduction (compared to the baseline lay-up) in the initiation strain level, approximately three times the reduction caused

by the addition of one layer of resin. These results indicate that the addition of soft resin layers on each side of the 0_2 plies significantly reduces the resistance to in-plane fiber microbuckling. These resin additions also allow more out-of-plane fiber microbuckling into the resin-rich regions.

5.4 Effects of Resin Constitutive Behavior

The lamina, and thus resin, constitutive behavior was varied by testing at two temperatures 21°C and 77°C. The change in the shear constitutive behavior, attributed to temperature effects, was shown in Fig. 35 for the lamina and in Fig. 36 for the neat resin. Some preliminary results showing the effects of the resin constitutive behavior on the initiation of fiber microbuckling in the baseline laminates are shown in Fig. 39. These average remote axial initial strain results show that for the baseline lay-up, in-plane fiber microbuckling initiates at $\approx$ 7042 $\mu\epsilon$ at 21°C and at $\approx$ 5830 $\mu\epsilon$ at 77°C. These results indicate that for the baseline lay-up, reducing the resin shear stress "yield strength" causes a 17% reduction in the strain level for in-plane fiber microbuckling initiation, and thus, significantly the resistance to in-plane fiber microbuckling.

6.0 FINITE ELEMENT RESULTS AND DISCUSSION

6.1 The Straight Fiber Problem

The critical buckling strains for the straight fiber problem are summarized in Table XIII. The infinite plate buckled at $\epsilon_{cr} = 2.77\%$ while the semi-infinite plate buckled at $\epsilon_{cr} = 2.49\%$. This result indicates that the free surface effect causes a 10% reduction in the critical buckling strain. Additionally, the finite plate (ten fibers and matrix) was modelled with both the anisotropic fiber properties and the two types of isotropic fiber properties to show the sensitivity of the critical strains to Young's modulus of the fiber. The finite plate with anisotropic fibers buckled at $\epsilon_{cr} = 1.53\%$, and the same plate with Type *a* isotropic fibers buckled at $\epsilon_{cr} = 1.64\%$ and Type *b* isotropic fibers buckled at $\epsilon_{cr} = 3.94\%$. This ten fiber model is similar to that of Rosen,[33] and thus, the results may be compared with Eqn. 2 where $\epsilon_{cr} = \frac{\sigma_c}{E_c}$. E_c is the composite modulus and using the Rule of Mixtures, $E_c \propto E_f$. Since the second term (Euler term for the fiber) of Eqn. 2 is only geometry dependent, the critical strain is dependent on the ratio $\frac{G_m}{E_f}$. As $\frac{G_m}{E_f}$ increases, the critical buckling strain also increases. The trends presented in Table XIII are consistent with Rosen's equation.

It should be noted that for the straight fiber problem, only linear-elastic constitutive behavior was assumed for the resin. Two reasons for this assumption exist. First, because the fibers are perfectly straight, no shear exists in the resin until after bifurcation buckling, and thus, nonlinear shear stress-strain behavior would not affect the results. Second, the eigenvalue analysis of all straight fiber problems with nonlinear resin behavior yielded hourglass modes. ABAQUS does not provide automatic hourglass control for nonlinear behavior for this particular shell element.

Consequently, the author did not show numerically that the finite element analysis would yield the same result for the straight fiber problem, regardless of linear or nonlinear constitutive behavior for the resin.

6.2 The Wavy Fiber Problem

The preliminary model used to illustrate the effect of the initial fiber waviness on the amount of shear strain in the matrix was shown in Fig. 31. The results for four different initial curvatures ($a_o/L = 0.000$, 0.005, 0.050, and 0.500) are shown in Fig. 43. In each case, Element 15 (approximately the element from each model with the maximum shear strain) is plotted. In Fig. 43, the absolute value of the elemental shear strain, γ_{12}, for Element 15 is plotted as a function of the absolute value of the elemental axial strain, ϵ_{11}. These results indicate that as the initial fiber curvature increases, the amount and rate of shear strain development in the resin per unit axial strain in the resin also increases. Results from the two fiber models show much larger shear shear strains and lower applied axial strains, due to the constraint provided by the fibers. Additionally, the curves (similar to Fig. 43) for the two fiber models turn upward asymtotically at axial strains $\approx 7\%$, caused by the shear strain in the matrix is approaching the resin shear stress "yield strength." It is expected that the infinite model will show lower axial strains, due to the additional constraints. Furthermore, as the initial curvature is increased, the axial strain at which the resin reaches its shear stress "yield strength" is decreased. Similar results were reported in Refs. 78 and 79 for an infinite model using a minimum potential energy approach. This preliminary result implies that excessive fiber waviness may cause localized shear strains to exceed the resin shear stress "yield strength" prematruely, reducing the support provided to the fiber. Consequently, the in-plane fiber microbuckling

initiation strain levels, and thus compression strength, are reduced.

7.0 SUMMARY OF ACCOMPLISHMENTS 08/01/88 THROUGH 11/30/89

The experimental results indicate that the local constraints (free surfaces, supporting ply orientation, and resin-rich regions) significantly affect the strain level for the initiation of in-plane fiber microbuckling. SEM examination of a damaged specimen indicates that multiple fiber breaks (shear and tensile type) appear to precede fiber microbuckling and occur at strain levels lower than those required for catastrophic damage. Additionally, preliminary results at an elevated temperature, 77°C, showed the shear stress "yield strength" of the resin was reduced and consequently, the resistance to fiber microbuckling was also reduced. Future work includes collecting additional data at room temperature and then a complete spectrum of fiber microbuckling initiation strain data at 77°C and 132°C.

The finite element analysis of the perfectly straight fiber problem indicates that the free surface effect causes a 10% reduction in the critical buckling strain. However, the experimentally measured reduction for fibers with an initial fiber curvature, was 35%. Furthermore, it was shown that increasing the initial fiber curvature causes a large increase in the rate and amount of shear strain developed in the matrix. This increase may cause localized shear strains to exceed the resin shear stress "yield strength" leading to premature fiber microbuckling initiation. Future modelling plans include completing this set of models for the shear strain in the matrix, a set of models to show the effects of the free surface on the wavy fiber problem, and a model to show the effects of a poor interface on fiber microbuckling.

8.0 REFERENCES

[1] Guynn, E.G., "Micromechanics of Compressive Failures in Open Hole Composite Laminates," Department of Mechanical Engineering, Texas A&M University, M.S. Thesis, December 1987.

[2] Guynn, E.G., Bradley, W.L., and Elber, W., "Micromechanics of Compression Failures in Open Hole Composite Laminates," in *Second Symposium on Composite Materials: Fatigue and Fracture, ASTM STP 1012*. Philadelphia, PA: American Society for Testing and Materials, 1989, pp. 118–136.

[3] Guynn, E.G. and Bradley, W.L., "Measurements of the Stress Supported by the Crush Zone in Open Hole Composite Laminates Loaded in Compression," *Journal of Reinforced Plastics and Composites*, vol. 8, March 1989, pp. 133–149.

[4] Guynn, E.G. and Bradley, W.L., "A Detailed Investigation of the Micromechanisms of Compressive Failure in Open Hole Composite Laminates," *Journal of Composite Materials*, vol. 23, May 1989, pp. 479–504.

[5] Leonard, L., "Compression Test Results—A Tough Nut to Crack," *Advanced Composites*, July/August 1989, pp. 57–63.

[6] Clark, R.K. and Lisagor, W.B., "Compression Testing of Graphite/Epoxy Composite Materials," in *Test Methods and Design Allowables for Fibrous Composites, ASTM STP 734*. C.C. Chamis, ED., Philadelphia, PA: American Society for Testing and Materials, 1981, pp. 34–53.

[7] Anon., "D695-85 Standard Test Method for Compressive Properties of Rigid Plastics," in *1985 Annual Book of ASTM Standards*. Philadelphia, PA: American Society for Testing and Materials, 1985, pp. 267–274.

[8] Anon., "D3410-75 (Reapproved 1982) Standard Test Method for Compressive Properties of Unidirectional or Crossply Fiber-Resin Composites," in *1982 Annual Book of ASTM Standards*. Philadelphia, PA: American Society for Testing and Materials, 1982, pp. 872–880.

[9] Anon., "C393-62 (Reapproved 1970) Standard Test Method of Flexure Test of Flat Sandwich Constructions," in *1962 Annual Book of ASTM Standards*. Philadelphia, PA: American Society for Testing and Materials, 1962, pp. 313–316.

[10] Anon., "D3410-87 Standard Test Method for Compressive Properties of Unidirectional or Crossply Fiber-Resin Composites," in *1987 Annual Book of ASTM Standards*. Philadelphia, PA: American Society for Testing and Materials, 1987, pp. 2573–2585.

8.0 REFERENCES (Continued)

[11] Shuart, M.J., "An Evaluation of the Sandwich Beam Compression Test Method for Composites," in *Test Methods and Design Allowables for Fibrous Composites, ASTM STP 734*. C.C. Chamis, ED., Philadelphia, PA: American Society for Testing and Materials, 1981, pp. 34–53.

[12] Hofer, K.E., Jr. and Rao, P.N., "A New Static Compression Fixture for Advanced Composite Materials," *Journal of Testing and Evaluation*, vol. 5, No. 4, July 1977, pp. 278–283.

[13] Camarda, C.J., "Application of the IITRI Compression Test Fixture at Elevated Temperature," NASA Langley Research Center, Hampton, VA, NASA Conference Publication 2079, March 1979.

[14] Woolstencroft, D.H., Curtis A.R., and Haresceugh, R.I., "A Comparison of Test Techniques Used for the Evaluation of the Unidirectional Compressive Strength of Carbon Fibre-Reinforced Plastic," *Composites*, October 1981, pp. 275–280.

[15] Gurdal, Z. and Starbuck, J.M., "Compressive Characterization of Unidirectional Composite Materials," in *Analytical and Testing Methodologies for Design with Advanced Materials*. G.C. Sih, J.T. Pindera, and S.V. Hoa, EDS., Elsevier Science Publishers B.V., 1988, pp. 337–347.

[16] Adsit, N.R., "Compression Testing of Graphite/Epoxy," in *Compression Testing of Homogeneous Materials and Composites, ASTM STP 808*. R. Chait and R. Papirno, ED., Philadelphia, PA: American Society for Testing and Materials, 1983, pp. 175–186.

[17] Ryder, J.T. and Black, E.D., "Compression Testing of Large Gage Composite Coupons," in *Composite Materials: Testing and Design (Fourth Conference), ASTM STP 617*. Philadelphia, PA: American Society for Testing and Materials, 1977, pp. 170–189.

[18] Chan, W., private communications, November 1987.

[19] Lamothe, R.M. and Nunes, J., "Evaluation of Fixturing for Compression Testing of Metal Matrix and Polymer/Epoxy Composites," in *Compression Testing of Homogeneous Materials and Composites, ASTM STP 808*. R. Chait and R. Papirno, ED., Philadelphia, PA: American Society for Testing and Materials, 1983, pp. 241–253.

[20] Chou, T., Stewart, W.B., and Bader, M.G., "On the Compression Strength of Glass-Epoxy Composites," *New Developments and Applications in Composites, TMS-AIME Publication*, 1979, pp. 331–346.

8.0 REFERENCES (Continued)

[21] Zhigun, I.G., Polyakov, V.A., and Mikhailov, V.V., "Compression Testing of Composites," Institute of Polymer Mechanics, Academy of Sciences of the Latvian SSR, Riga. Translated from Mekhanika Kompozitnykh Materialov, No. 6, pp. 1111-1118, November-December 1979. Original article submitted May 7, 1979.

[22] Rehfield, L.W., Armanios, E.A., and Changli, Q., "Analysis of Behavior of Fibrous Composite Compression Specimens," in *Recent Advances in Composites in the United States and Japan, ASTM STP 864*. J.R. Vinson and M. Taya, ED., Philadelphia, PA: American Society for Testing and Materials, 1985, pp. 236–252.

[23] Hahn, H.T. and Williams, J.G., "Compression Failure Mechanisms in Unidirectional Composites," in *Composite Materials: Testing and Design (Seventh Conference, ASTM STP 893*. J.M. Whitney, ED., Philadelphia, PA: American Society for Testing and Materials, 1986, pp. 115–139.

[24] Agarwal, B.D. and Broutman, L.J., *Analysis and Performance of Fiber Composites*, First Edition, New York, NY: John Wiley & Sons, 1980, pp. 48–57.

[25] Ewins, P.D. and Ham, A.C., "The Nature of Compressive Failure in Unidirectional Carbon Fibre Reinforced Plastics," *AIAA/ASME/SAE* 15^{th} *Structures, Structural Dynamics and Materials Conference*, Las Vegas, NE, April 1974.

[26] Greszczuk, L.B., "Compressive Strength and Failure Modes of Unidirectional Composites," in *Analysis of the Test Methods for High Modulus Fibers and Composites, ASTM STP 521*. Philadelphia, PA: American Society for Testing and Materials, 1973, pp. 192–217.

[27] Tsai, S.W., "Strength Theories of Filamentary Structures," in *Fundamental Aspects of Fiber Reinforced Plastics*. R.T. Schwartz and H.S. Schwartz, EDS., New York, NY: Interscience Publishers (a division of John Wiley & Sons), 1968, pp. 3–11.

[28] Shuart, M.J., "Short-Wavelength Buckling and Shear Failures for Compression-Loaded Composite Laminates," NASA Langley Research Center, Hampton, VA, NASA Technical Memorandum 87640, November 1985.

[29] Camponeschi, E.T., Jr., "Compression of Composite Materials: A Review," Center for Composite Materials, University of Delaware, CCM 87-40, August 1987.

[30] Piggott, M.R., "Compressive Properties of Resins and Composites," in *Developments in Reinforced Plastics*. G. Pritchard, ED., New York, NY: Elsevier Applied Science Publishers, 1985, pp. 131–163.

8.0 REFERENCES (Continued)

[31] Dow, N.F. and Gruntfest, I.J., "Determination of Most Needed Potentially Possible Improvements in Materials for Ballistic and Space Vehicles," General Electric, TIS 60SD389, June 1960.

[32] Timoshenko, S.P. and Gere, J.M., *Theory of Elastic Stability*, Second Edition, New York, NY: McGraw-Hill Book Company, 1961.

[33] Rosen, B.W., "Mechanics of Composite Strengthening," Fiber Composite Materials, American Society for Metals Seminar, 1965, pp. 37–75.

[34] Hayashi, T., "On the Shear Instability of Structures Caused by Compressive Load," presented at the AIAA/RAES/JSAS Aircraft Design and Technology Meeting, Los Angeles, CA, November 1965, AIAA Paper No. 65-770.

[35] Jones, R.M., *Mechanics of Composite Materials*, First Edition, New York, NY: McGraw-Hill Book Company, 1975.

[36] Schuerch, H., "Prediction of Compressive Strength in Uniaxial Boron Fiber-Metal Matrix Composite Materials," *AIAA Journal*, vol. 4, January 1966, pp. 102–106.

[37] Dow, N.F., Rosen, B.W., and Hashin, Z., "Studies of Mechanics of Filamentary Composites," NASA Langley Research Center, Hampton, VA, NASA Contractor Report 492, June 1966.

[38] Foye, R.L., "Compression Strength of Unidirectional Composites," presented at the AIAA 3rd Aerospace Sciences Meeting, New York, NY, November 1966, AIAA Paper No. 66-143.

[39] Sadowsky, M.A., Pu, S.L., and Hussain, M.A., "Buckling of Microfibers," *Journal of Applied Mechanics*, December 1967, pp. 1011–1016.

[40] Lager, J.R. and June, R.R., "Compressive Strength of Boron-Epoxy Composites," *Journal of Composite Materials*, vol. 3, January 1969, pp. 48–56.

[41] Chung, W.Y. and Testa, R.B., "The Elastic Stability of Fibers in a Composite Plate," *Journal of Composite Materials*, vol. 3, January 1969, pp. 58–80.

[42] Biot, M.A., *Mechanics of Incremental Deformation*, First Edition, New York, NY: John Wiley & Sons, 1965, pp. 227–259.

8.0 REFERENCES (Continued)

[43] Guz, O.M., "Determination of the Theoretical Compression Strength of Reinforced Materials," NASA Technical Translation F-13,443, Translated from "Pro Viznachennia Teoretichnoi Granitsi Mitsnosti Na Stisk armovanikh Nauk Ukrayns' koy RSR, Servia, Fiziko-Technichni i Matematichni Nauki, Vol. 31, March 1969, pp. 236–238.

[44] Hayashi, T., "Compressive Strength of Unidirectionally Fiber Reinforced Composite Materials," 7^{th} *International Reinforced Plastics Conference*, British Plastics Federation, Brighton England, 1970, vol. 11, pp. 1–3.

[45] Lanir, Y. and Fung, Y.C.B., "Fiber Composite Columns Under Compression," *Journal of Composite Materials*, vol. 6, July 1972, pp. 387–401.

[46] Suarez, J.A., Whiteside, J.B., and Hadcock, R.N., "The Influence of Local Failure Modes on the Compressive Strength of Boron/Epoxy Composites," in *Composite Materials: Testing and Design (Second Conference), ASTM STP 497.* Philadelphia, PA: American Society for Testing and Materials, 1972, pp. 237–256.

[47] Hayashi, I. and Fujikake, M., "Compressive Strength of Unidirectionally Fiber Reinforced Composite Materials," presented at the 18^{th} Japan Congress on Materials Research—Non Metallic Materials, Japan, March 1975, pp. 141–147.

[48] Kulkarni, S.V., Rice, J.S., and Rosen, B.W., "An Investigation of the Compressive Strength of Kevlar 49/Epoxy Composites," *Composites*, vol. 6, 1975, pp. 217–225.

[49] Greszczuk, L.B., "Interfiber Stresses in Filamentary Composites," *AIAA Journal*, vol. 9, July 1971, pp. 1274–1280.

[50] Greszczuk, L.B., "Microbuckling of Lamina-Reinforced Composites," in *Composite Materials: Testing and Design (Third Conference), ASTM STP 546.* Philadelphia, PA: American Society for Testing and Materials, 1974, pp. 5–29.

[51] Greszczuk, L.B., "Prediction of Transverse Strength and Scatter in Test Data for Unidirectional Composites," in *Composite Reliability, ASTM STP 580.* Philadelphia, PA: American Society for Testing and Materials, 1975, pp. 311–326.

[52] Greszczuk, L.B., "Microbuckling Failure of Circular Fiber-Reinforced Composites," *AIAA Journal*, vol. 13, October 1975, pp. 1311–1318.

8.0 REFERENCES (Continued)

[53] Greszczuk, L.B., "On Failure Modes of Unidirectional Composites Under Compressive Loading," in *Proceedings of 2nd USA-USSR Symposium on Fracture of Composite Materials*. G.C. Sih and U.P. Tamuze, EDS., Boston, MA: Martinus Nijhoff Publishers, 1982, pp. 231–244.

[54] Piggott, M.R. and Harris, B., "Compression Strength of Carbon, Glass and Kevlar-49 Fibre Reinforced Polyester Resins," *Journal of Materials Science*, vol. 15, 1980, pp. 2523–2538.

[55] Piggott, M.R. and Wilde, P., "Compressive Strength of Aligned Steel Reinforced Epoxy Resin," *Journal of Materials Science*, vol. 15, 1980, pp. 2811–2815.

[56] Piggott, M.R. and Harris, B., "Compression Strength of Hybrid Fibre-Reinforced Plastics," *Journal of Materials Science*, vol. 16, 1981, pp. 687–693.

[57] Martinez, G.M., Piggott, M.R., Bainbridge, D.M.R., and Harris, B., "The Compression Strength of Composites with Kinked, Misaligned and Poorly Adhering Fibres," *Journal of Materials Science*, vol. 16, 1981, pp. 2831–2836.

[58] Piggott, M.R., "A Theoretical Framework for the Compressive Properties of Aligned Fibre Composites," *Journal of Materials Science*, vol. 16, 1981, pp. 2837–2845.

[59] Guz, A.N., "Mechanics of Composite-Material Failure Under Axial Compression (Brittle Failure)," Institute of Mechanics, Academy of Sciences of the Ukrainian SSR, Kiev. Translated from Prikladnaya Mekhanika, Vol. 18, No. 10, October 1982, pp. 3–16.

[60] Gurdal, Z. and Haftka, R.T., "Compressive Failure Model for Anisotropic Plates with a Cutout," *AIAA Journal*, vol. 25, November 1987, pp. 1476–1481.

[61] Hanasaki, S. and Hasegawa, Y., "Compressive Strength of Unidirectional Fibrous Composites," *Journal of Composite Materials*, vol. 8, July 1974, pp. 306–309.

[62] Maewal, A., "Postbuckling Behavior of a Periodically Laminated Medium in Compression," *International Journal of Solids and Structures*, vol. 17, 1981, pp. 335–344.

[63] Kurashige, M., "Compressive Strength of Fiber-Reinforced Materials," *Acta Mechanica*, vol. 49, 1983, pp. 49–56.

8.0 REFERENCES (Continued)

[64] DeFerran, E.M. and Harris, B., "Compression Strength of Polyester Resin Reinforced with Steel Wires," *Journal of Composite Materials*, vol. 4, 1970, pp. 62–72.

[65] Kurashige, M., "Compressive Strength of a Laminated Fiber-Reinforced Material," *Bulletin of Japanese Society of Mechanical Engineering*, vol. 27, December 1984, pp. 2694–2697.

[66] Chang, F.K. and Lessard, L., "Effect of Load Distribution of the Fiber Buckling Strength of Unidirectional Composites," submitted to *Journal of Composite Materials.*

[67] Davis, J.G., Jr., "Compressive Strength of Fiber-Reinforced Composite Materials," in *Composite Reliability, ASTM STP 580.* Philadelphia, PA: American Society for Testing and Materials, 1975, pp. 364–377.

[68] Wang, A.S.D., "A Non-Linear Microbuckling Model Predicting the Compressive Strength of Unidirectional Composites," ASME Paper 78-WA/Aero-1, ASME, 1978.

[69] Wang, A.S.D., "Certification of Composite Aircraft Structures Under Impact, Fatigue and Environmental Conditions, Part III: Environmental Effects on Compression Strength," Naval Air Development Center, War Minster, PA, Report No. NADC-78259-60, January 1978.

[70] Petit, P.H., "A Simplified Method of Determining the In-Plane Shear Stress-Strain Response of Unidirectional Composites," in *Composite Materials: Testing and Design, ASTM STP 460.* Philadelphia, PA: American Society for Testing and Materials, 1969, pp. 83–93.

[71] Rosen, B. W., "A Simple Procedure for Experimental Determination of the Longitudinal Shear Modulus of Unidirectional Composites," *Journal of Composite Materials*, vol. 6, October 1972, pp. 552–554.

[72] Hahn, H.T., "A Note on Determination of the Shear Stress-Strain Response of Unidirectional Composites," *Journal of Composite Materials*, vol. 7, July 1973, pp. 383–386.

[73] Shuart, M. J., "Failure of Compression-Loaded Multi-Directional Composite Laminates," *Proceedings of the AIAA/ASME/ASCE/AHS* 29^{th} *Structures, Structural Dynamics and Materials Conference*, Williamsburg, VA, April 1988.

8.0 REFERENCES (Continued)

[74] Shuart, M.J. and Williams, J.G., "Compression Behavior of ±45°—Dominated Laminates With a Circular Hole or Impact Damage," *AIAA Journal*, vol. 24, January 1986, pp. 115–122.

[75] Chang, F.K., Lessard, L., and Tang, J.M., "Compression Response of Laminated Composites Containing an Open Hole," *SAMPE Quarterly*, vol. 19, July 1988, pp. 46–51.

[76] Chang, F.K. and Lessard, L., "Damage Tolerance of Laminated Composites Containing an Open Hole and Subjected to Compressive Loadings: Part I—Analysis," submitted to *Journal of Composite Materials*.

[77] Lessard, L. and Chang, F.K., "Damage Tolerance of Laminated Composites Containing an Open Hole and Subjected to Compressive Loadings: Part II—Experiment," submitted to *Journal of Composite Materials*.

[78] Davis, J., "The Effects of Fiber Waviness on the Compressive Response of Fiber-Reinforced Composite Materials," Department of Aerospace Engineering, Texas A&M University, M.S. Thesis, December 1989.

[79] Highsmith, A.L. and Davis, J., "The Effects of Fiber Waviness on the Compressive Response of Fiber-Reinforced Composite Materials," NASA Langley Research Center, Hampton, VA, Annual Progress Report for NASA Research Grant NAG-1-659, January 1990.

[80] Lee, J. W., "Deformation Analysis of Local Ply Curvature in Laminated Composites," Department of Aerospace Engineering, Texas A&M University, M.S. Thesis, December 1987.

[81] Collings, T.A., "Transverse Compressive Behaviour of Unidirectional Carbon Fibre Reinforced Plastics," *Composites*, May 1974, pp. 108–116.

[82] Hancox, N.L., "The Compression Strength of Unidirectional Carbon Fibre Reinforced Plastic," *Journal of Materials Science*, vol. 10, 1975, pp. 234–242.

[83] Kim, R.Y., "On the Off-Axis and Angle-Ply Strength of Composites," in *Test Methods and Design Allowables for Fibrous Composites, ASTM STP 734*. C.C. Chamis, ED., Philadelphia, PA: American Society for Testing and Materials, 1981, pp. 91–108.

8.0 REFERENCES (Continued)

[84] Fried, N., "The Compressive Strength of Parallel Filament Reinforced Plastics-The Role of the Resin," *Proceedings of the* 18^{th} *Annual Meeting of the Reinforced Plastics Division*, Society of the Plastics Industry, Chicago, IL, February 1963.

[85] Fried, N. and Kaminetsky, J., "The Influence of Material Variables on the Compressive Properties of Parallel Filament Reinforced Plastics," *Proceedings of the* 19^{th} *Annual Meeting of the Reinforced Plastics Division*, Society of the Plastics Industry, Chicago, IL, February 1964.

[86] Fried, N., "The Response of Orthogonal Filament Wound Materials to Compressive Stress," *Proceedings of the* 20^{th} *Annual Meeting of the Reinforced Plastics Division*, Society of the Plastics Industry, Chicago, IL, February 1965.

[87] Budiansky, B., "Micromechanics," *Computers and Structures*, vol. 16, 1983, pp. 3–12.

[88] Chou, T.W. and Kelly, A., "The Effect of Transverse Shear on the Longitudinal Compressive Strength of Fibre Composites," *Journal of Materials Science*, vol. 15, 1980, pp. 327–331.

[89] Wilkinson, E., Parry, T.V., and Wronski, A.S., "Compressive Failure in Two Types of Carbon Fibre-Epoxide Laminates," *Composites Science and Technology*, vol. 26, 1986, pp. 17–29.

[90] Lee, R.J., "Compression Strength of Aligned Carbon Fibre-Reinforced Thermoplastic Laminates," *Composites*, vol. 18, January, 1987, pp. 35–39.

[91] Whitney, J.M. and Nuismer, R.J., "Stress Fracture Criteria for Laminated Composites Containing Stress Concentrations," *J. Composite Materials*, vol. 8, July 1974, pp. 253–265.

[92] Nuismer, R.J. and Whitney, J.M., "Uniaxial Failure of Composite Laminates Containing Stress Concentrations," *Fracture Mechanics of Composites, ASTM STP 593*, 1975, pp. 117–142.

[93] Nuismer, R.J. and Labor, J.D., "Applications of the Average Stress Criterion: Part II—Compression," *J. Composite Materials*, vol. 13, January 1979, pp. 49–60.

8.0 REFERENCES (Continued)

[94] Reifsnider, K.L, Stinchcomb, W.W., Bakis, C.R., and Yih, R.Y., "The Mechanics of Micro-Damage in Notched Composite Laminates," in *Composite Materials: Fatigue and Fracture (Second Symposium), ASTM STP 1012*. Philadelphia, PA: American Society for Testing and Materials, 1989, pp. in print.

[95] Renault, M., Valentin, D., and Perez, F., "A Damage Tolerance Study of Notched CFRP Laminates," *Engineering Conference on Fracture: Failure Analysis, Theory and Practice*, Budapest, Hungary, September 1988.

[96] Guz, A.N. and Lapusta, Y.N., "Stability of Fibers Near a Free Cylindrical Surface," Institute of Mechanics, Academy of Sciences of the Ukrainian SSR, Kiev. Translated from Prikladnaya Mekhanika, Vol. 24, No. 10, October 1988, pp. 3–9.

[97] Burns, S.W., Herakovich, C.T., and Williams, J.G., "Efficient 3-D Finite Element Failure Analysis of Compression Loaded Angle-Ply Plates with Holes," *Sixth International Conference on Composite Materials—Second Europe Conference on Composite Materials*, London England, July 1987, vol. 5, pp. 231–240.

[98] Pattnaik, A., Koczak, M.J., and Rogers, H.C., "Compressive Failure Behavior of FP Alumina/Aluminum Composites," in *New Developments and Applications in Composites*. D. Kuhlmann-Wilsdorf and W.C. Harrigan, EDS., AIME Publication, 1979, pp. 261–282.

[99] Chaplin, C.R., "Compressive Fracture in Unidirectional Glass-Reinforced Plastics," *Journal of Materials Science*, vol. 12, 1977, pp. 347–352.

[100] Parry, T.V. and Wronski, A.S., "Kinking and Tensile, Compressive and Interlaminar Shear Failure in Carbon-Fibre-Reinforced Plastic Beams Tested in Flexure," *Journal of Materials Science*, vol. 16, 1981, pp. 439–450.

[101] Parry, T.V. and Wronski, A.S., "Kinking and Compressive Failure in Uniaxially Aligned Carbon Fibre Composite Tested Under Superposed Hydrostatic Pressure," *Journal of Materials Science*, vol. 17, 1982, pp. 893–900.

[102] Wronski, A.S. and Parry, T.V., "Compressive Failure and Kinking in Uniaxially Aligned Glass-Resin Composite Under Superposed Hydrostatic Pressure," *Journal of Materials Science*, vol. 17, 1982, pp. 3656–3662.

[103] Evans, A.G. and Adler, W.F., "Kinking as a Mode of Structural Degradation in Carbon Fiber Composites," *Acta Metallurgica*, vol. 26, 1978, pp. 725–738.

8.0 REFERENCES (Continued)

[104] Potter, R.T. and Purslow, D., "The Environmental Degradation of Notched CFRP in Compression," *Composites*, July 1983, pp. 206–225.

[105] Purslow, D. and Potter, R.T., "The Effect of Environment on the Compression Strength of Notched CFRP-A Fractographic Investigation," *Composites*, vol. 15, April 1984, pp. 112–120.

[106] Marom, G., Davidovitz, M., Mittelman, A., and Roman, I., "Fracture Mechanisms in Bending of Unidirectional Kevlar-Reinforced Epoxy Composites," *Proceedings of the International Conference on Testing, Evaluation, and Quality Control of Composites*, University of Surrey, Guildford, United Kingdom, September 1983.

[107] Davidovitz, M., Mittelman, A., Roman, I., and Marom, G., "Failure Modes and Fracture Mechanisms in Flexure of Kevlar-Epoxy Composites," *Journal of Materials Science*, vol. 19, 1984, pp. 377–384.

[108] Rajendran, G. , Rogers, H.C., and Koczak, M.J., "The Compressive Failure Modes of Alumina/Aluminum Composites: Dead Weight vs. Machine Loading," *Powder Metallurgy International*, vol. 18, 1986, pp. 397–400.

[109] Waas, A. and Babcock, C., "Observation of the Initiation and Progression of Damage in Compressively Loaded Composite Plates Containing a Cutout," NASA Langley Research Center, Hampton, VA, NASA Progress Report for Grant NSG-1-483, November 1986.

[110] Starnes, J.H. and Williams, J.G., "Failure Characteristics of Graphite/Epoxy Structural Components Loaded in Compression," in *Mechanics of Composite Materials—Recent Advances*. Z. Hashin and C.T. Herakovich, EDS., New York, NY: Pergamon Press, 1982, pp. 283–306.

[111] Williams J.G., "Effect of Impact Damage and Open Holes on the Compression Strength of Tough Resin/High Strain Fiber Laminates," NASA Langley Research Center, Hampton, VA, NASA Technical Memorandum 85756, February 1984.

[112] Rhodes, M.D., Mikulas, M.M., and M^{c}Gowan, P.E., "Effects of Orthotropy and Width on the Compression Strengths of Graphite/Epoxy Panels with Holes," *AIAA Journal*, vol. 22, September 1984, pp. 1283–1292.

[113] Sohi, M.M., Hahn, H. T. and Williams, J. G., "The Effect of Resin Toughness and Modulus on Compressive Failure Modes of Quasi-Isotropic Graphite/Epoxy Laminates," in *Toughened Composites, ASTM STP 937*. N.J. Johnston, ED., Philadelphia, PA: American Society for Testing and Materials, 1987, pp. 37–60.

8.0 REFERENCES (Continued)

[114] Hahn, H.T. and Sohi, M.M., "Buckling of a Fiber Bundle Embedded in Epoxy," *Composites Science and Technology*, vol. 27, 1986, pp. 25–41.

[115] Hahn, H. T., "Compressive Failure of Unidirectional Composites," presented at the 13^{th} International Symposium for Testing and Failure Analysis, Los Angeles, CA, November 1987.

[116] DeTeresa, S.J., Allen, S.R., Farris, R.J., and Porter, R.S., "Compressive and Torsional Behaviour of Kevlar 49 Fibre," *Journal of Materials Science*, vol. 19, 1984, pp. 57–72.

[117] Chang, I.Y., "Thermoplastic Matrix Continuous Filament Composites of Kevlar Aramid or Graphite Fiber," *Composites Science and Technology*, vol. 24, 1985, pp. 61–79.

[118] Chang, I. Y., "Static Mechanical Properties of Thermoplastic Matrix Composites," *Proceedings of the International Symposium on Composite Materials and Structures*, Beijing, People's Republic of China, June 1986.

[119] Mabson, G.E., Wharram, G.E., Tennyson, R.C., and Hansen, J.S., "On the Compressive Strength of Graphite Composite Laminates Containing Interlaminar Flaws," *Polymer Plastics Technology in Engineering*, vol. 22, 1984, pp. 99–113.

[120] Sternstein, S.S., Yurgartis, S.W., and Srinivasan, K., "Deformation, Microdeformation and Toughness in Graphite-Polymeric Matrix Composites," *Proceedings of the Sixth International Conference on Deformation, Yield and Fracture of Polymers*, Cambridge, England, April 1985.

[121] Bishop, S.M., "The Mechanical Performance and Impact Behaviour of Carbon-Fibre Reinforced PEEK," *Composite Structures*, vol. 3, 1985, pp. 295–318.

[122] Miyano, Y. and Kanemitsu, M., Kunio, T., and Kuhn, H.A., "Role of Matrix Resin on Fracture Strengths of Unidirectional CFRP," *Journal of Composite Materials*, vol. 20, November 1986, pp. 520–538.

[123] van Dreumel, W.H.M., "A Short Note on the Compressive Behaviour of Aramid Fibre Reinforced Plastics Plastics," Dreft University of Technololgy, Dreft, The Netherlands, Report No. LR-341, January 1982.

[124] Turner, R.M. and Cogswell, F.N., "The Effect of Fibre Characteristics on the Morphology and Performance of Semi-Crystalline Thermoplastic Composites," *SAMPE Journal*, vol. 23, January/February 1987, pp. 40–44.

8.0 REFERENCES (Continued)

[125] Vinson, J.R. and Sierakowski, R.L., *The Behavior of Structures Composed of Composite Materials*, First Edition, Boston, MA: Kluwer, 1986, pp. 303.

[126] DeTeresa, S.J., Porter, R.S., and Farris, R.J., "A Model for the Compressive Buckling of Extended Chain Polymers," *Journal of Materials Science*, vol. 20, 1985, pp. 1546–1659.

[127] DeTeresa, S.J., Porter, R.S., and Farris, R.J., "Experimental Verification of a Microbuckling Model for the Axial Compressive Failure of High Performance Polymer Fibres," *Journal of Materials Science*, vol. 23, 1988, pp. 1886–1894.

[128] DeTeresa, S.J., Allen, S.R., and Farris, R.J., "The Axial Compressive Strength of High Performance Polymer Fibers," submitted to *Advances in Chemistry Series, Composites: Chemical and Physiochemical Aspects*, T.L. Vigo and V.J. Kinzig, EDS., July 1989.

[129] Yau, S.S. and Chou, T.W, "Strength of Woven-Fabric Composites with Drilled and Molded Holes," in *Composite Materials: Testing and Design (Eighth Conference), ASTM STP 972*. J.D. Whitcomb, ED., Philadelphia, PA: American Society for Testing and Materials, 1988, pp. 423–437.

[130] Klein, A.J., "Which Weave," *Advanced Materials and Processes*, March 1986, pp. 40–43.

[131] Schapery, R.A., "Mechanical Characterization and Analysis of Inelastic Composite Laminates with Growing Damage," Texas A&M University, College Station, TX, Report No. MM 5742-89-10, April 1989.

[132] Landro, L.D., and Pegoraro, M., "Carbon Fibre-Thermoplastic Matrix Adhesion," *Journal of Materials Science*, vol. 22, 1987, pp. 1980–1986.

[133] Ewins, P.D. and Potter, R.T., "Some Observations on the Nature of Fiber Reinforced Plastics and the Implications for Structural Design," *Philosophical Transactions of the Royal Society of London*, vol. A294, 1980, pp. 507–517.

[134] Malik, B., Palazotto, A., and Whitney, J., "Notch Strength of GR/PEEK Composite Material at Elevated Temperatures," 26^{th} *Structures, Structural Dynamics, and Materials Conference*, Orlando, Florida, April 1985.

8.0 REFERENCES (Continued)

[135] Ramey, J., Palazotto, A., and Whitney, J., "Comparison of Notch Strength Between Gr/PEEK (APC-1 and APC-2) and Gr/Epoxy Composite Material at Elevated Temperature," *Proceedings (A86-48676 24-35) 1986 SEM Spring Conference on Experimental Mechanics*, Society of Experimental Mechanics, New Orleans, LA, June 1986.

[136] Kar, R.J., Herfert, R.E., and Kessler, R.T., "Fractographic and Microstructural Examination of Compression Failures in Wet Compression Graphite/Epoxy Coupons," in *Composite Materials: Testing and Design (Seventh Conference), ASTM STP 893*. J.M. Whitney, ED., Philadelphia, PA: American Society for Testing and Materials, 1986, pp. 140–157.

[137] Fiberite Corporation — An ICI (Imperical Chemical Industries) Company, Orange, CA, "APC-2: The Product of High Technology," trade name material data sheets, 1988.

[138] Carlile, D.R., Leach, D.C., Moore, D.R., and Zahlan, N., "Mechanical Properties of the Carbon Fibre/PEEK Composite APC-2/AS4 for Structural Applications," *ASTM Symposium on Advances in Thermoplastic Matrix Composite Materials*, Bal Harbor, FL, October 1987.

[139] Hartness, J.T., "Polyether Matrix Composites," *SAMPE Quarterly*, January 1983, pp. 33–36.

[140] Lee, W.I., Talbott, M.F., Springer, G.S., and Berglund, L.A., "Effects of Cooling Rate on the Crystallinity and Mechanical Properties of Thermoplastic Composites," *Journal of Reinforced Plastics and Composites*, vol. 6, January 1987, pp. 2–12.

[141] Iaconis, J.M., "Process Variables Evaluation of PEEK APC-2 Thermoplastic Matrix Composites," 32^{nd} *International SAMPE Symposium and Exhibition*, Anaheim, CA, April 1987.

[142] Blundell, D.J. and Osborn, B.N., "The Morphology of Poly(aryl-ether-ether-ketone)," *Polymer*, vol. 24, August 1983, pp. 953–958.

[143] Pagano, N.J. and Pipes, R.B., "The Influence of Laminate Stacking Sequence on Laminate Strength," *Journal of Composite Materials*, vol. 5, January 1971, pp. 50–57.

8.0 REFERENCES (Continued)

[144] Quadrax Corporation, Providence, Rhode Island, "Quadrax Interlaced Unidirectional Tapes," Advertising Brochure, 1988.

[145] Guynn, E.G. and Bradley, W.L., "Micromechanics of Composite Laminate Compression Failures," NASA Langley Research Center, Hampton, VA, Annual Progress Report for NASA Research Grant NAG-1-659, August 1988.

[146] Trademark of The Dow Chemical Company.

[147] Barron, D., private communications, October 1988.

[148] Carlsson, L.A. and Pipes, R.B., *Experimental Characterization of Advanced Composites Materials*, First Edition, Englewood Cliffs, New Jersey: Prentice-Hall, Inc., 1987, pp. 54–65.

[149] Whitney, J.M., Daniel, I.M., and Pipes, R.B., *Experimental Mechanics of Fiber Reinforced Composite Materials*, Revised Edition, Englewood Cliffs, New Jersey: Prentice-Hall, Inc., 1984, pp. 185–199.

[150] Gray, R.J., "Experimental Techniques for Measuring Fibre/Matrix Interfacial Bond Shear Strength," *Journal of Adhesion and Adhesives*, vol. 3, No. 4, October 1983, pp. 197–201.

[151] Caldwell, D.L., "Determination of Interfacial Strength of Composites," *Proceedings of the Advanced Composites Conference*, Detroit, MI, 1987.

[152] Caldwell, D.L. and Cortez, F.M., "A New Method for Determining the Interfacial Strength of Composites," presented at the Society of the Plastics Industry Conference, Cincinnati, OH, February 1988.

[153] Caldwell, D.L. and Jarvie, D.A., "Determination of the Interfacial Strength of Advanced Composites," presented at the 33rd International SAMPE Symposium, Anaheim, CA, March 1988.

[154] Mandell, J., Grande, D.H., Tsiang, T., and M^{c}Garry, F.J.,, "Modified Microdebonding Test for Direct In-Situ Fiber/Matrix Bond Strength Determination in Fiber Composites," in *Composite Materials: Testing and Design (Seventh Conference), ASTM STP 893*. J.M. Whitney, ED., Philadelphia, PA: American Society for Testing and Materials, 1986, pp. 87–108.

8.0 REFERENCES (Continued)

[155] Whitney, J.M., Browning, C.E., and Hoogsteden, W., "A Double Cantilevered Beam Test for Characterizing Mode I Delamination of Composite Materials," *Journal of Reinforced Plastics Composites*, vol. 1, 1982, pp. 297–310.

[156] Keary, P.E., Ilcewicz, L.B., Shaar, C., and Trostle, J., "Interlaminar Fracture Toughness of Composites Using Slender Double Cantilever Beam Specimens," *Journal Composite Materials*, vol. 19, March 1985, pp. 154–175.

[157] Bathe, K.J., *Finite Element Procedures in Engineering Analysis*, First, Englewood Cliffs, NJ: Prentice-Hall, Inc., 1982.

[158] Zienkiewicz, O.C., *The Finite Element Method (The third, expanded and revised edition of The Finite Element Method in Engineering Science)*, First, London, England: McGraw Hill Book Company (UK) Limited, 1977.

[159] Leeser, D., private communications, June 1989.

[160] DeTeresa, S.J., private communications, December 1989.

Table I. Composite Laminate Material Test Matrix.

Stacking Sequence	Variable Investigated
$[(\pm 45/0_2)_3/\pm 45/0]_s$	Baseline APC-2
$[(0_2/\pm 45)_3/0/\pm 45]_s$	Interchange 0's and 45's to observe surface 0's
$[\pm 45/0/90]_{3s}$	Theoretically "straight" fibers
$[\pm 45/\langle 0/90\rangle]_{3s}$	Replace 0/90 with Quadrax $\langle 0/90\rangle$, 1 harness, to compare fiber waviness effects
$[\pm 45/\langle 0/90\rangle]_{3s}$	Replace 0/90 with Quadrax $\langle 0/90\rangle$, 8 harness, to compare fiber waviness effects
$[(\pm 45/0_2)_3/\pm 45/0]_s$	Use non-surface treated AS4 fibers in PEEK to provide a poor interface
$[(\pm 15/0_2)_3/\pm 15/0]_s$	Vary support to 0's
$[(\pm 75/0_2)_3/\pm 75/0]_s$	Vary support to 0's
$[(90_2/0_2)_3/90_2/0]_s$	Vary support to 0's
$[(\pm 45/f/0_2/f)_3/\pm 45/f/0]_s$	Vary resin rich region: $f = 0.025$ mm, one layer of PEEK film
$[(\pm 45/f_3/0_2/f_3)_3/\pm 45/f_3/0]_s$	Vary resin rich region: $f = 0.025$ mm, one layer of PEEK film
$[\pm 45]_{2s}$	Measure G_{12}, tension tests
$[\pm 45]_{8s}$	Measure G_{12}, compression tests
$[0]_{24}$	Measure G_{Ic}, APC-2
$[0]_{24}$	Measure G_{Ic}, Use non-surface treated AS4 fibers in the PEEK resin

Table II. Effects of Supporting Fiber Orientation.

Stacking Sequence	Variable Investigated
$[(0_2/\pm 45)_3/0/\pm 45]_s$	Vary support to 0's
$[(\pm 15/0_2)_3/\pm 15/0]_s$	Vary support to 0's
$[(\pm 45/0_2)_3/\pm 45/0]_s$	Baseline lay-up
$[(\pm 75/0_2)_3/\pm 75/0]_s$	Vary support to 0's
$[(90_2/0_2)_3/90_2/0]_s$	Vary support to 0's

Table III. Effects of Initial Fiber Waviness.

Stacking Sequence	Variable Investigated
$[\pm 45/0/90]_{3s}$	Theoretically "straight" fibers
$[\pm 45/\langle 0/90\rangle]_{3s}$	Replace 0/90 with Quadrax $\langle 0/90\rangle$, 1 harness, to compare fiber waviness effects
$[\pm 45/\langle 0/90\rangle]_{3s}$	Replace 0/90 with Quadrax $\langle 0/90\rangle$, 8 harness, to compare fiber waviness effects

Table IV. Effects of Interfacial Bond Strength.

Stacking Sequence	Variable Investigated
$[(\pm 45/0_2)_3/\pm 45/0]_s$	Baseline APC-2
$[(\pm 45/0_2)_3/\pm 45/0]_s$	Use non-surface treated AS4 fibers in the PEEK resin to provide a poor interface

Table V. Effects of Resin-Rich Regions.

Stacking Sequence	Variable Investigated
$[(\pm 45/0_2)_3/\pm 45/0]_s$	Baseline APC-2, no PEEK film added
$[(\pm 45/f/0_2/f)_3/\pm 45/f/0]_s$	Vary resin rich region: $f = 0.025$ mm, one layer of PEEK film
$[(\pm 45/f_3/0_2/f_3)_3/\pm 45/f_3/0]_s$	Vary resin rich region: $f = 0.025$ mm, one layer of PEEK film

Table VI. Mechanical Properties of Constituent Materials.[137]

Material	E_{11}, GPa	E_{22}, GPa	G_{12}, GPa	ν_{12}
PEEK Resin	3.60	3.60	1.30	0.42
AS4 Fiber	235	14.0	28.0	0.20
APC-2 Lamina	134	8.90	5.10	0.30
Quadrax†	70.7	70.7	6.10	0.03
Isotropic Fiber[a]	235	235	97.9	0.20
Isotropic Fiber[b]	67.2	67.2	28.0	0.20

[a] Assumed for isotropic straight fiber analysis.
[b] Assumed for wavy fiber analysis.
† Assumed same for both 1- and 8- harness.[144]

Table VII. APC-2 Coefficients of Thermal Expansion.[137]

Temperature Range, °C	α_1, /°C	α_2, /°C
23–143	0.5E-06	30E-06
143–343	1.0E-06	75E-06

Table VIII. Laminate Engineering Constants.

Stacking Sequence	E_{xx}, GPa	E_{yy}, GPa	G_{xy}, GPa	ν_{xy}	ν_{yx}
$[(\pm 45/0_2)_3/\pm 45/0]_s$	72.7	22.8	20.8	0.69	0.22
$[(0_2/\pm 45)_3/0/\pm 45]_s$	72.7	22.8	20.8	0.69	0.22
$[\pm 45/0/90]_{3s}$	51.7	51.7	19.8	0.31	0.31
$[\pm 45/\langle 0/90\rangle]_{3s}$ 1-&8-harness	53.6	53.6	19.8	0.27	0.27
$[(\pm 15/0_2)_3/\pm 15/0]_s$	121.6	9.2	9.0	0.69	0.05
$[(\pm 75/0_2)_3/\pm 75/0]_s$	67.5	66.9	9.0	0.10	0.10
$[(90_2/0_2)_3/90_2/0]_s$	67.5	75.8	5.1	0.04	0.04

Table IX. Determination of G_{12}.

Stacking Sequence	Variable Investigated
$[\pm 45]_{2s}$	Measure G_{12}, tension tests
$[\pm 45]_{8s}$	Measure G_{12}, compression tests

Table X. Determinination of G_{Ic}.

Stacking Sequence	Variable Investigated
$[0]_{24}$	Measure G_{Ic}, APC-2
$[0]_{24}$	Measure G_{Ic}, Use non-surface treated AS4 fibers in the PEEK resin

Table XI. Ramberg-Osgood Parameters for Resin Nonlinear Constitutive Behavior.

Temperature, °C	σ_o, MPa	n
21	115.5	8.0748
77	84.02	5.8676

Table XII. Strain Concentration Factors.

Stacking Sequence	SCF
$[(0_2/\pm 45)_3/0/\pm 45]_s$	3.28364
$[(\pm 15/0_2)_3/\pm 15/0]_s$	4.19298
$[(\pm 45/0_2)_3/\pm 45/0]_s$	3.28364
$[(\pm 75/0_2)_3/\pm 75/0]_s$	3.41052
$[(90_2/0_2)_3/90_2/0]_s$	3.69487

Table XIII. Critical Buckling Strains.

Model	ϵ_{cr}, %
Infinite Plate	2.77
Semi-Infinite Plate	2.49
Ten Anisotropic Fibers and Matrix	1.53
Ten Isotropic Fibers[a] and Matrix	1.64
Ten Isotropic Fibers[b] and Matrix	3.94

[a] Assumed for isotropic straight fiber analysis.
[b] Assumed for wavy fiber analysis.

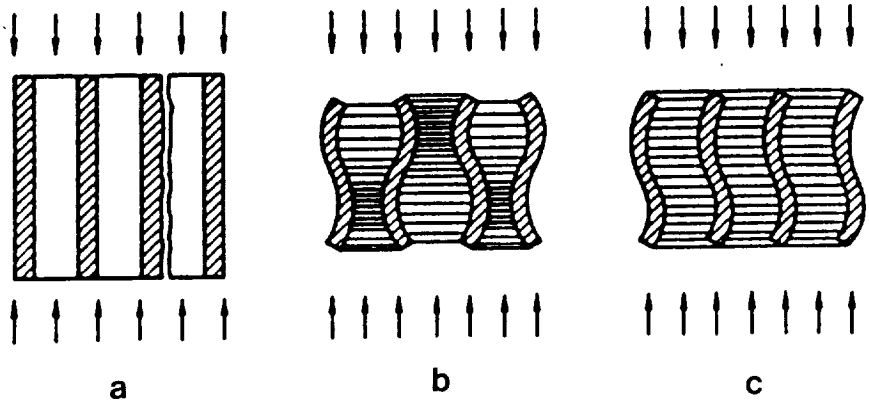

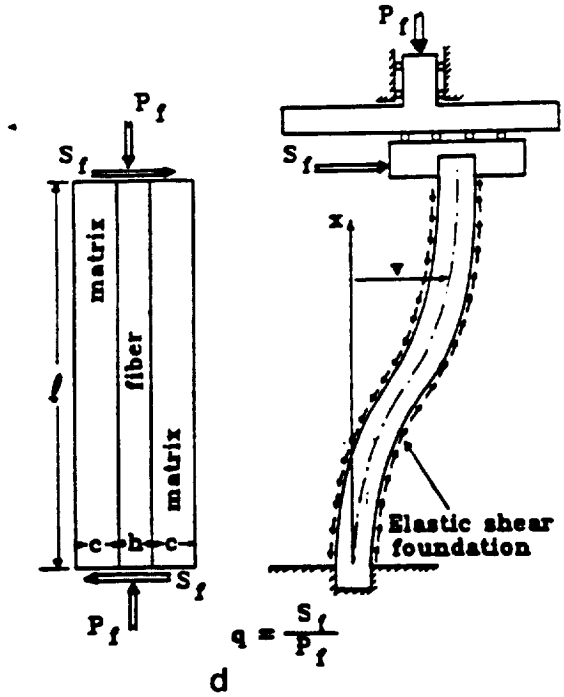

Fig. 1 Failure modes and model of a unidirectional composite subjected to a longitudinal compressive load.
a) Longitudinal splitting due to secondary transverse tensile stresses.
b) Fiber microbuckling out-of-plase (extension mode).
c) Fiber microbuckling in-phase (shear mode).[24]
d) In-phase fiber microbuckling, including the localized induced shearing stresses.[60]

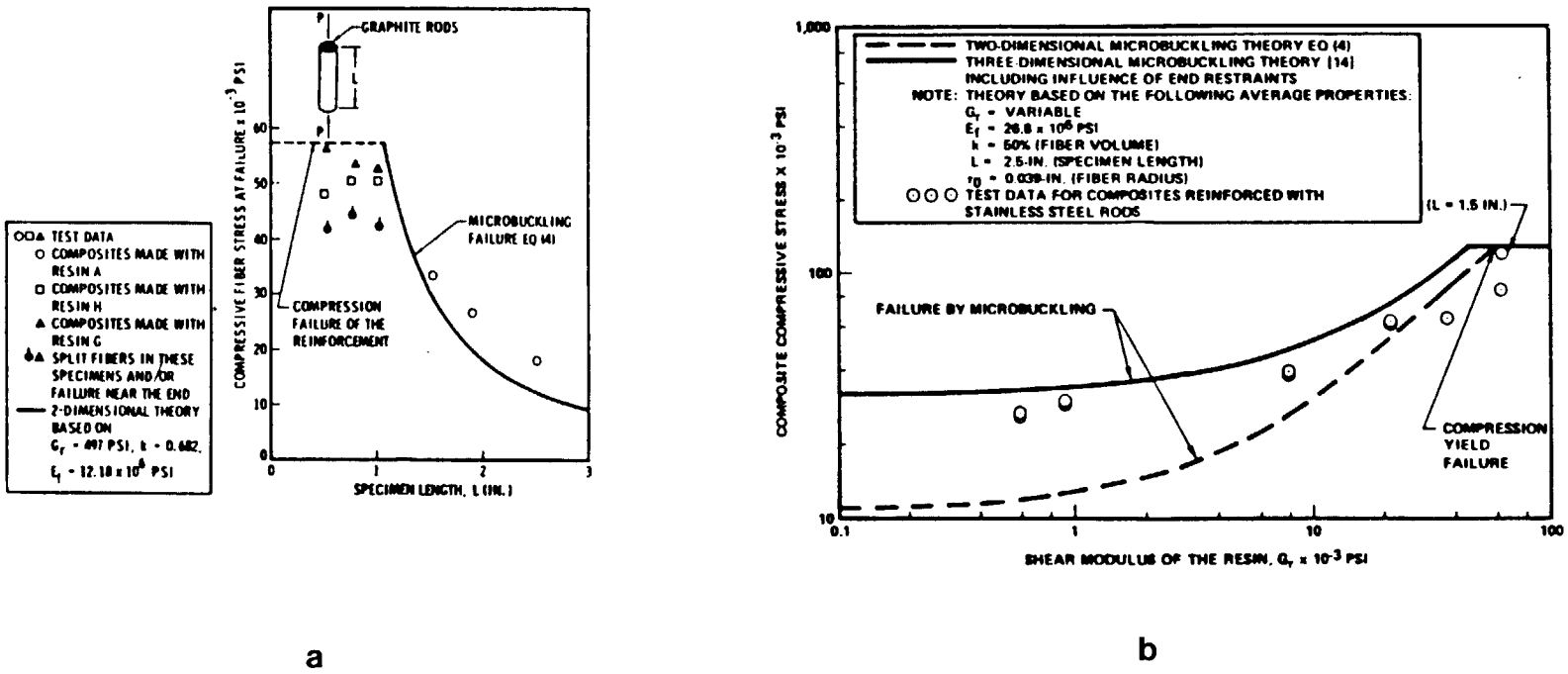

Fig. 2 Test-theory correlation by Greszczuk[26] for compressive strength of composites.
a) Comparison of reinforcement and microbuckling failures.
b) Effect of resin shear modulus on microbuckling strength.

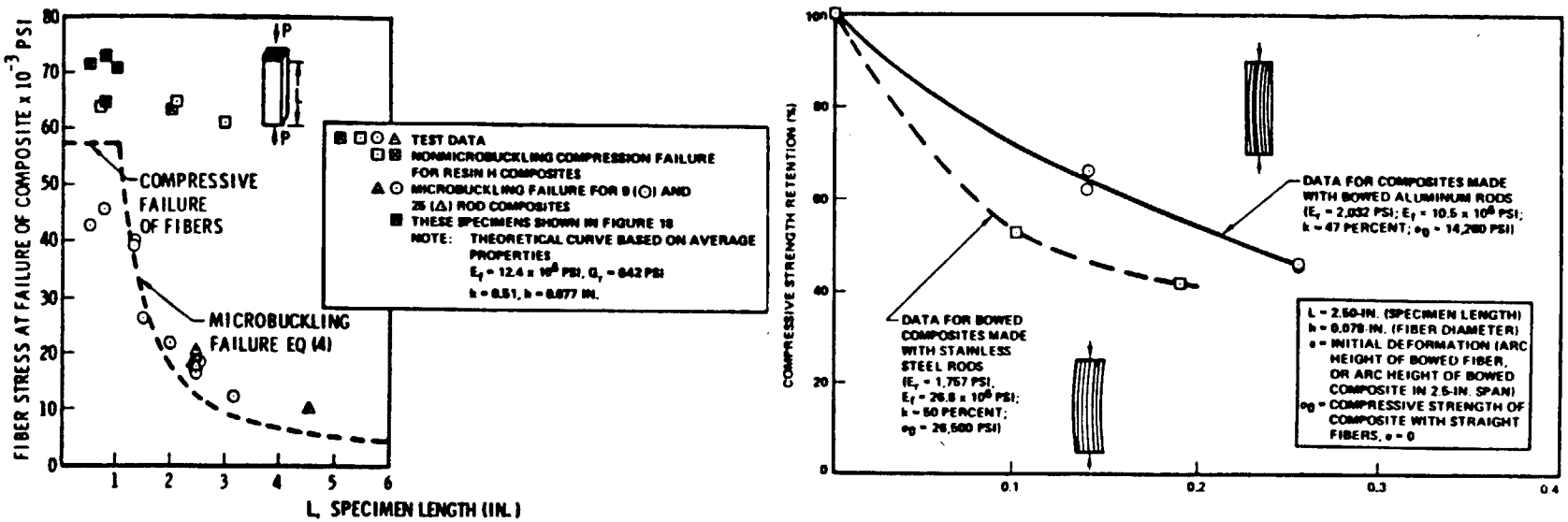

c d

Fig. 2 Continued
c) Comparison of reinforcement and microbuckling failures.
d) Effect of initial deformations on microbuckling strength.

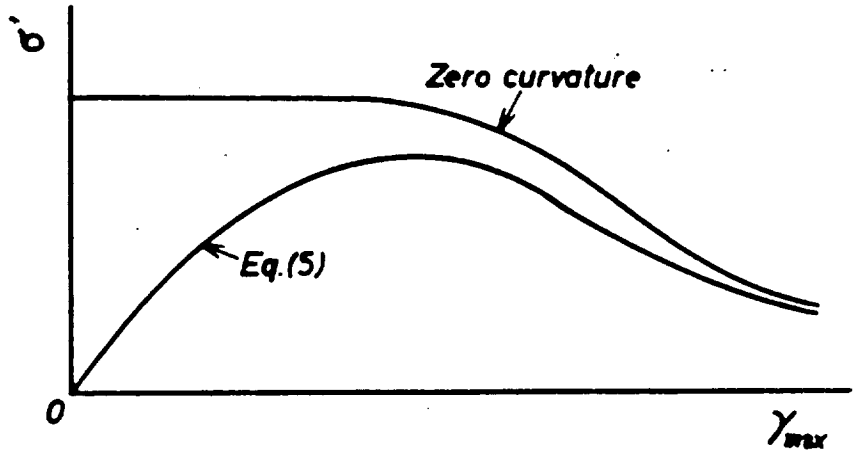

Fig. 3 Schematical representation of Eqns. 16 and 18,[61] the relation between the nominal compressive stress of the composite material and the shearing strain of the matrix.

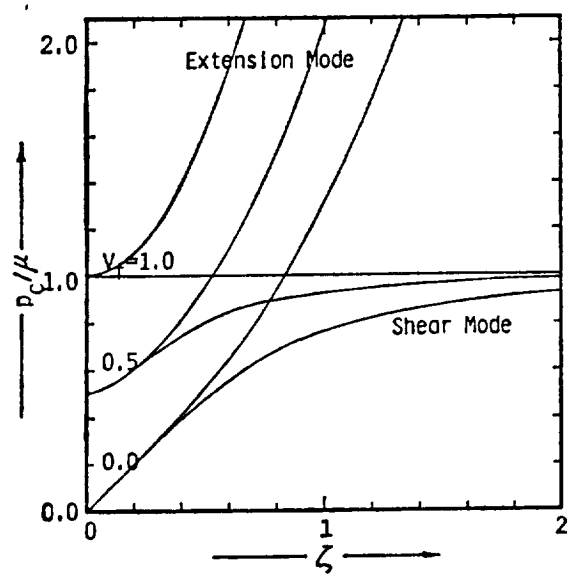

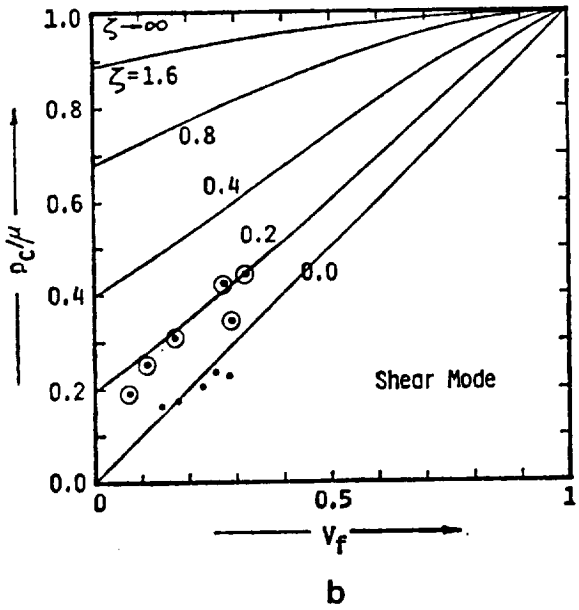

Fig. 4 Kurashige's results for unidirectional composites.[63]
a) Dependence of compressive strength on buckling wavelength.
b) Dependence of compressive strength on fiber volume fraction for shear mode fiber microbuckling.

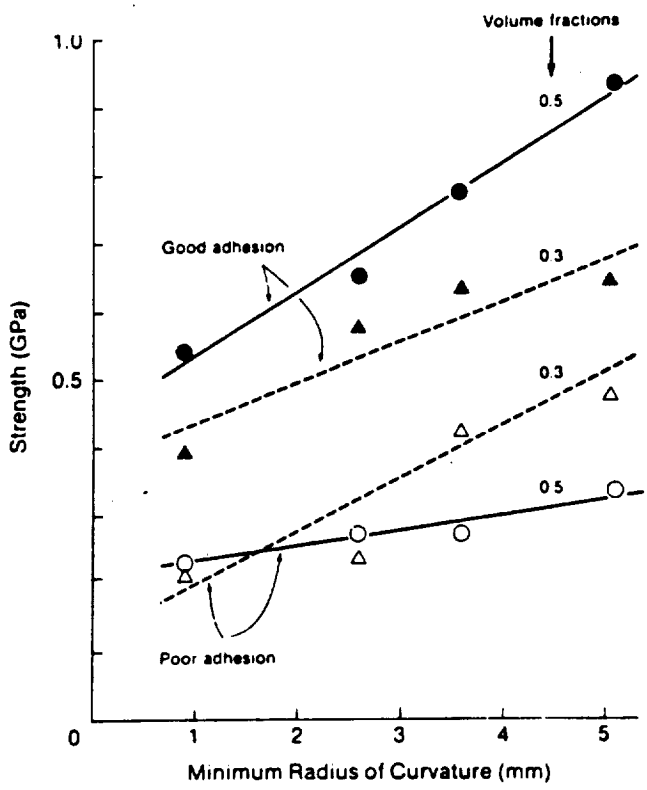

Fig. 5 Composite compressive strength as a function of the minimum radius of curvature for glass fibers in a polyester resin.[57]

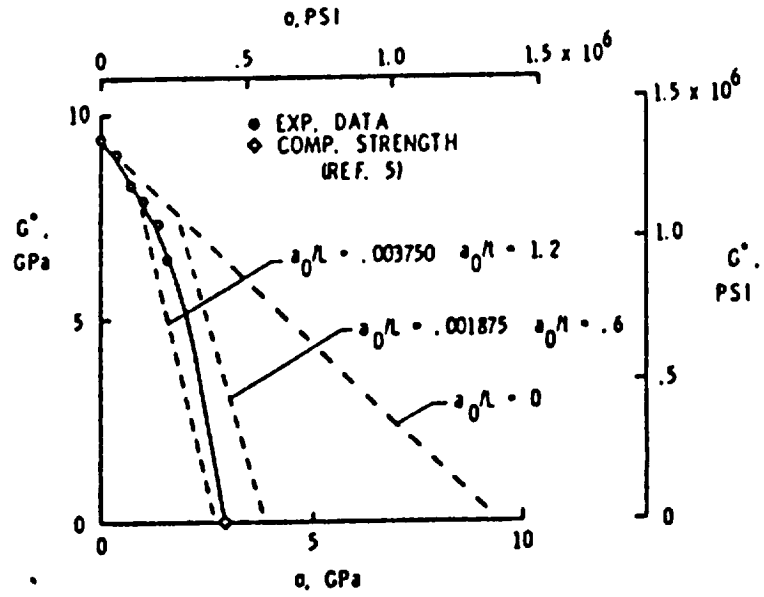

Fig. 6 Comparison of measured and predicted values of apparent shear modulus as a function of axial compressive stress for unidirectional boron/epoxy composites.[67]

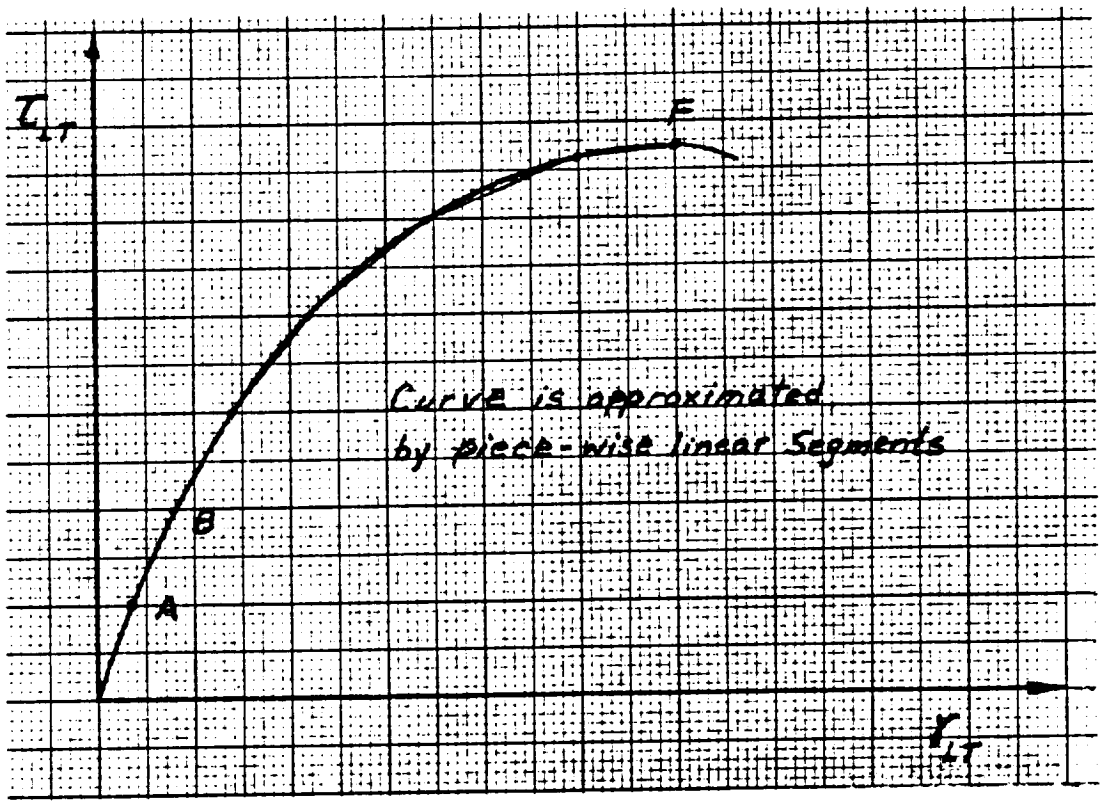

Fig. 7 A hypothetical shear stress versus shear strain curve for a graphite/ epoxy unidirectional composite, suggested by Wang.[68,69]

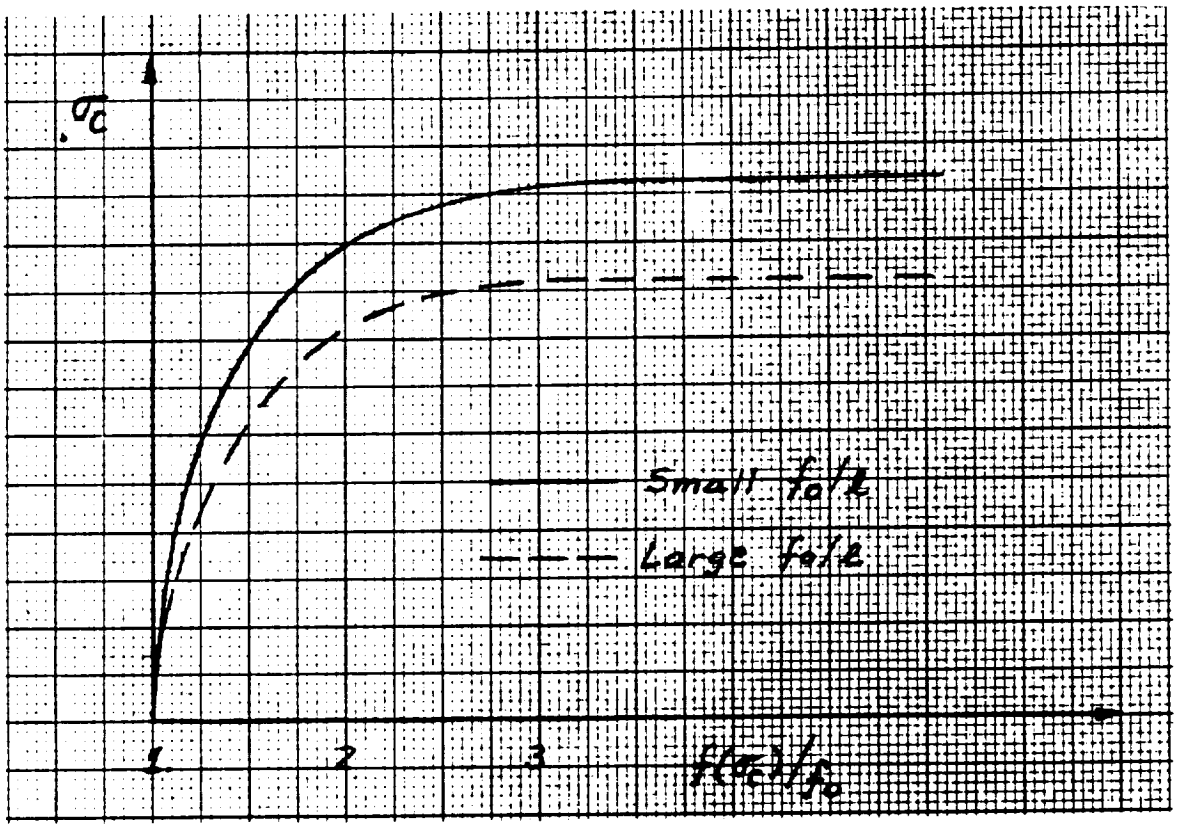

Fig. 8 A hypothetical compression strength, σ_c, as a function of lateral fiber deflection, $f(\sigma_c)$, suggested by Wang.[68,69]

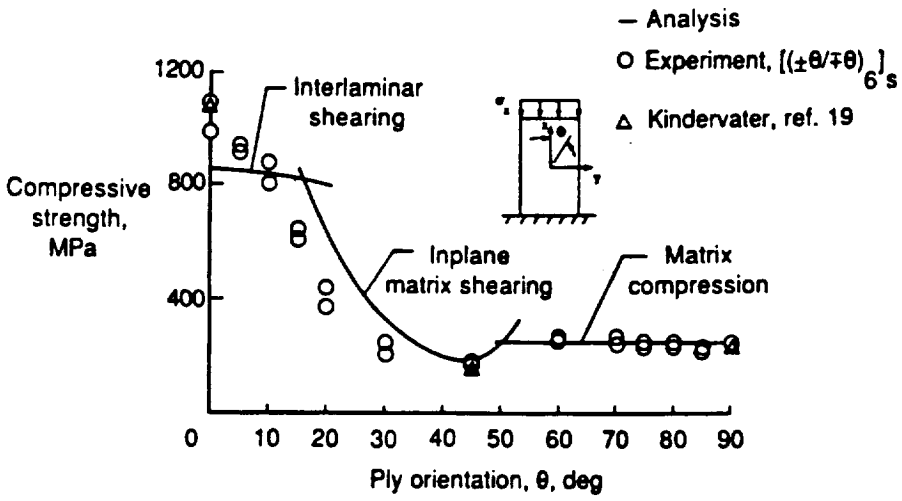

Fig. 9 Compressive strength as a function of ply orientation for $[\pm\theta]_s$-class AS4/3502 laminates.[73]

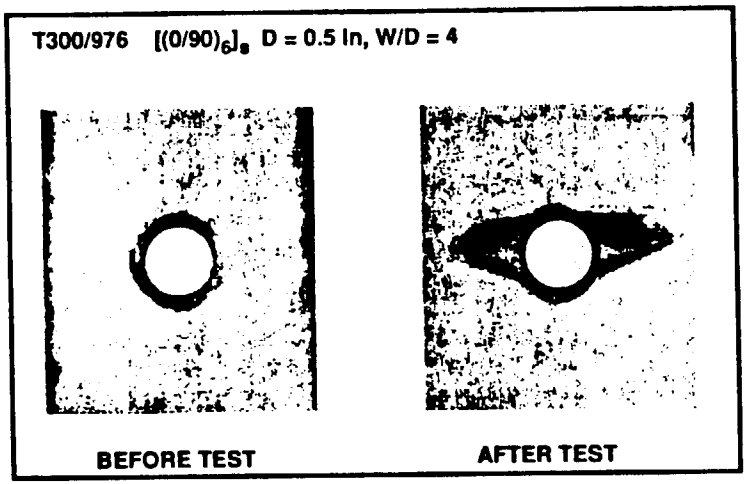

a

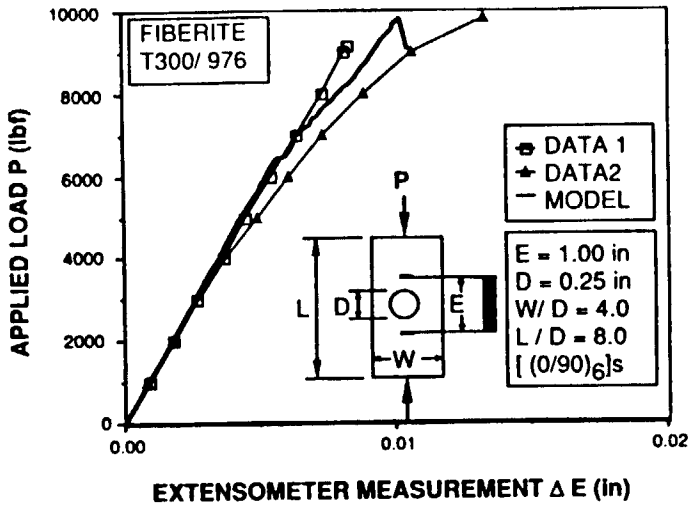

b

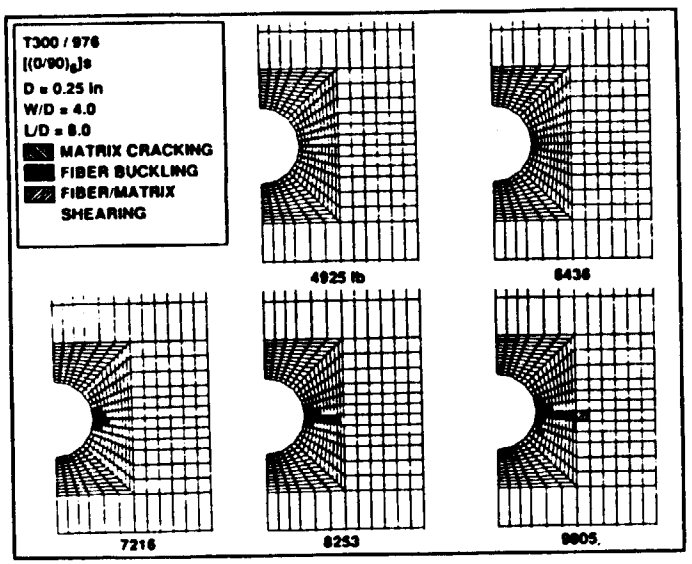

c

Fig. 10 Typical analytical and experimental results for a graphite/epoxy $[(0/90)_6]_s$ laminate.[72]
a) X-radiographs.
b) Load-displacement curves.
c) Illustration of specimen damage.

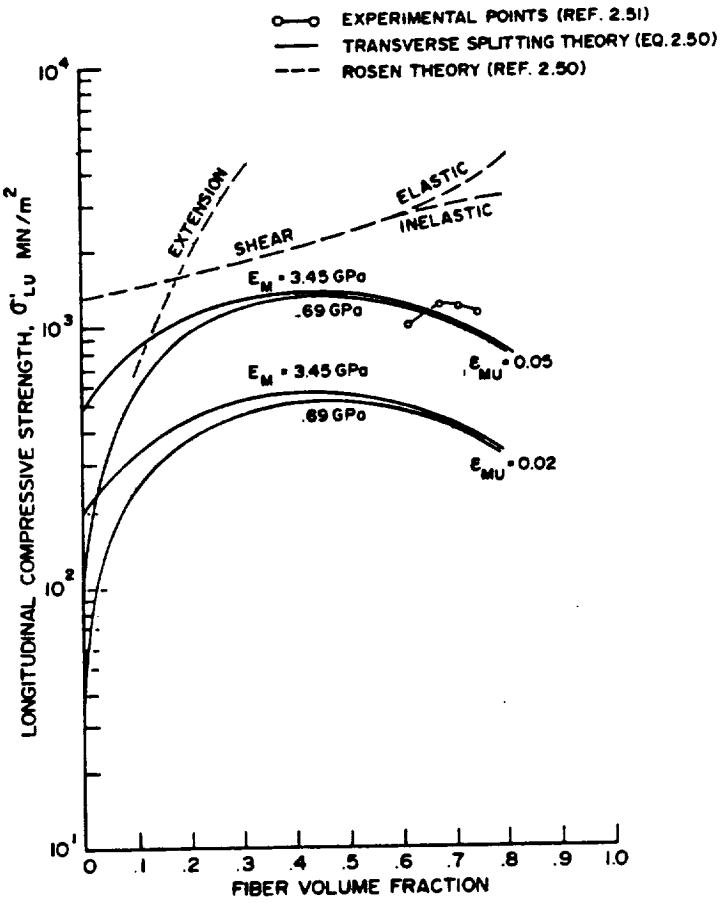

Fig. 11 Predicted and experimental values of longitudinal compressive strength, theories of Rosen (Eqns. 1 and 3) and Broutman(Eqn. 4).[24]

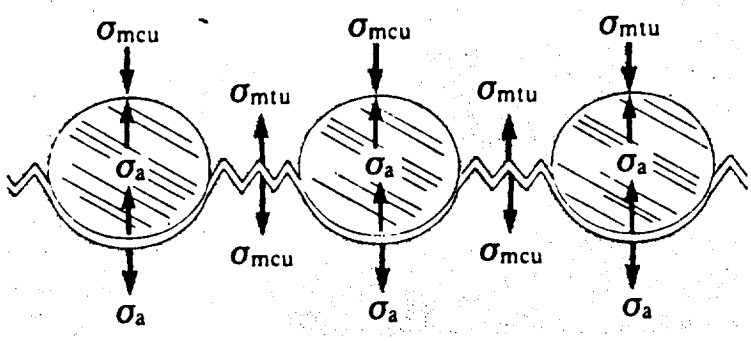

Fig. 12 Stresses involved in the longitudinal splitting failure of a composite, developed by Piggott.[58]

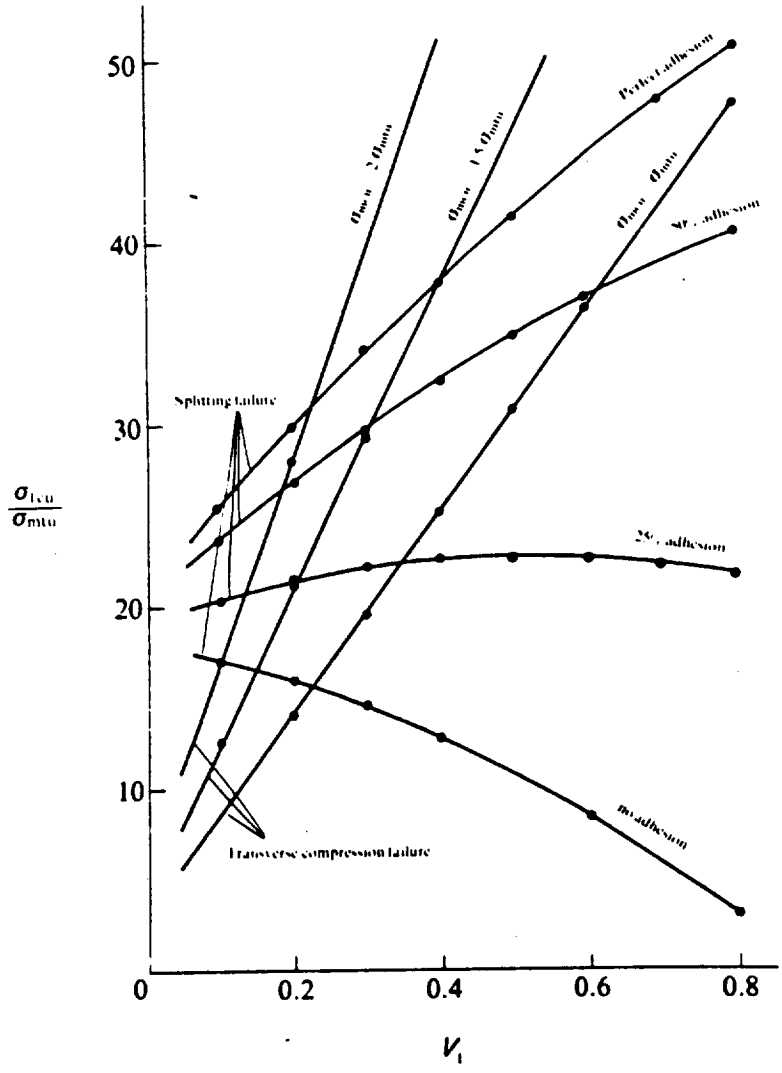

Fig. 13 Dimensionless plot, developed by Piggott,[58] for composite compressive strength when controlled by transverse splitting and transverse matrix compression failure.

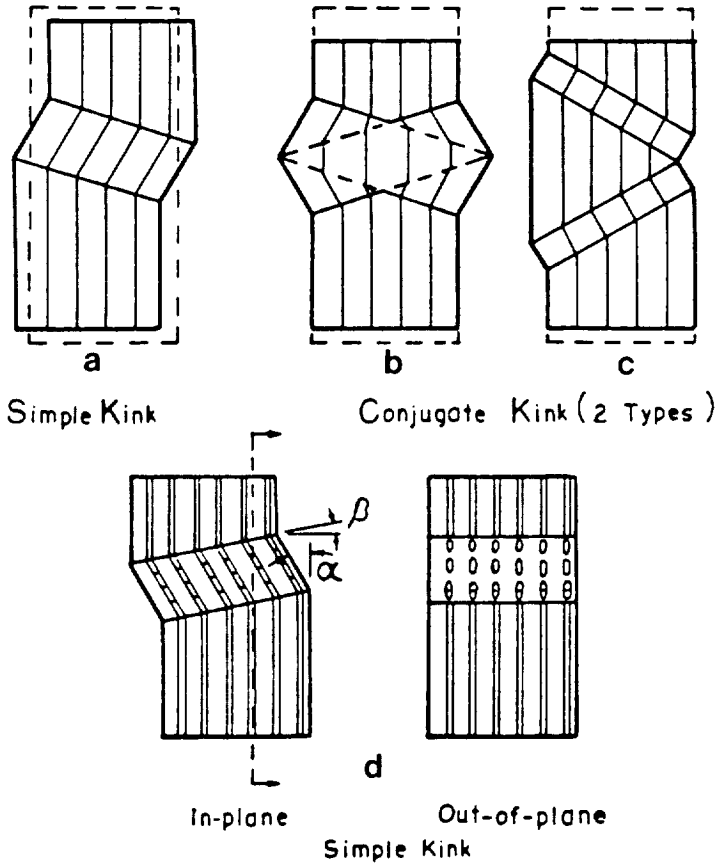

Fig. 14 Schematics describing kink bands.[98]
a) Simple kink.
b) Conjugate kink, type 1.
c) Conjugate kink, type 2.
d) Notation for a simple kink, in-plane and out-of-plane.

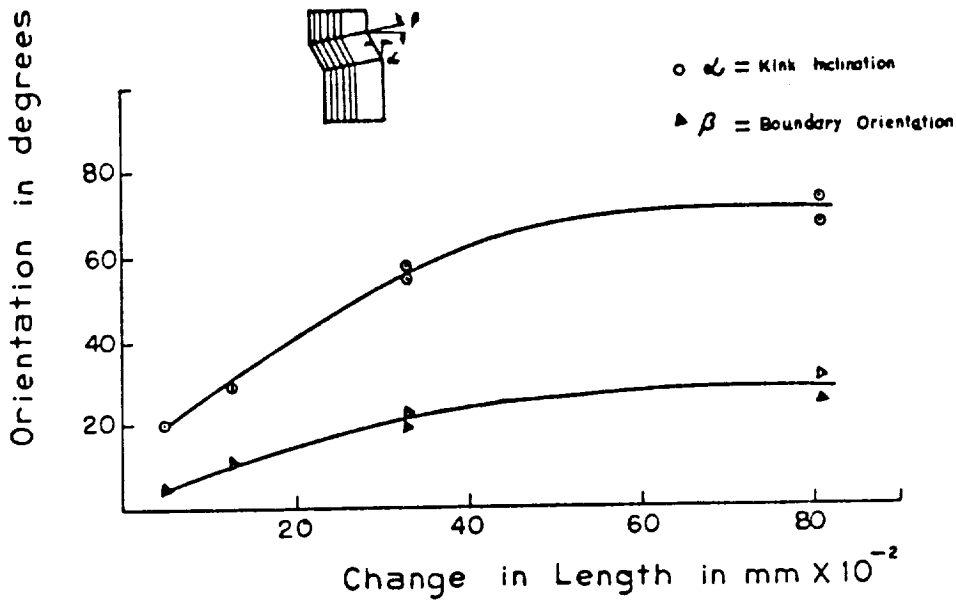

Fig. 15 Kink orientation relationship as a function of post-failure deformation, Δl.[98]

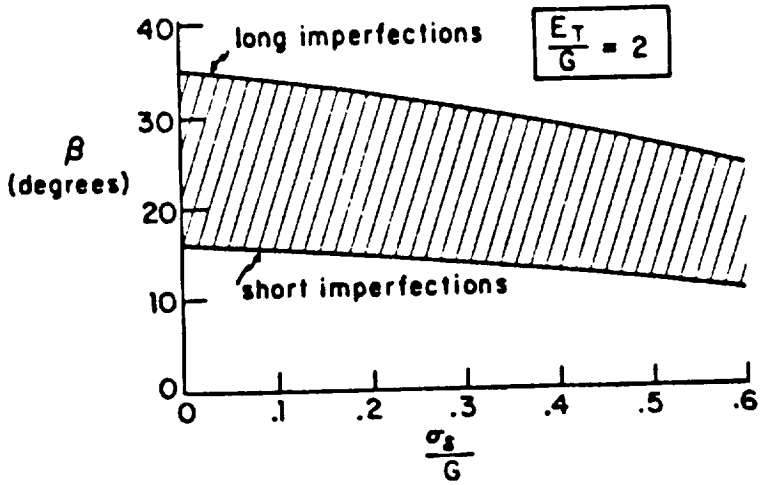

a

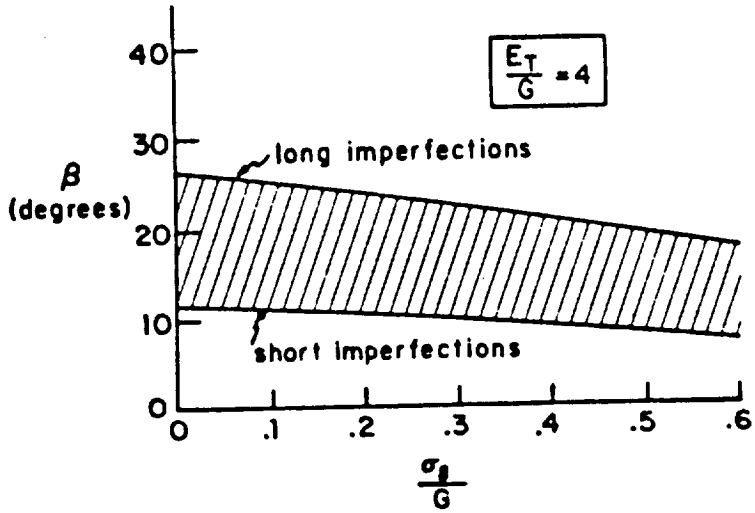

b

Fig. 16 Estimated kink-band inclinations.[87]
a) $\frac{E_T}{G} = 2$.
b) $\frac{E_T}{G} = 4$.

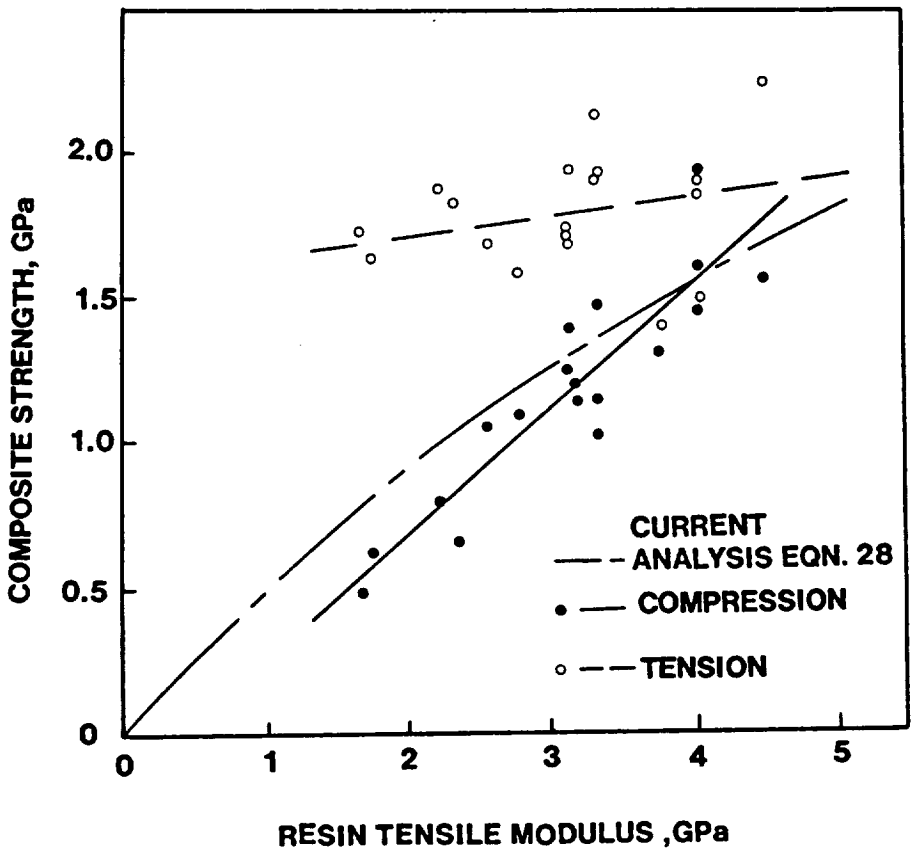

Fig. 17 Effect of resin tensile modulus on composite tensile and compressive strengths.[23]

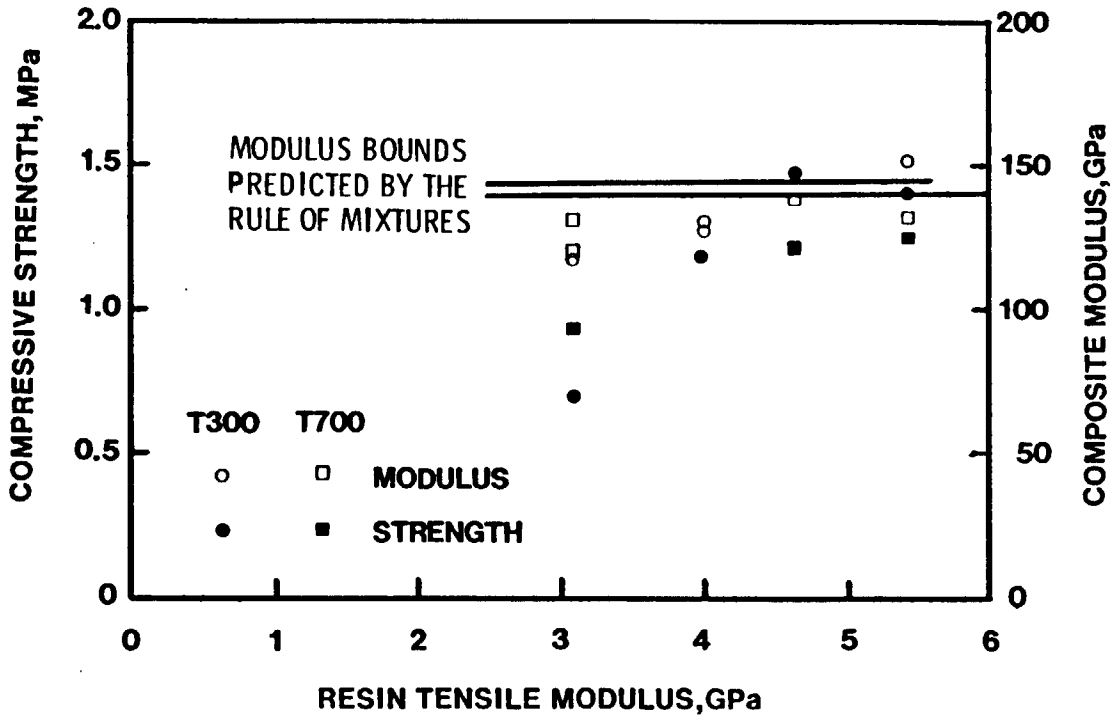

Fig. 18 Effect of resin tensile modulus on compressive modulus and strength of T300 and T700 composites.[23]

Table 1. Young's Moduli of Fibers.

Fiber	E_f kg/mm²
For Polyester Specimen	7.28×10^3
For Epoxy Specimen	7.13×10^3

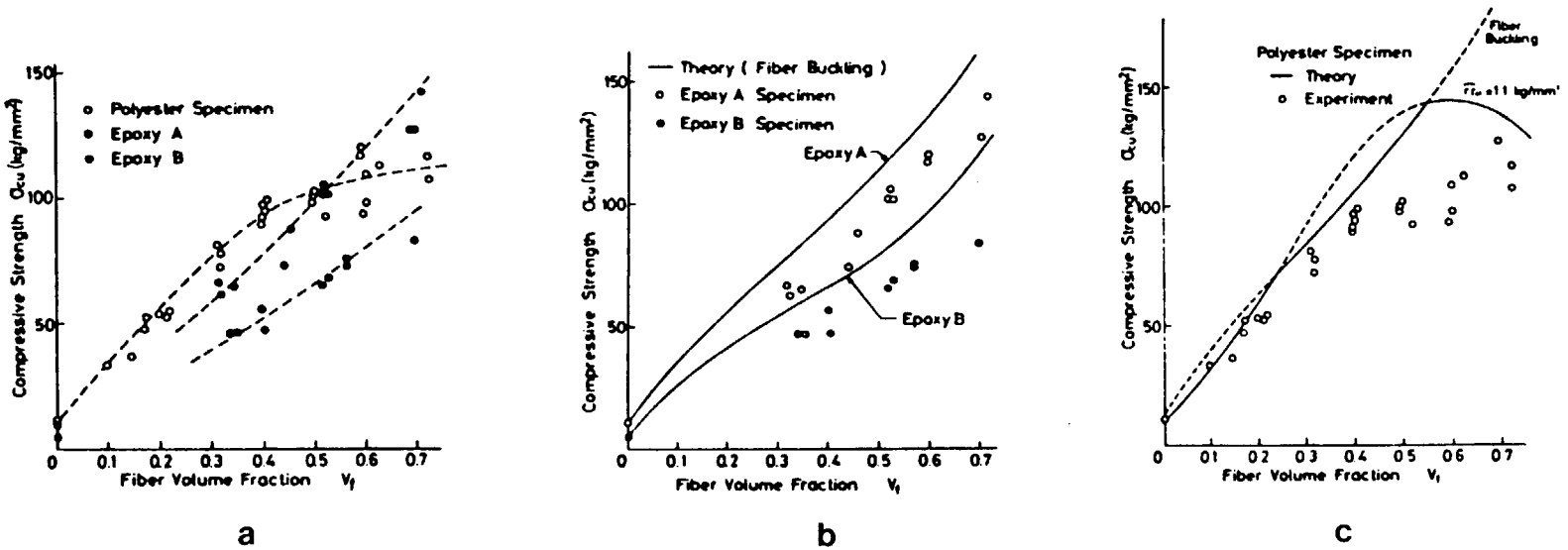

Fig. 19 Compression strength as a function of fiber volume fraction.[47]
a) Experimental data.
b) Comparison of fiber buckling theory and experimental data for two epoxy composites.
c) Comparison of fiber buckling and interfacial debonding failure theories.

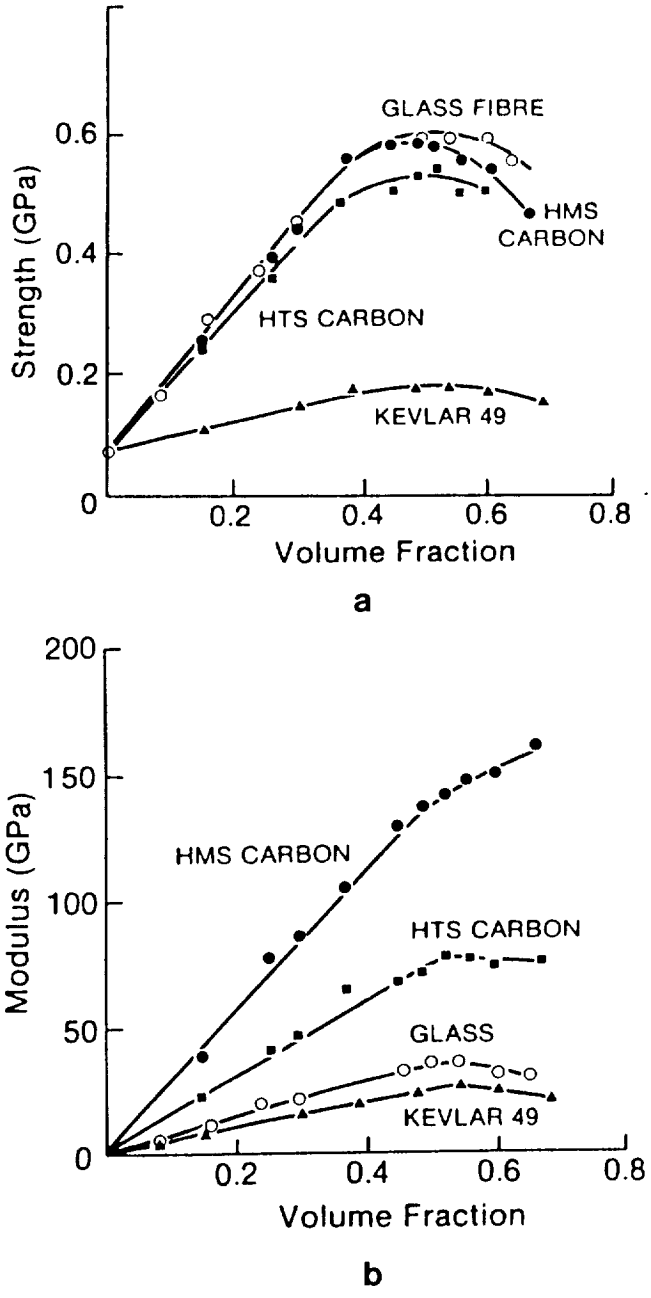

Fig. 20 The effects of fiber volume fraction on compressive strength and modulus.[57]

a) Compressive strength as a function of fiber volume fraction for various fibers embedded in a polyester resin.

b) Compressive modulus as a function of fiber volume fraction for various fibers embedded in a polyester resin.

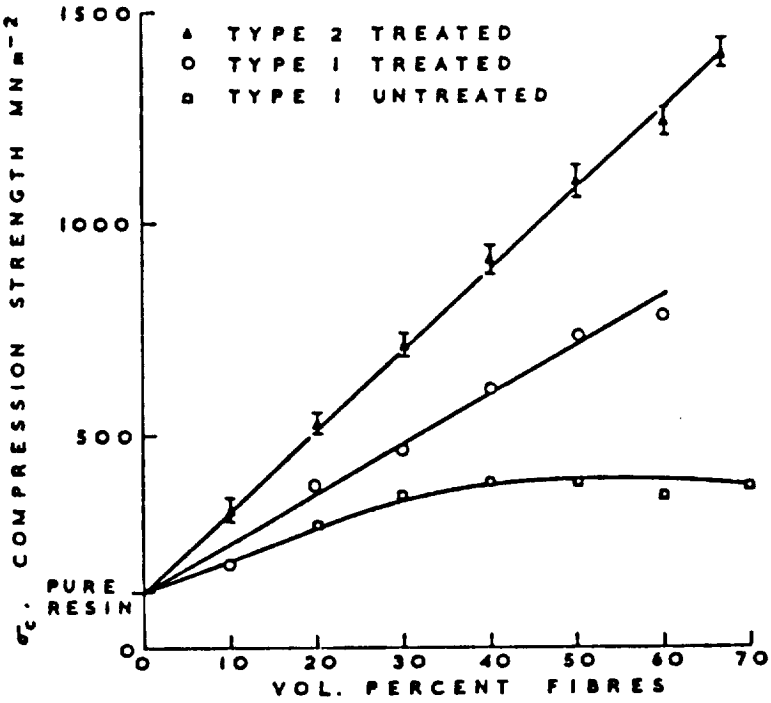

Fig. 21 Variation of compression strength as a function of fiber volume fraction.[82]

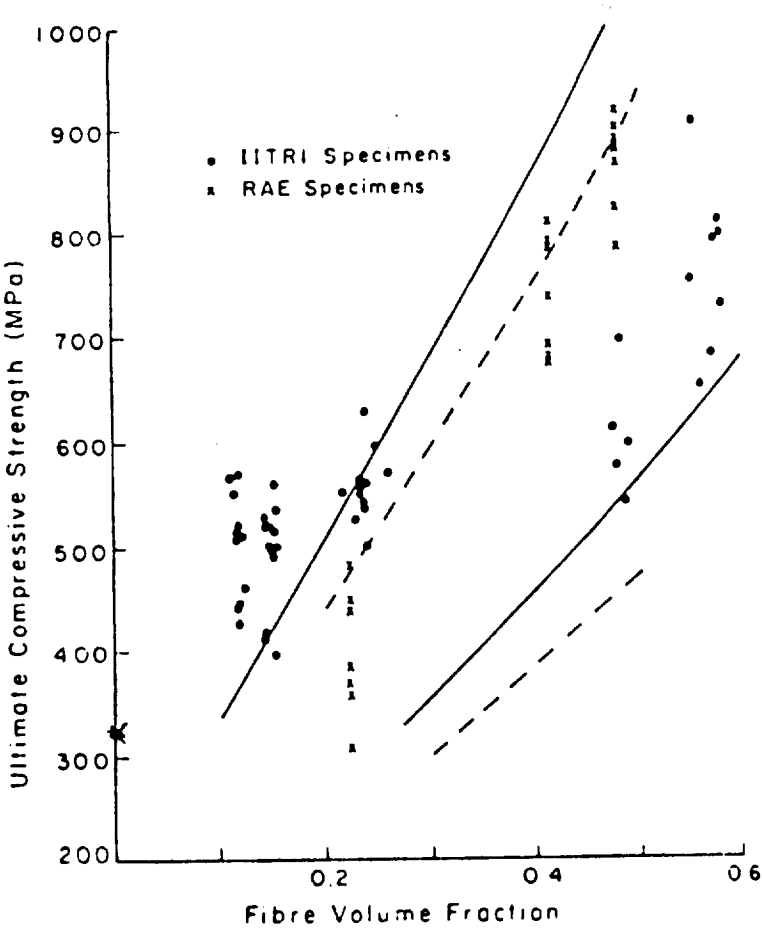

Fig. 22 Compressive strength of composites obtained from IITRI and RAE test fixtures.[88]

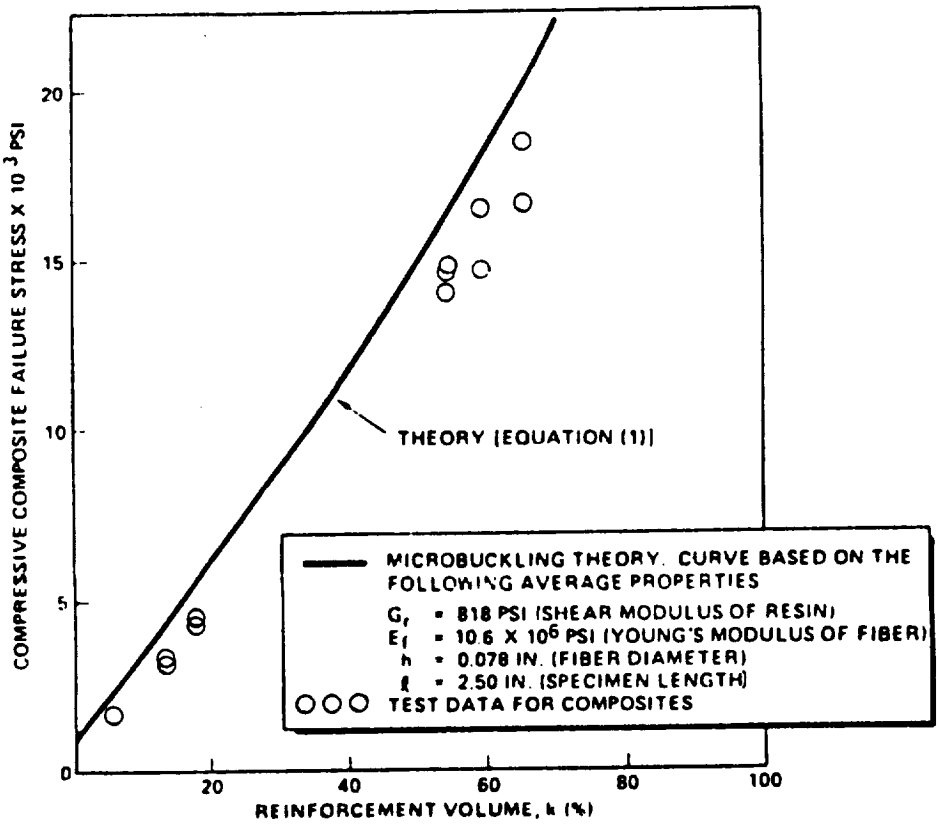

Fig. 23 Test-theory comparison of compressive microbuckling strength of circular fiber-reinforced composites having various fiber volume fractions.[53]

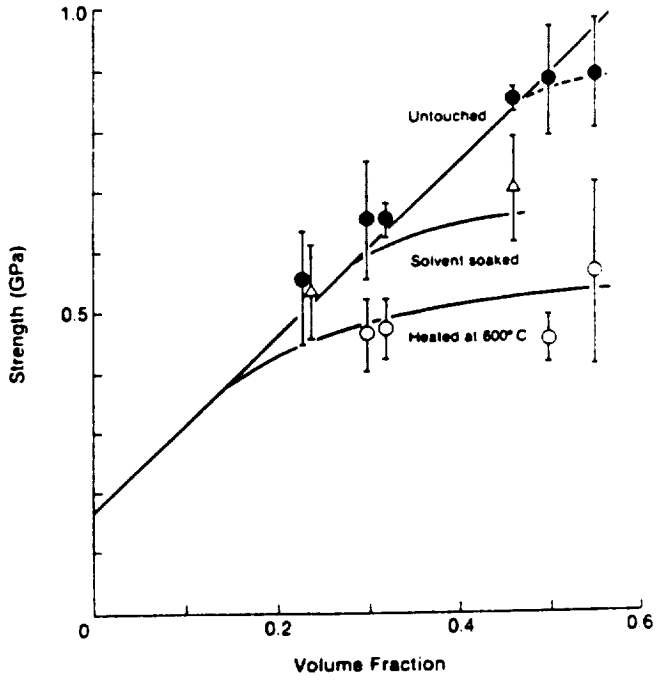

Fig. 24 Effect of interfacial bonding on the compressive strength of glass/polyester composites.[57]

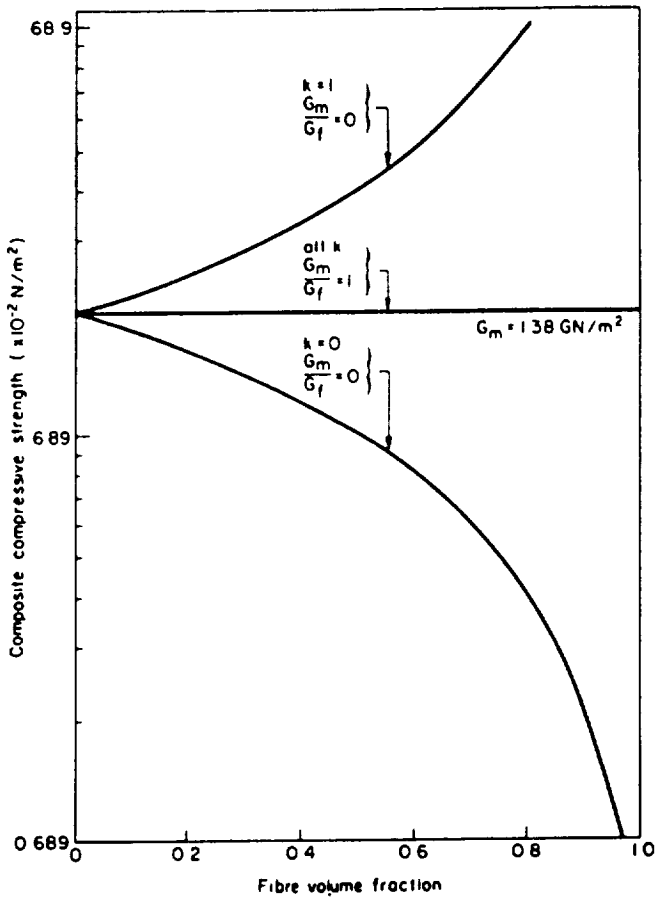

Fig. 25 Variation of composite compressive strength with fiber volume fraction for good interfacial bonding ($k = 1$) and for poor interfacial bonding ($k = 0$).[48]

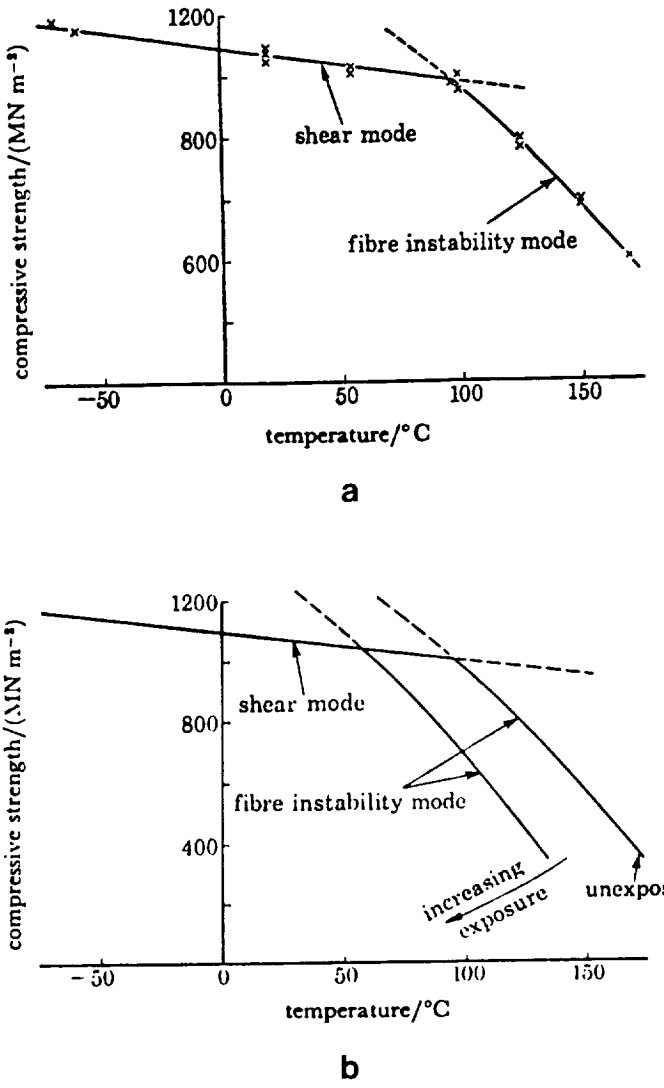

Fig. 26 Environmental effects on the unidirectional compressive strength of CFRP[133]

a) Experimentally determined variation of compressive strength with temperature.

b) Expected variation of compressive strength with temperature-humidity exposure.

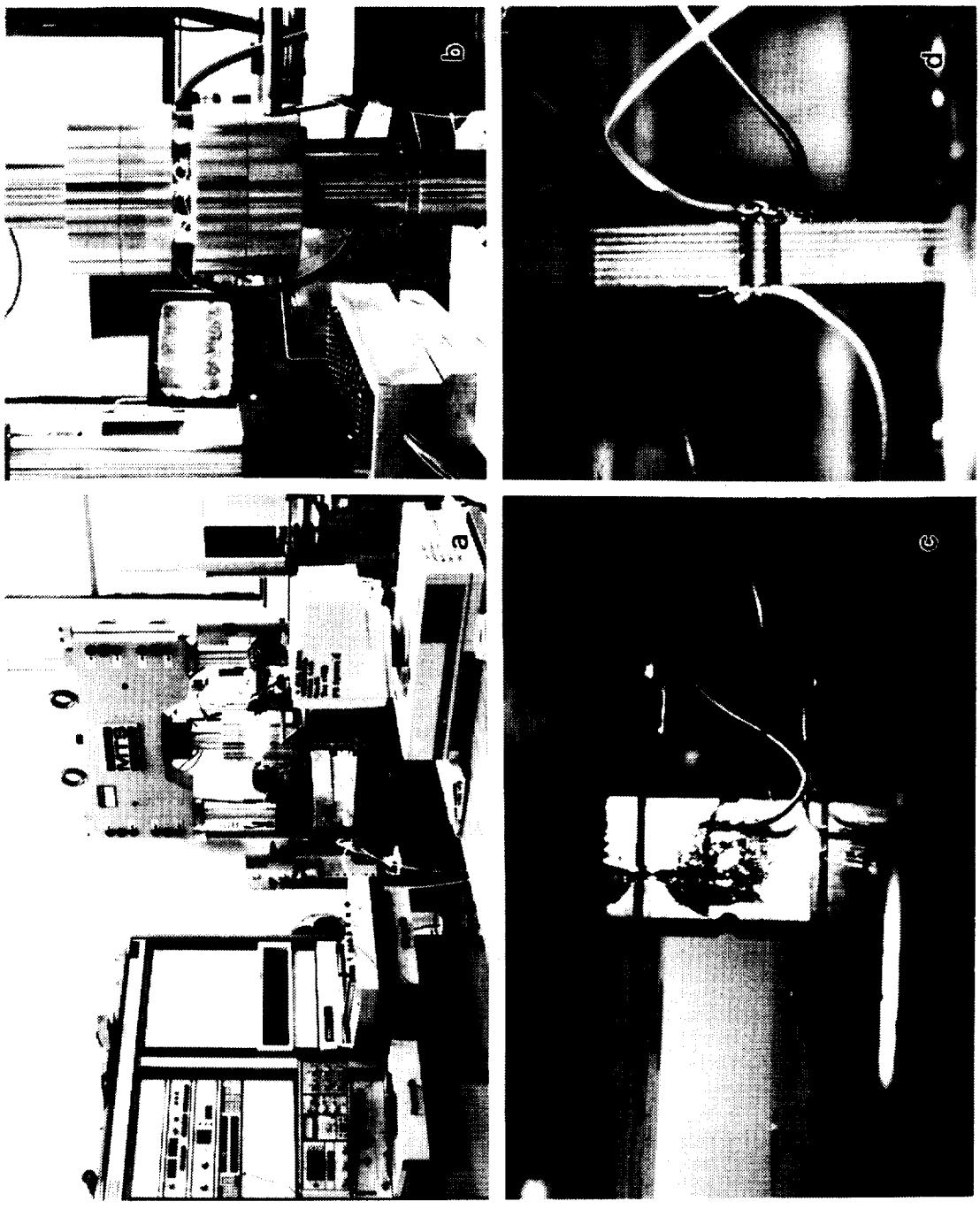

Fig. 27 Compression test facilities.
a) Overview of MTS test stand, controller, and data acquisition.
b) Close-up showing gripped specimen, stereomicroscope in the background, and video image of notch edge.
c) Surface view of edge-notched specimen with strain gages, gripped in MTS test stand.
d) Edge view of specimen with strain gages.

Fig. 28 Shim casting fixture.

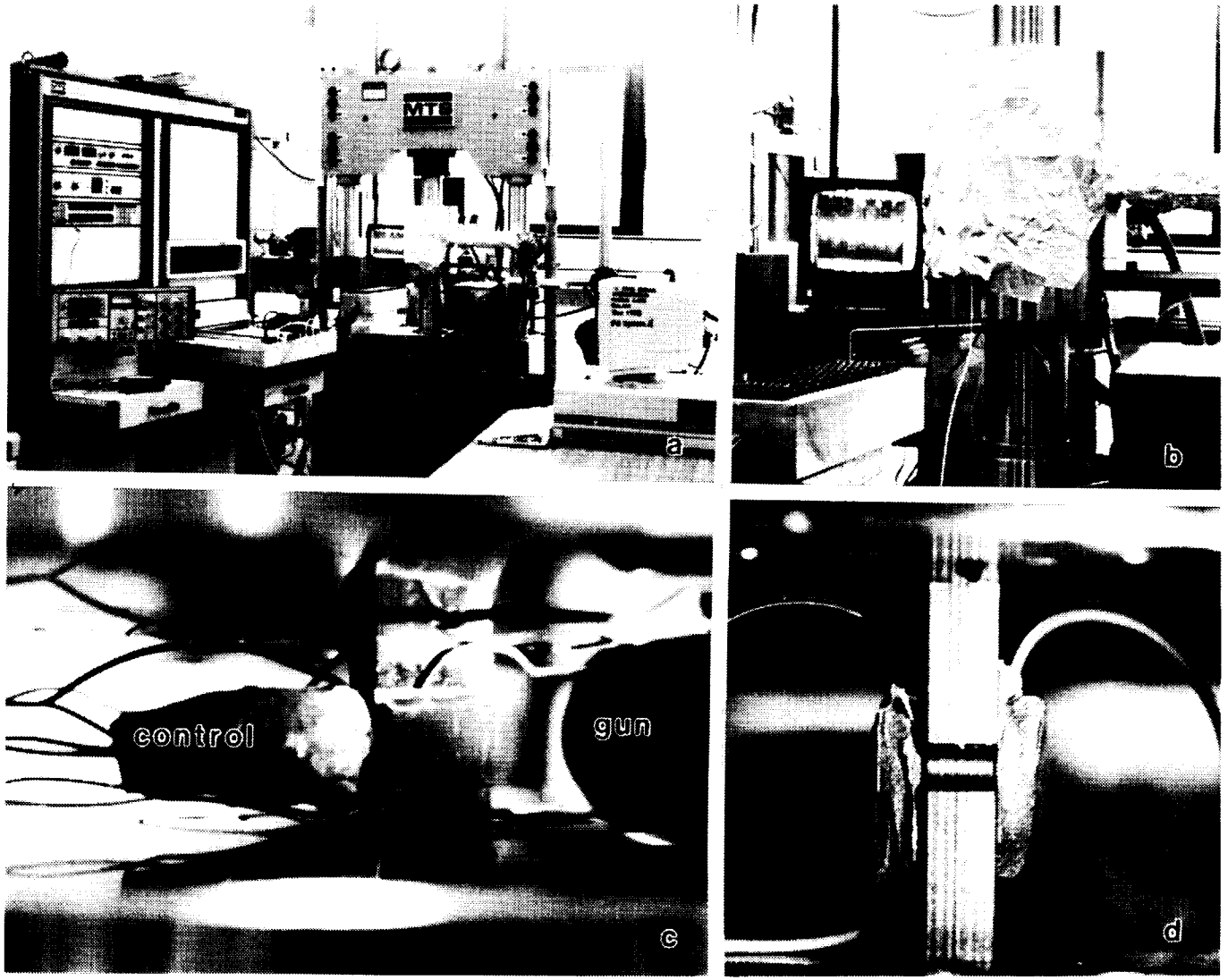

Fig. 29 High temperature compression test facilities.
a) Overview of MTS test stand, controller, and data acquisition.
b) Close-up showing gripped specimen, stereomicroscope in the background, video image of notch edge, and the heat gun.
c) Surface view of edge-notched specimen with strain gages, gripped in MTS test stand.
d) Edge view of specimen with strain gages.

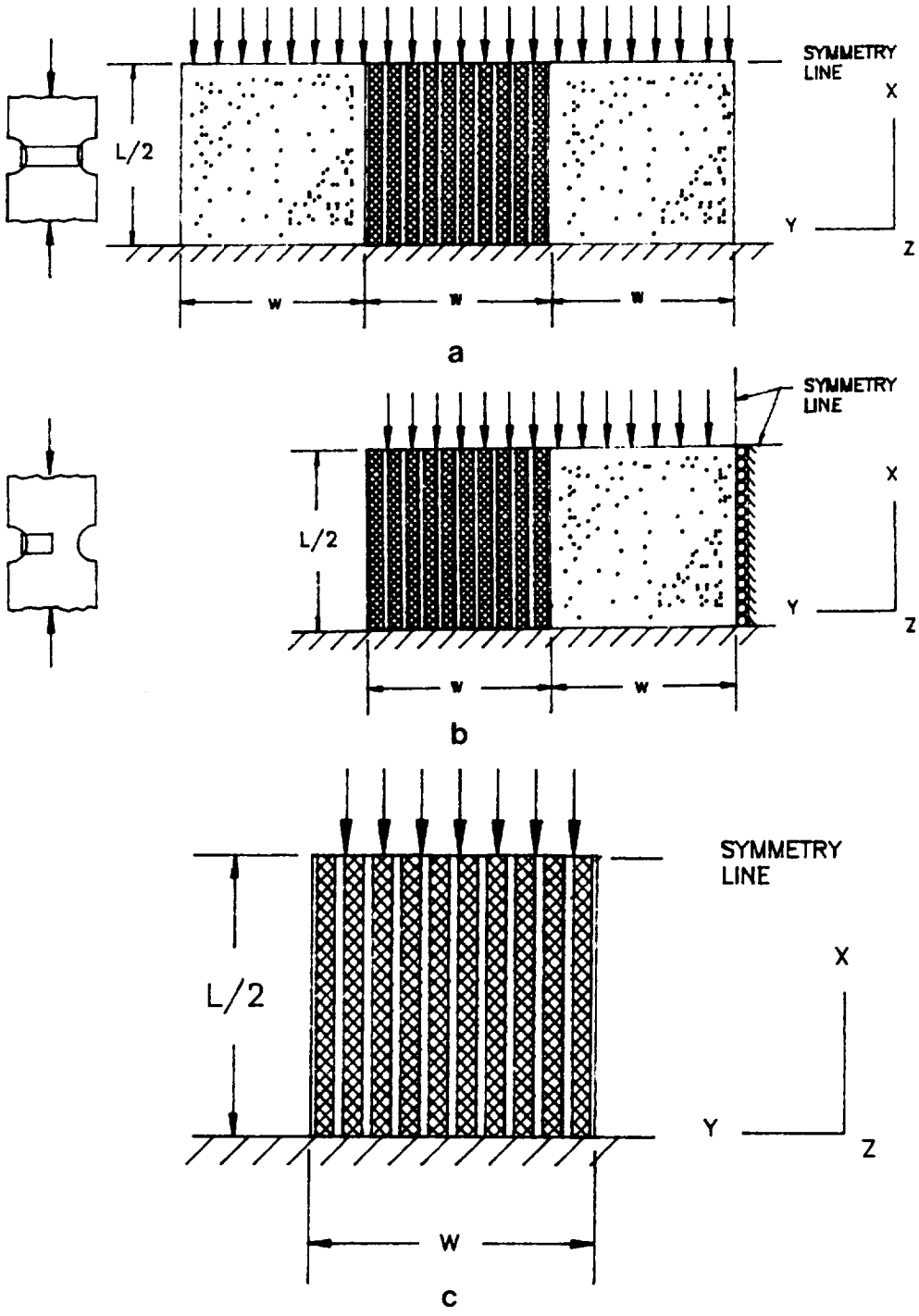

Fig. 30 Models for straight fiber problem.
a) Infinite model.
b) Semi-infinite model.
c) Finite, ten fiber/matrix model.

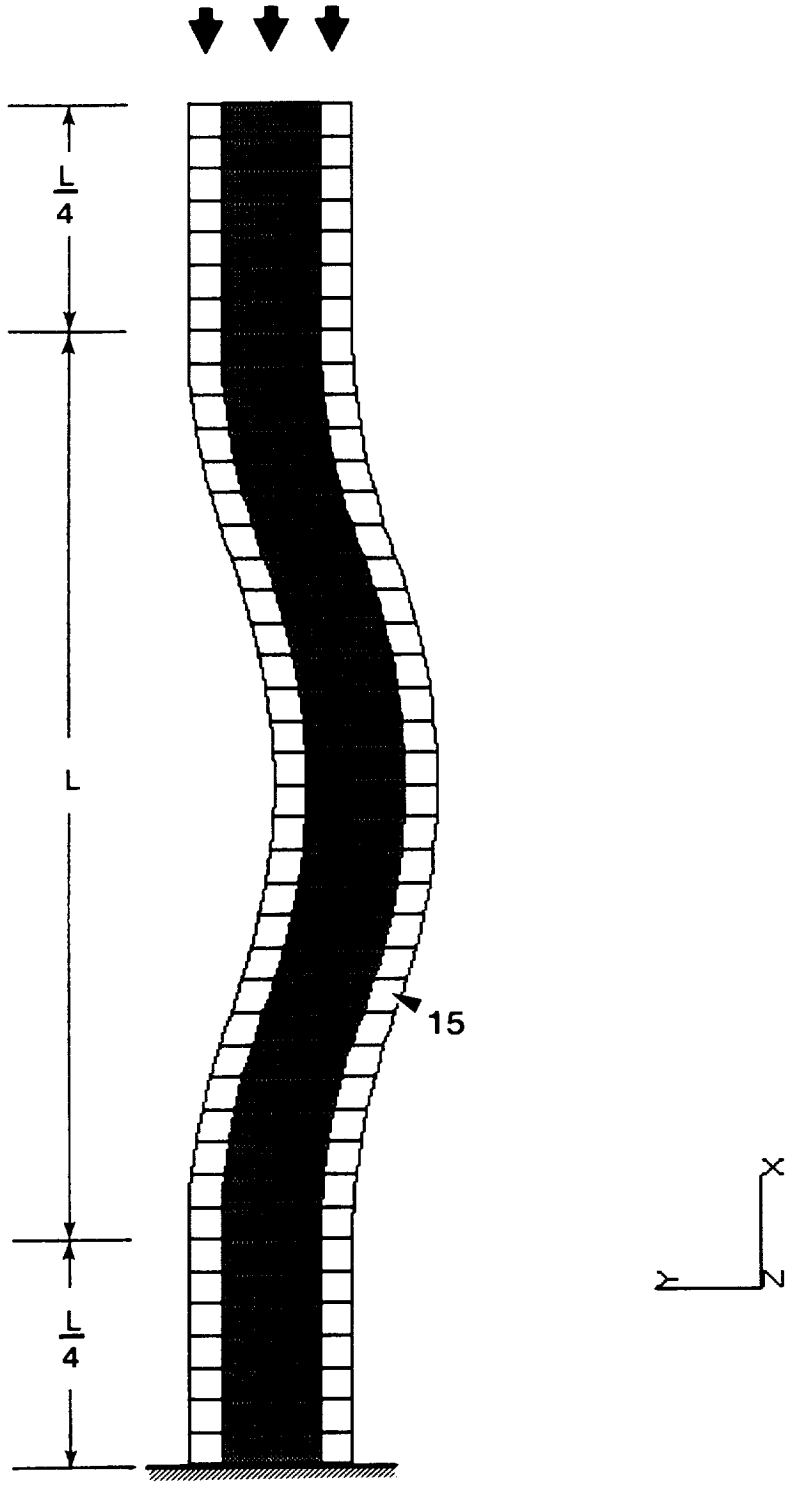

Fig. 31 Meshed geometry for one fiber (dark gray region) with half-matrix (white regions) with an initial curvature $\frac{a_o}{L}$.

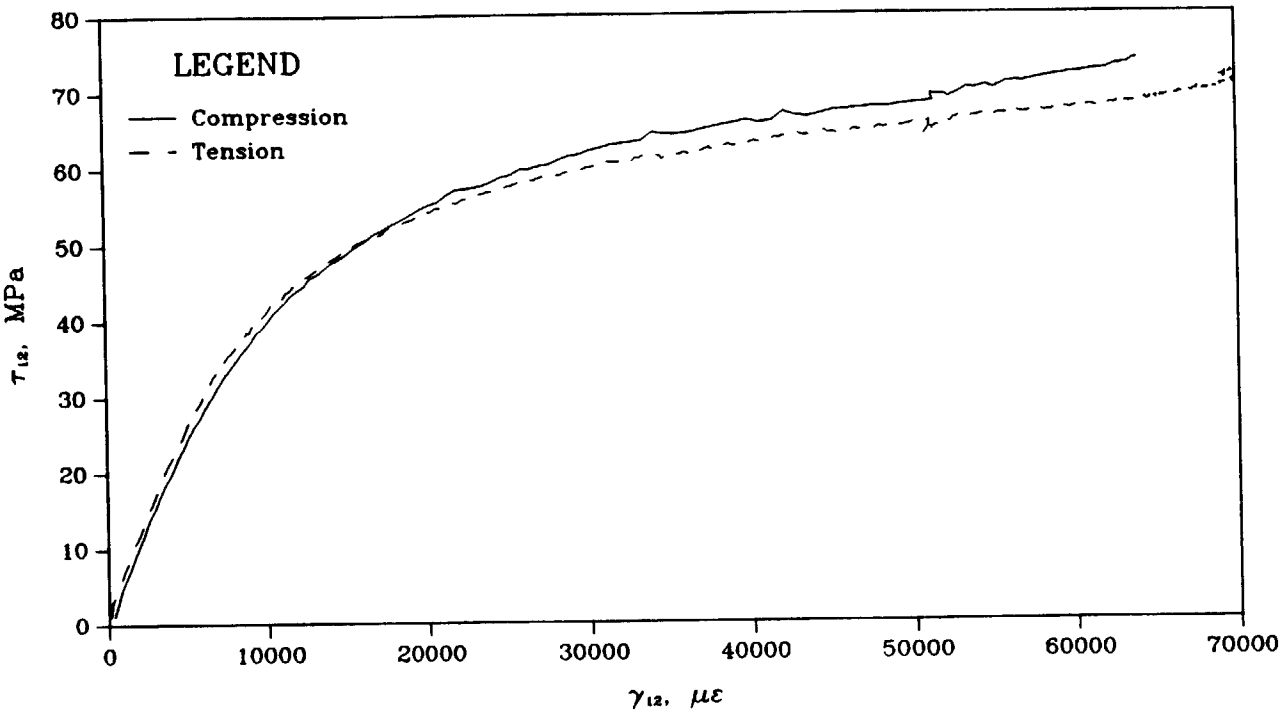

Fig. 32 Shear stress-strain curves obtained from the tension and compression testing of $[\pm 45]_{ns}$ specimens at 21°C.

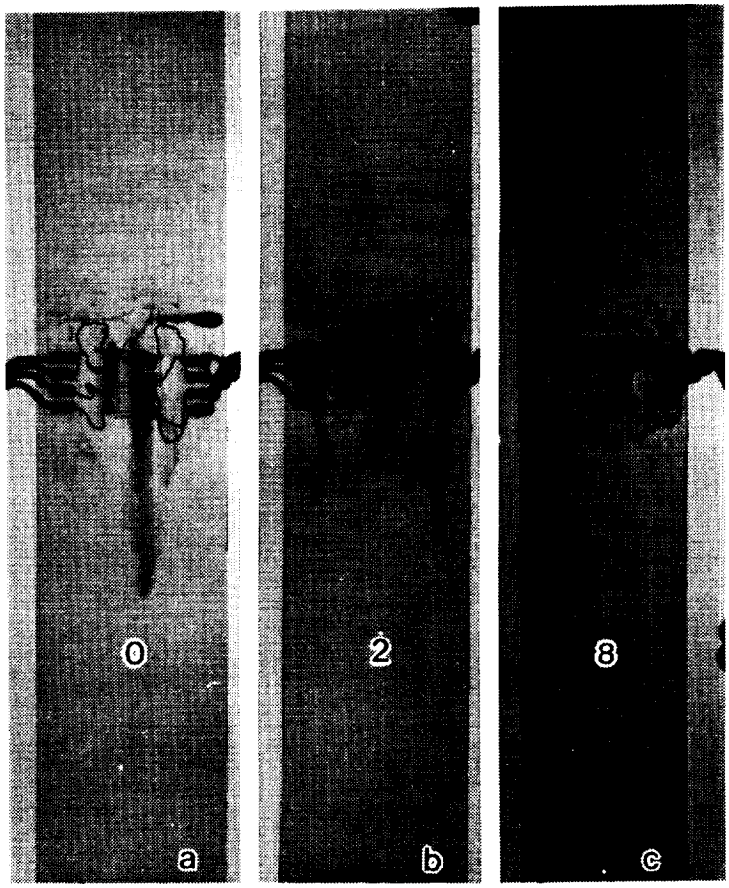

Fig. 33 Dye-penetrant enhanced radiographs of a tension-loaded $[\pm 45]_{2s}$ specimen.
a) Virgin specimen, prior to loading.
b) Applied axial strain level is 2%.
c) Applied axial strain level is 8%.

Fig. 34 Dye-penetrant enhanced radiograph of a compression-loaded $[\pm 45]_{8s}$ specimen. Applied axial strain level is 9.7%.

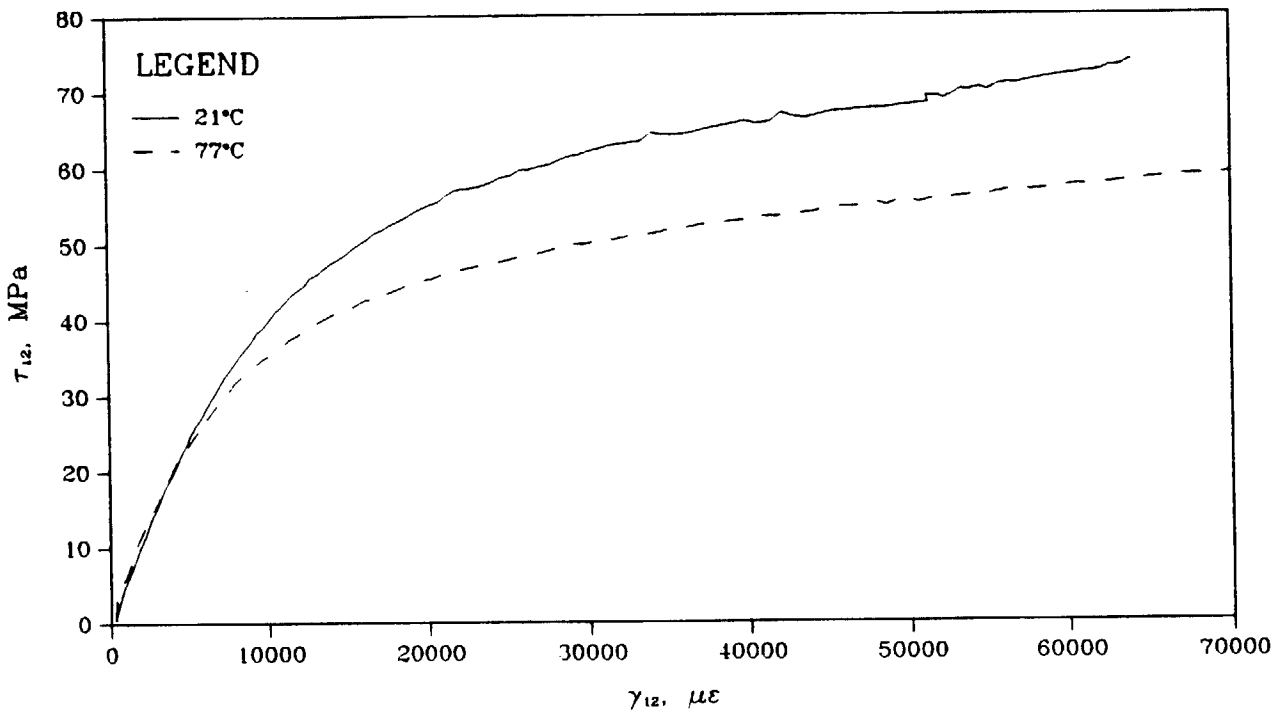

Fig. 35 Shear stress-strain curves obtained from compression-loaded $[\pm 45]_{8s}$ specimens tested at 21°C and 77°C.

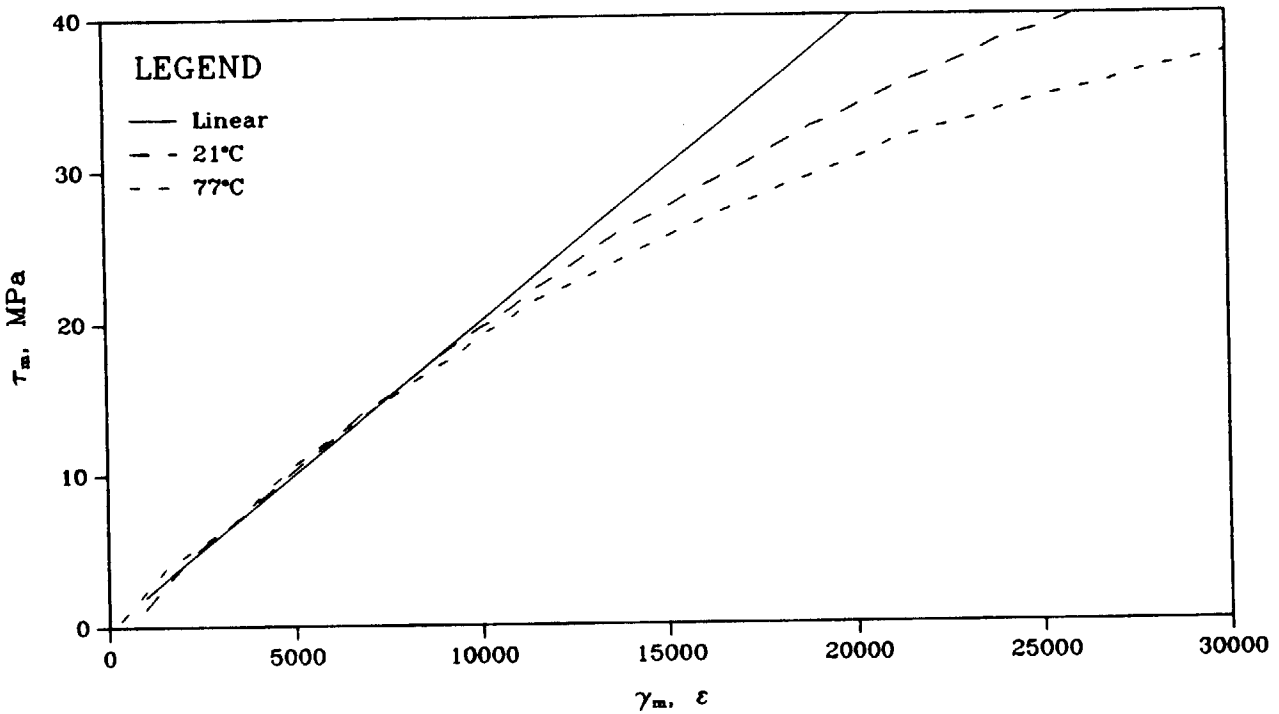

Fig. 36 Shear constitutive behaviors of the PEEK resin at 21°C and 77°C.

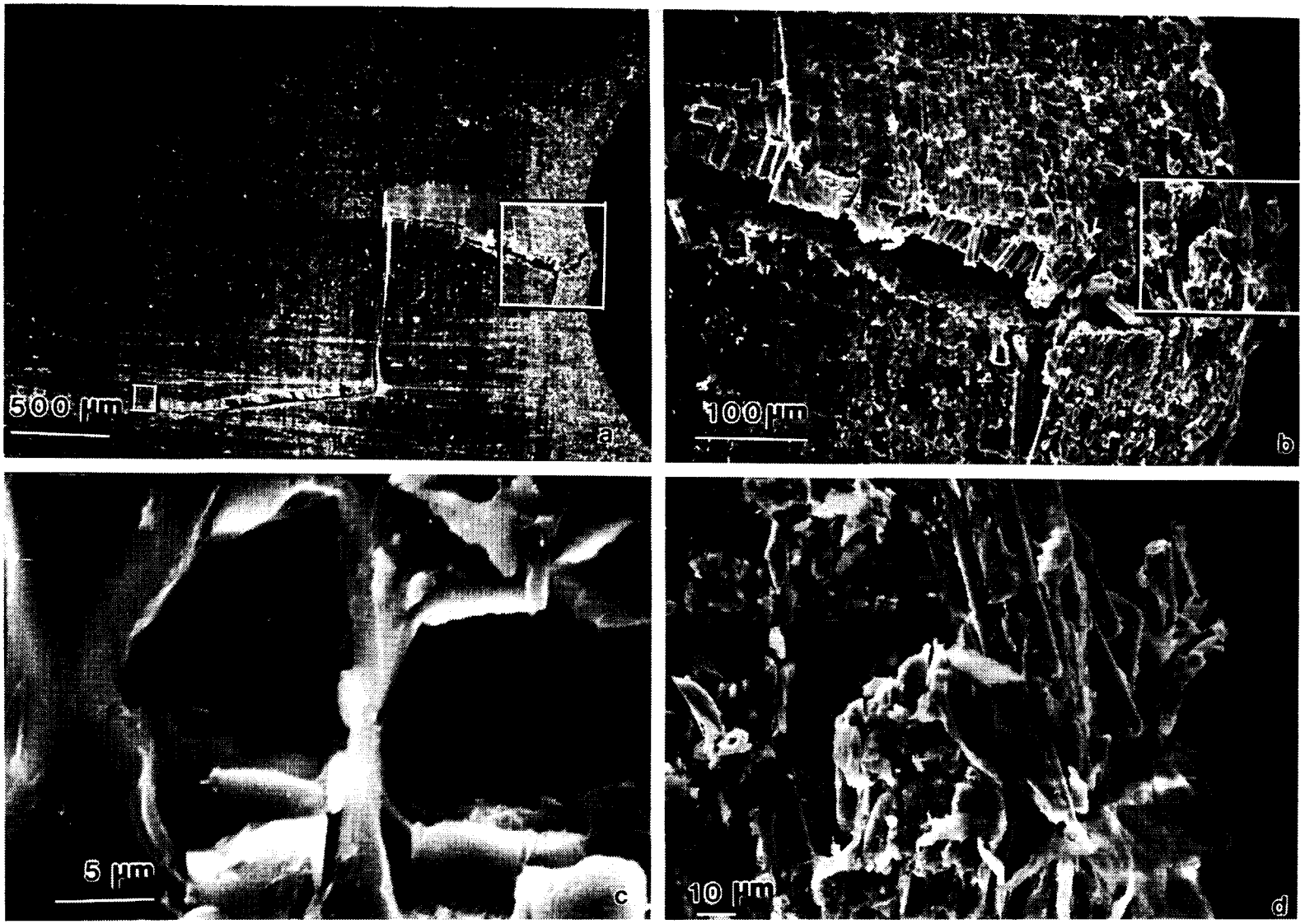

Fig. 37 Surface view of in-plane and out-of-plane fiber microbuckling of a $[(0_2/\pm 45)_3/0/\pm 45]_s$ laminate tested at 21°C.
a) In-plane and out-of-plane fiber microbuckling.
b) Detail of (a) showing in-plane fiber microbuckling.
c) Detail of (a) showing matrix deformation and tensile-type fiber breaks in the surface ply.

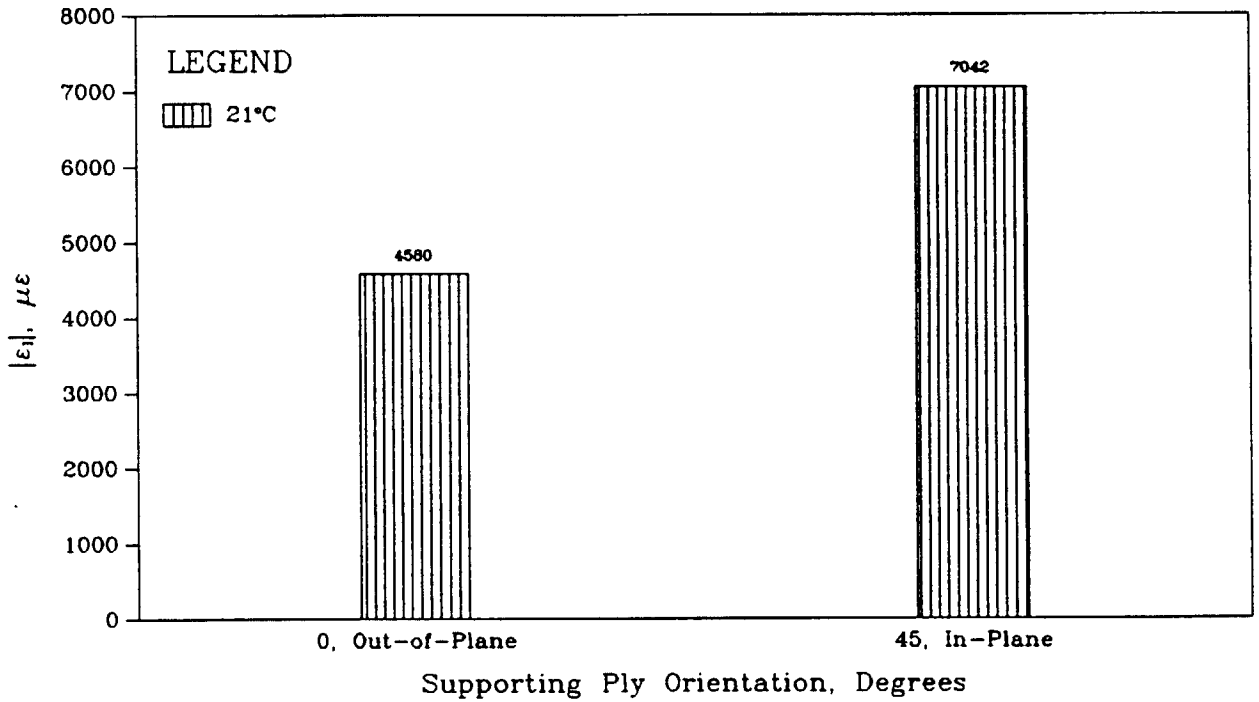

Fig. 38 Bar chart showing the free surface effects on fiber microbuckling initiation in $[(\pm 45/0_2)_3/\pm 45/0]_s$ and $[(0_2/\pm 45)_3/0/\pm 45]_s$ laminates tested at 21°C.

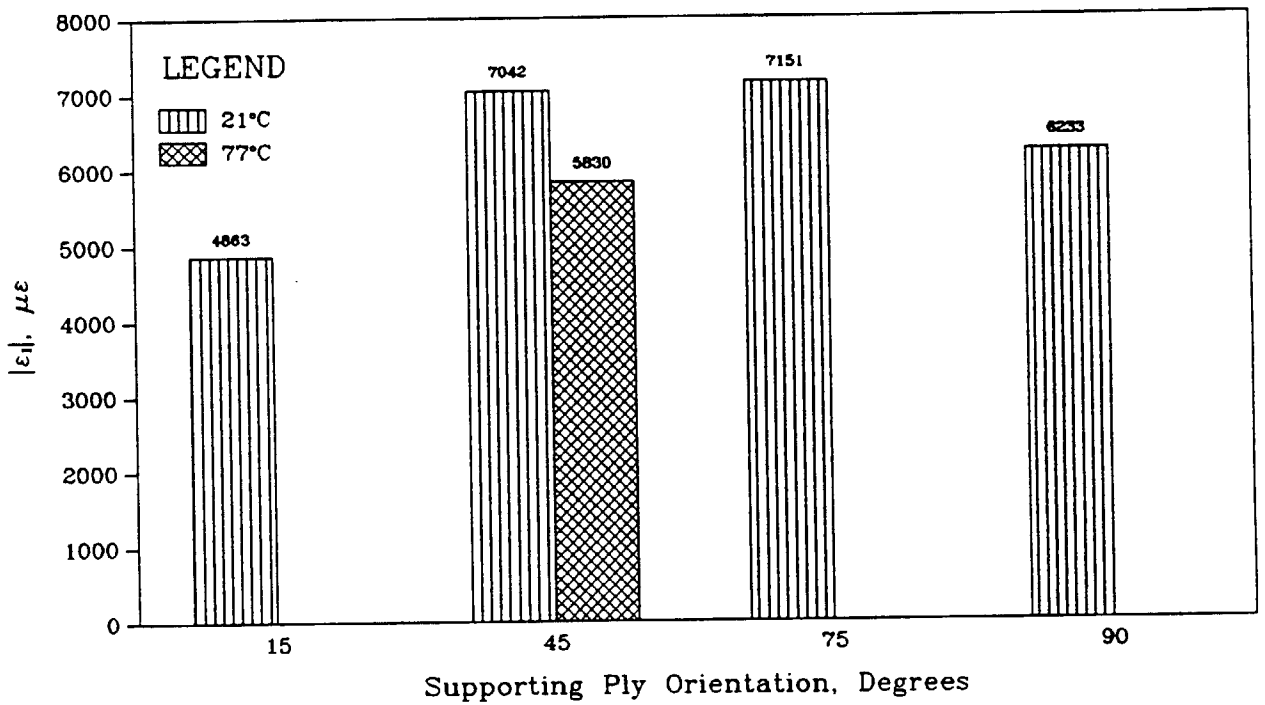

Fig. 39 Bar chart showing the effects of supporting ply orientation on fiber microbuckling initiation in $[(\pm 15/0_2)_3/\pm 15/0]_s$, $[(\pm 45/0_2)_3/\pm 45/0]_s$, $[(\pm 75/0_2)_3/\pm 75/0]_s$, and $[(90_2/0_2)_3/90_2/0]_s$ laminates tested at 21°C.

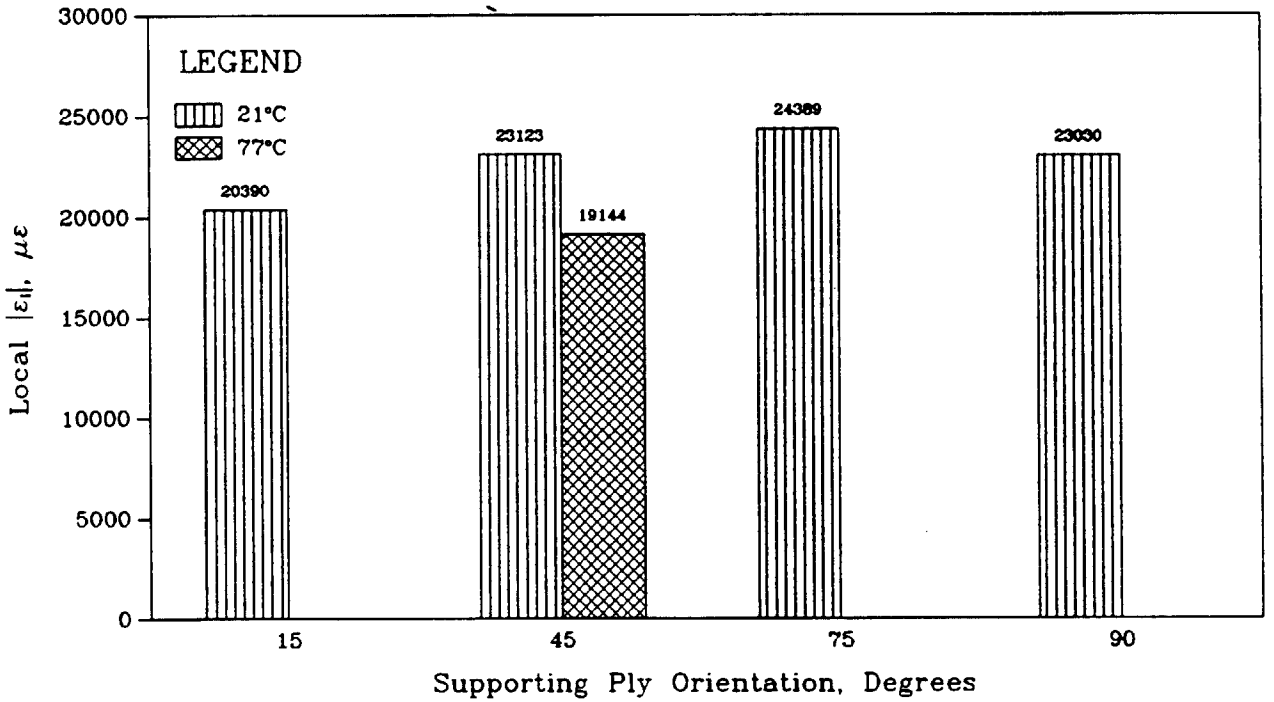

Fig. 40 Bar chart showing the local fiber microbuckling initiation strain levels for the laminates in Fig. 39.

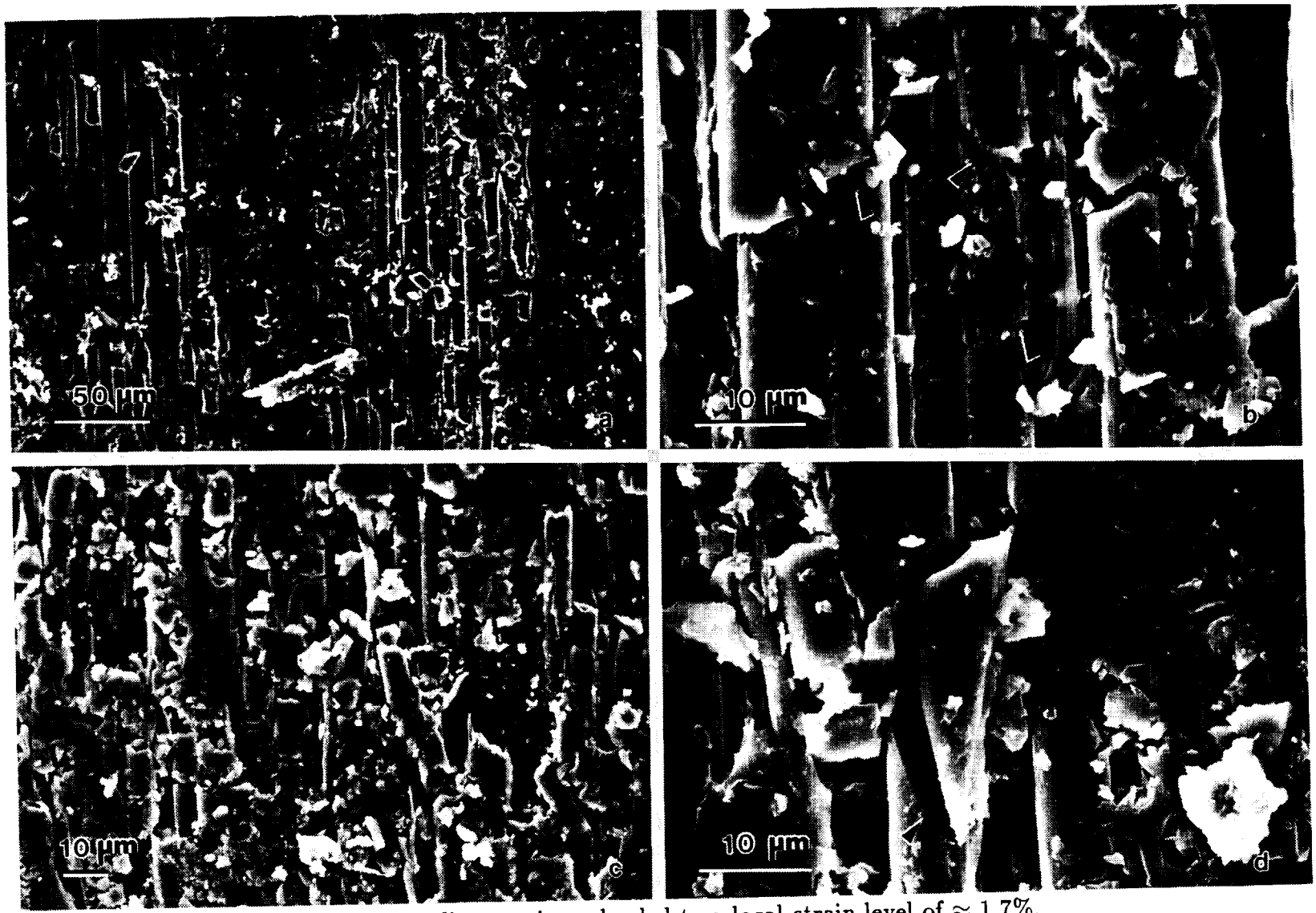

Fig. 41 Baseline specimen loaded to a local strain level of $\approx 1.7\%$.
a) Multiple fiber breaks in 0_2 plies near the free surface.
b) Detail of (a) showing multiple fiber shear breaks.
c) Multiple fiber breaks in the center 0_2 plies.
d) High magnification of a fiber shear failure.

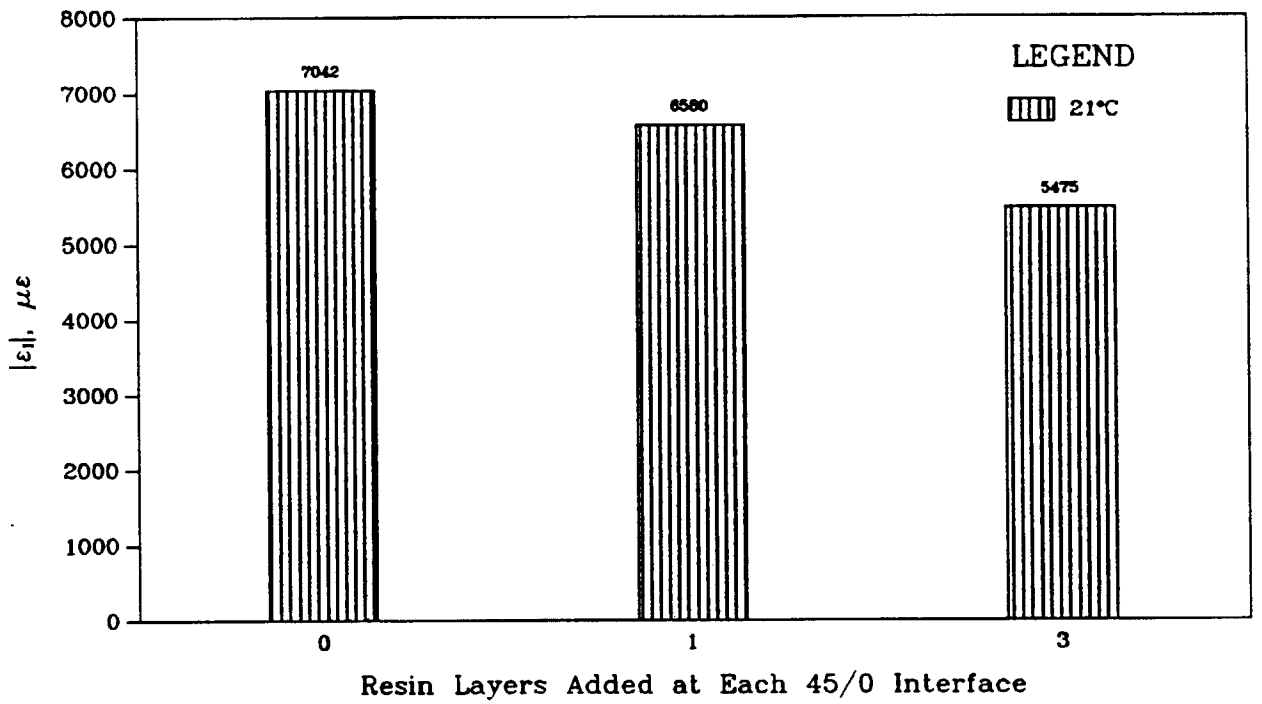

Fig. 42 Bar chart showing the effects of resin-rich regions on fiber microbuckling initiation on $[(\pm 45/0_2)_3/\pm 45/0]_s$, $[(\pm 45/f/0_2/f)_3/\pm 45/f/0]_s$, and $[(\pm 45/f_3/0_2/f_3)_3/\pm 45/f_3/0]_s$ laminates tested at 21°C.

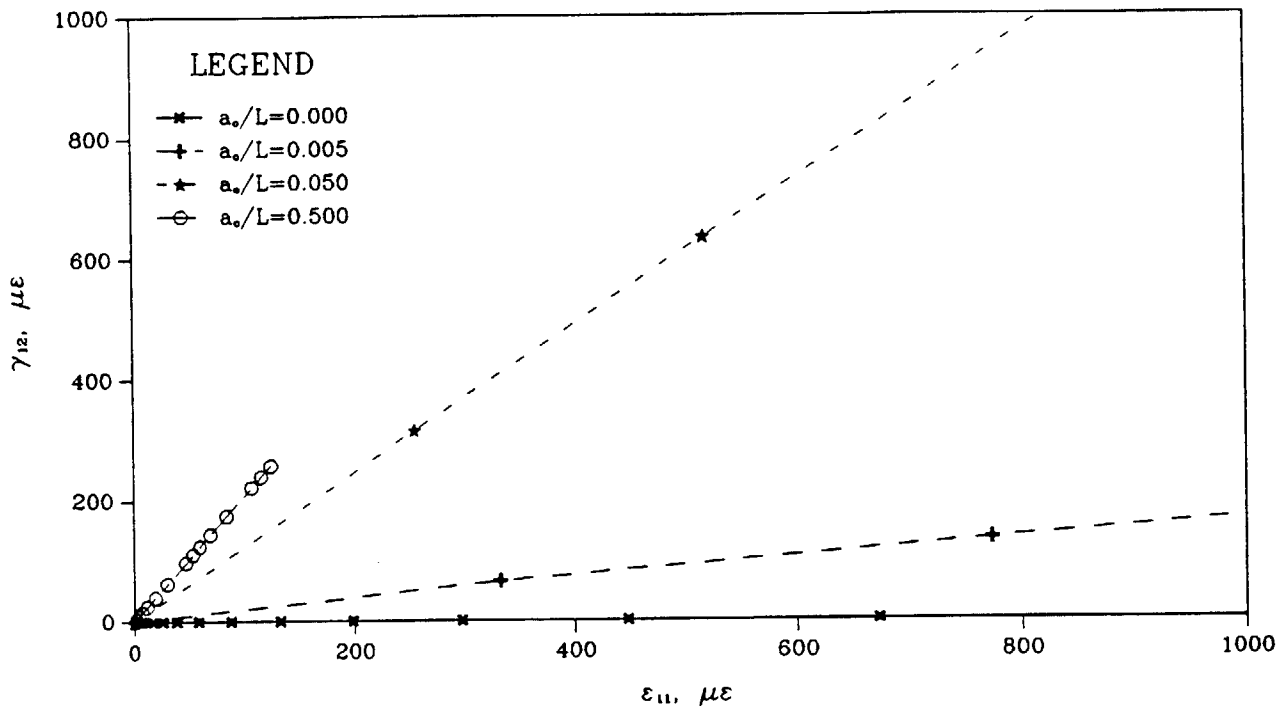

Fig. 43 Elemental shear strain plotted as a function of elemental axial strain for four different values of initial fiber curvature, $\frac{a_o}{L}$.